UNIVERSITÀ POLITECNICA DELLE MARCHE

FACOLTÀ DI INGEGNERIA

Corso di Laurea in Biomedical Engineering

Identification of R peaks and Electrocardiographic Alternans during sport activity

Advisor:

Prof. Laura Burattini

Coadvisor:

Dott. Ilaria Marcantoni

Candidate:

Alessia Di Menna

Academic Year 2020-2021

Abstract

The central organ of the circulatory system is the heart, and the standard diagnostic tool for heart disease is the electrocardiogram. Electrocardiographic changes in competitive athletes have an occurrence of about 80% related to the physiological adaptation induced by physical exercise. This physiological condition is called "athlete's heart" and its manifestation can be confound with underlying cardiomyopathies in 10-14% cases, leading to erroneous diagnosis during the medical preparticipation screening. Heart monitoring through the evaluation of cardiac risk indexes is the main weapon to contrast sport-related sudden cardiac death. A heart-rate related phenomenon acting as a risk index of cardiac electrical instability and sudden cardiac death is the electrocardiographic alternans. The electrocardiographic alternans is an electrophysiological phenomenon manifesting in the electrocardiogram as the fluctuation of one of its waves, so resulting in P-wave alternans, QRS-complex alternans and/or T-wave alternans. The electrocardiographic alternans could be an important index for monitoring heart in high-risk athletes, due to the presence of the "athlete's heartquot; a not pathological condition, which can mask pathological disease. In sport literature, there is a lack of studies for the identification of cardiac risk through electrocardiographic alternans during physical activity. The aim of the thesis is the complete characterization of electrocardiographic alternans, in terms of P wave alternans, QRS alternans and T wave alternans, during different physical activity in healthy subjects. The starting point for a reliable analysis of electrocardiographic alternans is the correct identification of R-peak positions, thus, the present thesis is composed of two parts: the introduction of a new method for identification of R peaks and the analysis of electrocardiographic alternans in electrocardiogram acquired on subjects while performing sport. An algorithm, based on the Ensemble Empirical Model Decomposition, was proposed for the identification of R peaks. During validation, the algorithm showed a good level of performance working on noisy electrocardiogram, with a sensitivity of 95%, positive predictive value of 94%, and cumulative statistical index of 89%. Regarding the electrocardiographic alternans analysis, the first approach for its identification was recently proposed in the last year (2020), while previous studies focused only on the analysis of T wave alternans. In this work, the enhanced adaptive matched filter, a method based on signal enhancement, is applied to analyze electrocardiographic alternans. Besides features already used to characterize electrocardiographic alternans (as amplitude, duration and magnitude), the alternans area was introduced to allow a reliable comparison of different types of alternans. The analysis performed on electrocardiogram acquired

during sport activities indicates that the highest alternans area was found on the T wave (1450 μ×ms for P wave, 1240 μ×ms for QRS complex and 2323 μ×ms for T wave). So, the prevalent alternans wave is the T wave. The literature did not provide a similar evaluation of electrocardiographic alternans on athletes, since previous studies considered only T-wave alternans and was not quantified in terms of area. The thesis demonstrates the presence of physiological electrocardiographic alternans in healthy subjects performing several sports.The preliminary knowledge of the physiological values of alternans is necessary to establish which value can be considered abnormal and therefore when the electrocardiographic alternans highlights a risk. The relationship with the heart rate will be useful to understand if there are any heart rate values related to a higher alternans. Further follow-up studies are needed, and they should involve a larger population of athletes to significantly evaluate the reference alternans value for healthy subjects during physical exercise, but also a wider range of heart-rate values.

Contents

List of Figures

List of Tables

Introduction

The athlete's heart identifies structural and functional changes that occur in the heart of people who train at high intensity for more than one hour per days. Athletic heart syndrome is a heart condition that is usually harmless. The muscular walls of the heart increase in thickness, particularly in the left ventricle, providing a more powerful contraction. The left ventricle's internal dimensions increase as a result of increased ventricular filling. Electrocardiographic changes in competitive athletes have an occurrence of about 80% further to the physiological adaptation related to exercise training, with pathological cardiomyopathy hidden in these changes of about 10-14%. The gold standard for the evaluation of athlete's status is the standard 12 lead electrocardiogram (ECG) which provides information about the measurement of heart rate variability, that can be integrated with continuous ECG monitoring thought the use of a small disposable wireless adhesive patch , and signal-averaged ECGs. Given the exercise-related physiological adaptation, distinguishing physiological from pathological conditions for athletes continues to be challenging despite the access to a multi-parametric approach and the combination of different innovative technologies. The continuous monitoring and the quantification of parameters acting as cardiac risk indexes can be fundamental in the prevention of sport-related sudden cardiac death The increased risk of cardiac attack and sudden cardiac death can have devastating consequences in the sports world. In 2018, Italian football was deeply rocked by the sudden death of Davide Astori, captain of the Fiorentina soccer team, further to a cardiac arrest in his room the night before a match. Autopsy records attest that the death's cause is biventricular arrhythmogenic cardiomyopathy, a congenital heart muscle disease causing irregular and potentially life-threatening heart rhythms. The disease has manifested itself through ventricular escape beats during the routine stress testing, an unrecognize symptom that causes the 31-years-old player's death. For the same pathology, a most shocking episode occurs during a Serie B match at Pescara, where the 25-years-old Piermario Morosini collapses to the ground in the 31st minute after suffering cardiac arrest. The most recent but significant episode occurs when Christian Eriksen collapsed on the pitch suddenly after suffering cardiac arrest during Denmark's Euro 2020 opener on June 12, 2021. But his luck was the presence of the first aid on hand and the ability of the medical team to revive him. This episode underlines the relevance of a continuous monitoring system, able to detect when the subject's heart is at risk of cardiac attack. For about 80% of cases, the cardiac attack comes without any pre-warming symptoms, suggesting the necessity of continuous cardiovascular screening processes for the identification of

high-risk athletes. A heart rate (HR) dependent phenomenon related to cardiac electrical instability and a risk index for arrhythmias and sudden cardiac death is the electrocardiographic alternans (ECGA). ECGA is the manifestation of an electrophysiological phenomenon occurring at stable heart rhythm consisting in the every-other-beat alternation of the morphology of one or more electrocardiographic waves. Usually in sport, only the alternans of T wave is used as index for cardiac risk, but with the evaluation of ECGA (including also the P wave and QRS complex) is possible to obtain a complete characterization of the cardiac cycle. The continuous evaluation of ECGA through a wearable monitoring system could be a valuable tool to detect athlete's risk during physical activity. Indeed, the aim of the thesis is the complete characterization of alternans, in terms of PWA, QRSA and TWA, during different physical activity in healthy subjects.For the first time, the ECGA evaluation is done through the identification of healthy alternans reference value. The starting point for the assessment of ECGA is the correct identification of R peaks position in the electrocardiographic trace. Although, this process is challenging in recordings acquired during sport activity since they are often affected by movement artefacts and deep baseline wondering. Thus the present thesis is composed of two parts: the development of an algorithm for identification of R peaks in electrocardiograms characterized by a very low signal to noise ratio and the consequent evaluation of ECGA in signals acquired on subjects while performing sport.

Chapter 1

The heart

1.1 Anatomy

The heart is a muscle pump with two main functions: collection of deoxygenated blood from tissues and organs in the peripheral body and pumping it into the lungs and collection of oxygenated blood from the lungs and pumping it into the peripheral body. The human heart is located centrally in the thoracic cavity, just behind and slightly left of the breastbone, and it rests in the superior surface of the diaphragm. The size is about that of a fist, weighing approximately 300–350 grams in males and 250–300 grams in females [12] .It occupies a place in the middle mediastinum, the compartiment of the thoracic cavity situated between the two pleural sacs. The heart is contained in the pericardium, a fibro-serous, fluid-filled sack, which has physiological functions: it fixes the heart in the mediastinum, prevents overfilling, enhances the lubrification and the protection from infection. The internal organization includes four cavities composed of cardiac muscles or myocardium: two upper chambers, called atria that receive the blood from the vasculature, and two lower chambers, called ventricles filled from atria that produce the force for the pumping action. A functional division separates the heart in left and right halves: the right atrium (RA) and right ventricles (RV) referred to the right heart are aimed at gathering blood from the body pumping it to the lungs. The left atrium (LA) and left ventricle (LV) constitute the left heart; their role is to distribute blood throughout the body. The heart is characterized by a one-way flow maintained by a set of four valves: two atrioventricular valves (tricuspid and bicuspid) allowing the flow from the atria to ventricles and two semilunar valves (aortic and pulmonary) allowing the outflow from ventricles [5].

1.1.1 The pericardium

The pericardium is the covering around the heart and great vessels (Fig. 1.4). The main functions are to keep the heart in a stable place in the mediastinum enhancing its movements while separating it from the lungs and other structures and supporting physiological function. It is composed of two distinct but continuous layers: the fibrous and the serous [1]. The fibrous layer consists in a dense irregular connective tissue sac. The base lays over the diaphragm by the pericardiophrenic ligament,

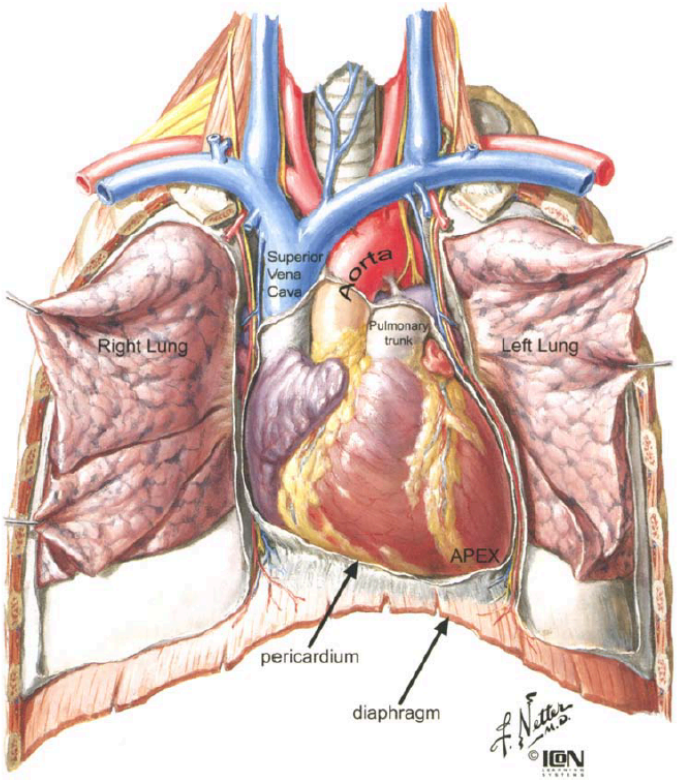

Figure 1.1: The anterior surface of the heart. The atria are positioned superior to their respective ventricles. The base of the heart is defined by a plane, called the atrioventricular groove or sulcus, that separates the atria from the ventricles. The great arteries, aorta, and pulmonary trunk arise from the base of the heart. The pericardium surrounds the muscular body of the heart. [1]

whereas the apex is continuous and fused with the roots of the great vessels that leave the heart . As regard the border, the posterior is connected with the structures of the posterior mediastinum through the loose connective tissue and the anterior is directly located on the posterior surface of the sternum. The serous layer is formed by the visceral pericardium (viscus=" internal organ") close to the heart, and by the parietal pericardium (parietes= "walls") which form the outer edge, specifically the part of the visceral layer that covers the heart, but not the great vessels is called the epicardium. These layers are separated by a space filled with 15-40 millimetres of lubricating substance called serous pericardial fluid, which reduces the friction between the parietal and visceral layer during heart contractions. The pericardial sac places the heart in the mediastinum and provides a lubricated surface for the heart to contract inside and for the lungs to move outside. Namely, the attachments of the pericardium to the surrounding structures enable the heart to be kept in a fixed location, preventing the excessive dilatation and the overfilling of the heart and providing protection. Rather, the serous layers, which contain collagen and elastin, are involved in the support of strength and elasticity of the parietal pericardium. The

pericardium is even responsible for the control of the pressure-volume relationship of cardiac chambers, hydrostatic, inertial and gravitational forces and acts as a mechanical barrier against infection.

1.1.2 The right heart

The right heart is primarily involved in the pulmonary circulation, the RA collect deoxygenated blood from the superior and inferior vena cavae and from the coronary veins and propels it through the tricuspid valve into RV [13].In the RA, the cardiac pacemaking and conduction system are located. They include the sinoatrial node (SAN), that generates the electrical impulses and sets the rhythm and rate of the heart, and the atrioventricular node (AVN), responsible for channelling electrical conduction to the ventricles [14]. The RV is a hollow muscular chamber, that pumps the blood from the RA through the outflow tract to the pulmonary trunk and extends from the inferior border of the right atrium to the cardiac apex [2]. The RV wall is about 2-5 mm in thickness and the traditional description divides it in two parts, the sinus and the conus, thus resulting inadequate for the understanding of the congenital malformation [15]. In 1977, Goor and Lillehi suggest a complete three-part description of the RV, from a embryological point of view: the inlet, including the tricuspid valve, chordae tendineae and pupillary muscles, the trabeculated apical myocardium and the outlet, including the conus and the pulmonary valve [16, 17] (Fig. 1.4). During the contraction of the RV, the control of blood back-flow is mediated by the right atrioventricular valve, the tricuspid ("three cusps") valve (TV). It is composed by three leaflets, i.e. the anterior, posterior and septal leaflets, attached to the ventricles via chordae tendineae to a large number of papillary muscles. The annulus fibrosus of the cardiac skeleton strengthen the TV orifice and it is located on the base of RA connected with the septum. The TV is sensitive to structural modification, resulting from a continuous increase of pressure and volume load. The papillary muscles, instead, prevent the prolapse of the leaflets into the atrium: the contraction and dropping on chordae tendineae prepare and secure them for the contraction of the heart [18]. The ventricular systole enables the exit of the blood from the right ventricle into the pulmonary trunk and arteries as a part of the pulmonary circulation. During the diastole, the right ventricle relaxes, and the pulmonary semilunar valve prevents the back flow into the ventricle. The pulmonary valve consists in three symmetric, semilunar-shaped cups: anterior, right and left. The cups are attached to an annulus, a structure anchored to the right ventricular infundibulum (the funnel-shaped outflow tract) and the pulmonary trunk. When the contraction occurs, the three cups collapse against the arterial wall, and the blood flows into the pulmonary artery. Once the filling is complete, the cups contact each other preventing the retrograde flow of the blood [5].

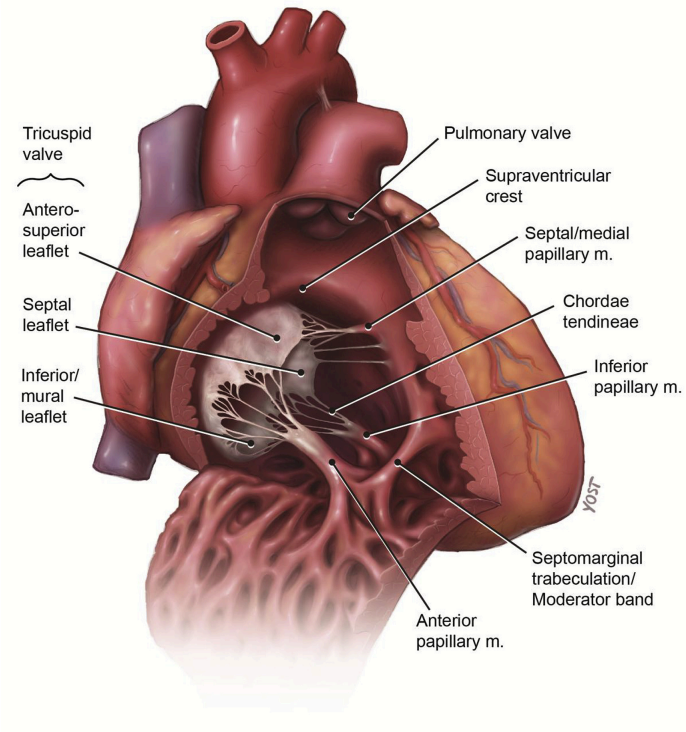

Figure 1.2: Anatomy of the right heart: internal structure [2]

1.1.3 The left heart

The left part of the heart is involved in the collection of oxygen-rich blood in the atrium, flowing blood in the left ventricle via mitral valve and pumping of blood in the whole body, including tissues and organs. The role of the LA is the modulation of the left ventricular filling and cardiovascular performance. Indeed, the LA is a reservoir for pulmonary venous return during ventricular systole able to adapt its functioning in case of late or early ventricular systole. The atrial function and ventricular performance show a strong and important interplay throughout the cardiac cycle [19](which be discussed in the next chapter). During the contraction of the LA, the blood is pumped into the LV through the left atrioventricular orifice, the mitral valve or bicuspid ("two cups"). The mitral valve is one of the two atrioventricular valves and it is composed by: the annulus, two leaflets, two papillary muscle and two sets of chordae tendineae [5]. The atrioventricular valve attaches to the ventricular wall via chordae tendineae, which in turn attach to the papillary muscle preventing the collapsing into the atrium. The extended attachment of the chordae tendineae and papillary muscle is known as the subvalvular apparatus (Figure 3). The mitral valve, as previously stated, has two cups, anterior and superior, named according to their position. Although neither description is anatomically correct, the terms aortic (anterior) and mural (posterior) leaflets are preferred. Each leaflet is characterized by a basal, clear and rough zones [3]. In a normal condition, the LV relaxes, the mitral valve opens and allow it to be filled. When the systole occurs, the increased pressure

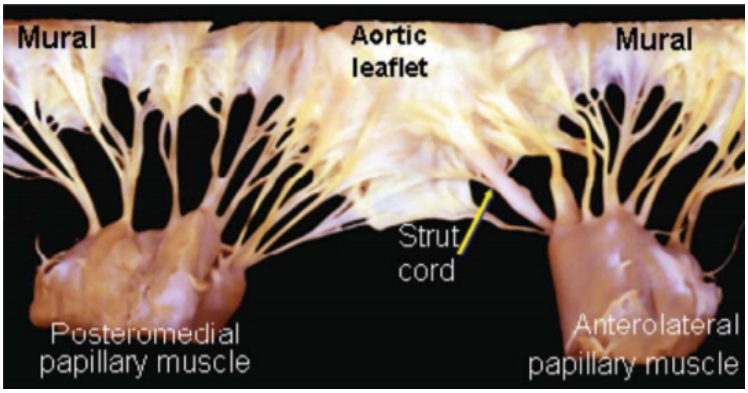

Figure 1.3: View of the ventricular surface of an adult mitral valve[3]

within the ventricle triggers the closure of the valve, with the aim of blocking blood from leaking backward and ensuring that all the blood is ejected into the aorta and to the body. Therefore, the LV pumps blood at higher pressures compared to the other heart chambers, owing to a higher workload and mechanical afterload, resulting in a thicker LV free wall in comparison to that of RV. Namely, the thickness is more pronounced at the cardiac base and it gradually becomes thinner toward the apex. The normal thickness of the LV ventricle for an adult heart is 12-15mm [20]. The ventricular contraction provides the necessary strength for the pumping of the blood into the aortic artery thereby building the aortic root, a direct continuation of the left ventricular outflow. The term 'aortic root' refers to the aortic valve from the LV outlet to its junction with the ascending aorta and it consists in the aortic valve leaflets, the leaflet attachments, the sinuses of Valsalva, the interleaflet trigones, the sinotubular junction and the annulus [21]. Like the pulmonary semilunar valve, the aortic semilunar valve prevents the backflow of the blood and forms the hemodynamic junction and physical boundary between the LV and the ascending aorta. The three leaflets constitute the aortic valve providing the main sealing mechanism (Figure 4). From an anatomical point of view the valve leaflets can be distinguished into three parts: the free margin, the "belly" of the leaflet and leaflet attachments. The distal structures to the hemodynamic junction are subject to arterial pressure and the proximal parts are subjected to the ventricular hemodynamics. The optimal solution for low resistance valve opening is represented by its trileaflet design [4]. Rather, the sinuses of Valsalva are three bulges of the aortic wall and two of the three sinuses give origin to the coronary arteries, termed by the left, right and non-coronary sinus.

1.1.4 Fetal heart

The formation of the heart and its major vessels is basically complete at the third month of fetal development and the blood-flow direction is generally the same as the adult. Some differences arise between fetal and postnatal circulation: umbilical

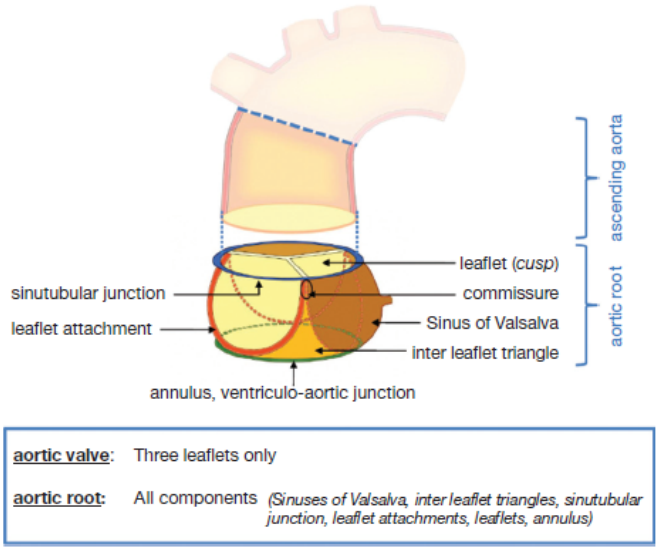

Figure 1.4: Aortic root and aortic valve nomenclature [4]

veins carry the oxygen-rich blood toward the fetus and from umbilical arteries the deoxygenated blood flows away from the fetus, the placenta provides a support of oxygenated blood toward the heart and mostly the RA contains a mixture of oxygenated and deoxygenated blood. The fetal lungs are not completely formed and functional and so a little portion of the blood in the RA is required. Most of it is shunted from the right part, the pulmonary side, to the left part, the systemic one while the LA and RA are separated by the interatrial septum. To ensure the flow from RA to LA, three features are found in the fetal heart. First, the foramen ovale, an oval hole in the interatrial septum allowing the passages from the RA to the LA (Fig 1.5). Indeed, the pressure in the RA is higher respect to the LA due to the large vasculature from the placenta. Precisely, the foramen oval is not a real hole but a two flaps valve to avoid regurgitation of blood. The second feature is the ligament of the inferior vena cava which extends to atrial septum passing to the foramen ovale. Lastly, the ductus arteriosus or "duct of the arteries" connects the left pulmonary artery and the aortic artery thus a little portion of blood reaches the nonfunctional lungs. At any rate, after birth several processes occur: the umbilical cord is cut and the newborn is able to perform the first breath, the increased secretion of the hormone prostaglandin promotes the closure of the ductus arteriosus, the lungs receive more blood, and the pressure is boosted in the LA, wrapping up the two flaps of the foreman ovale and preventing the flow from the right to the left atrium [5].

1.2 Physiology

The adequately pumping action of the blood in the circulatory system is provided by a highly synchronized contraction of the cardiac muscle: firstly, the contraction of the

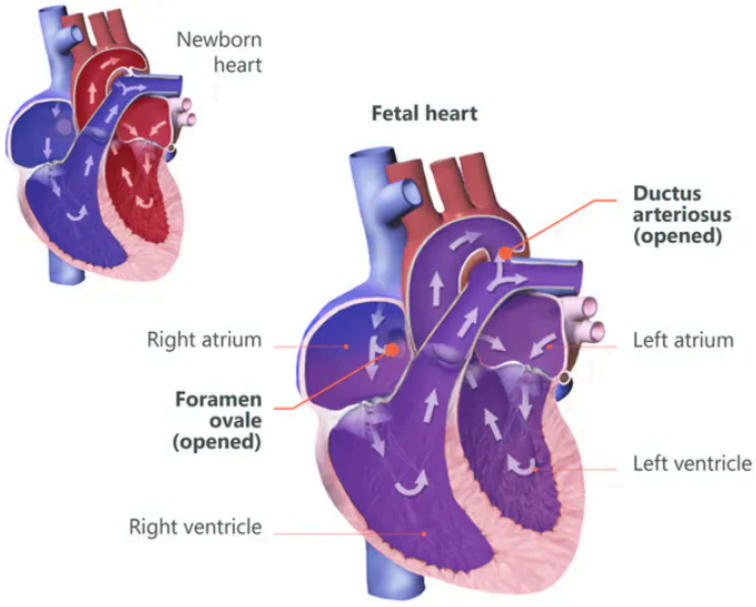

Figure 1.5: The fetal hear

atria occurs followed by the contraction of ventricles. The cardiac conduction system controls and determines the sequence of excitation of cardiac cells coordinating the contraction of the heart [12].

1.2.1 The heart electrical activity

The cardiac cells have the ability to contract without the backing of the central nervous system (CNS), triggering signal originating within the muscle itself. The inherent properties of the cardiac muscle to function in ordered rhythmic fashion is defined as **myogenic**, whereas the ability of the cardiac cells to initiate and generate its own rhythm is called **autorhythmicity**.The latter propriety arises from a small portion of muscle cells, called autorhythmic cell, essential for the contraction and a normal heartbeat. Two autorhythmic cells are distinguished in: the pacemaker cells, highly specialized cardiomyocytes which initiate the heart rhythm and generate the action potential (AP), and the conduction fibers, with function of transmit and coordinate the AP through the heart. Lastly, the cell that produce the contractile force are named **contractile cells**.The pacemaker cells are involved in the generation of the biological pacemaker through the production of spontaneously AP. Generally, pacemaker cells are situated in all the parts of the human heart, but a higher contraction is found in two specific regions of the myocardium: the sinoatrial node (SAN) in the RA near the junction with the superior vena cava, and the atrioventricular node (AVN), near the tricuspid valve in the interatrial septum. In particular, the SAN is the real pacemaker of the heart with own automaticity determining the heart rate (HR) [5]. For this reason, the rate of the SAN and AVN

for spontaneously generate the AP is different. The main difference between SA node and AV node is that the SA node generates cardiac impulses whereas the AV node relays and intensifies cardiac impulses. The spontaneous frequency of depolarization of the SAN is 70 depolarization per min. The electrical activity of the heart can be represented in slow response (the AP generated by pacemaker cells both at SAN and AVN) and fast response (generated by muscles from ventricles myocardial cells). The slow is spontaneous, the fast must receive an input from for the pacemaker cells. The conduction fibers are specialized cells skilled at transmitting the AP with a higher velocity of conduction respects the cardiac muscle fiber since they are larger in diameter: the rate is 0.5 meter per second in the conduction fibers opposed to the 0.02–0.05 meter per second in other regions of the conductive system [5, 22]. The transmission of the AP is a wave of excitation which starts in SAN and moves through the ventricles, causing the depolarization and the contraction. This can be achieved by the presence of intercalated disc, fundamental for the transmission of force, mechanical continuity and chemical communication between cardiomyocytes [23], which contains two functional structures: gap junction and desmosome. The gap junctions are an aggregation of intracellular channel that allow the diffusion of the electrical current in form of ions from one cell to another [24]. Instead, the desmosomes are physical bond between the disks that resist the mechanical stress and adopt a strongly adhesive state [25] (Figure 6).

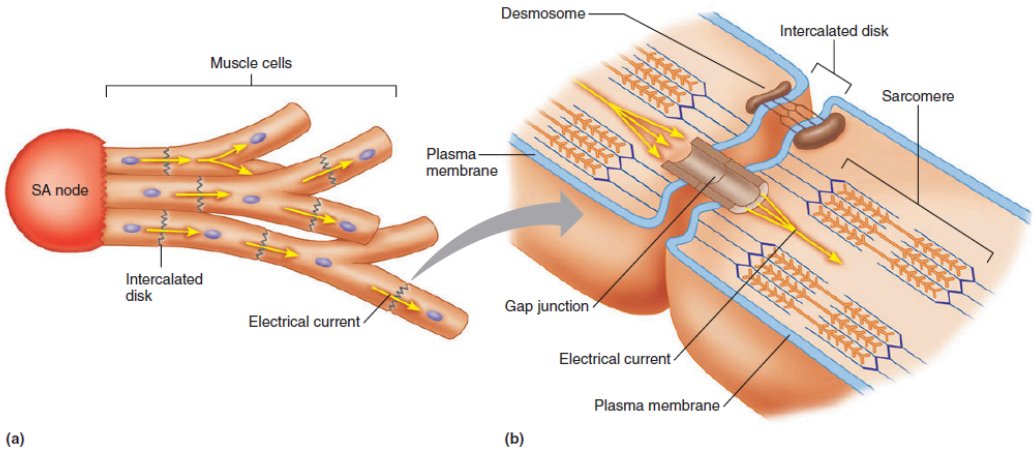

Figure 1.6: Electrical communication between cardiac muscle cells. **(a)** Spontaneously generation of the action potential in the senoatrial node and the transmission to the adjacent cell by means of electrical current. **(b)** Internal view of the connection between adjacent cells displaying gap junction and desmosome. [5]

The triggering of the heartbeat occurs following five different electrical events (Figure 7):

1. In the SAN, the pacemaker cells cause the triggering of the APs, which travel

in two different regions: the AV node and atrial muscles. The internodal pathway, a systems of conduction fibers, leads the impulses to the AV node and simultaneously the interatrial pathway spread the APs through the atrial muscle.

2. The APs reach the AVN and the AV nodal delay occurs: the impulses are delayed by about 0.1 second since in AVN the transmission of the APs is slower than the other cells in the conduction system.

3. The AV node fires the APs through the bundle of His, an atrioventricular bundle, situated in the interventricular septum and together with the AVN constitute the electrical connection between atria and ventricles, divided only by the fibrous skeleton.;

4. In this phase, the travelling of the APs through the bundle of His is relatively short because it branches into right and left bundle, in order to conduct the impulses toward the right and left ventricles, respectively.

5. The impulses arrive at the Purkinje fibers, a large network of branches that transmit the APs through the ventricular myocardium from the apex to the valves and to the rest of the ventricular myocardial cells.

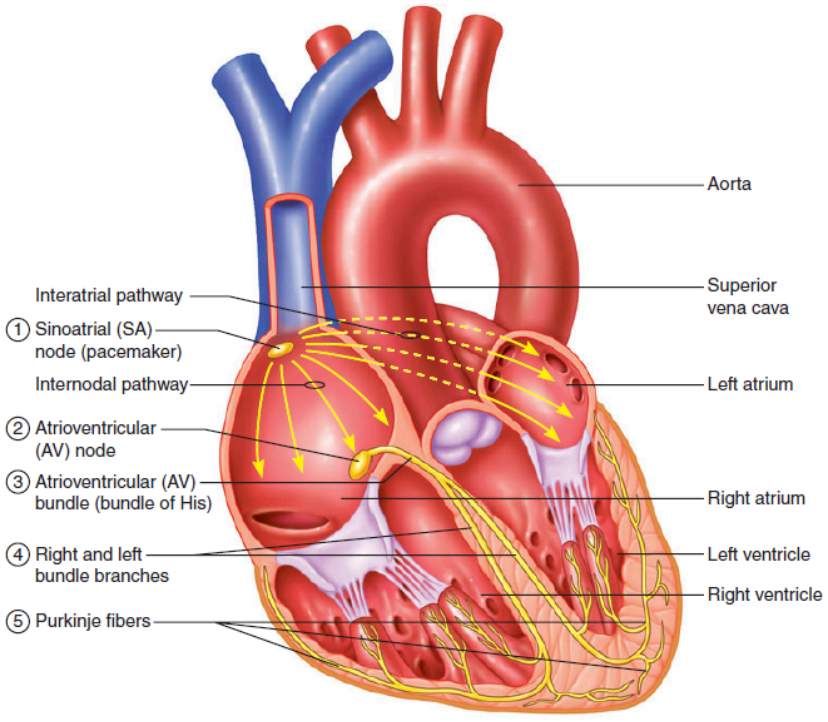

Figure 1.7: The conduction system and the five electrical events

As previously explained, the heart contains different population of cells specialized for different functions. Generally, all the heart's cells have the ability to conduct

the APs but some cluster of cells are specialized in the generation and propagation of the impulses through the heart, **the conducting cells**, other group of cells are involved in the contraction and in the pumping blood activity and they are referred to **the working cells**.These cells are mainly the ventricular myocytes and constitute the majority cells in the heart whereas the conductive cells are situated in the SAN, AVN and Purkinje fibers. These two kinds of cells differentiate not merely to their purpose, but also to the shape and types of the AP, specifically we can distinguish a fast-response action potential for ventricular myocytes and slow-response action potential for the pacemaker cells. Firstly, the concept of membrane potential must be introduced. The living cells are composed by a cell membrane and different distribution of ions which crossing the membrane change its voltage. The most significant ions that contribute to the membrane potential are sodium (Na+), potassium (K+), calcium (Ca++) and choride (Cl-). A higher concentration of potassium is found inside the cell respect to the outside and contrarily, the concentration of sodium, potassium, calcium and chloride is higher outside. Consequently, the phases of the cardiac AP are associated with changes in cell membrane permeability. Furthermore, the cardiac resting membrane (Vm) are negative, meaning a net negative charge inside the cell [26].

Fast-response action potential

The ventricular muscle cells and the Purkinje fiber have a resting potential of about –90mV. When a stimulus depolarizes the Vm to a critical value, defined as threshold (-65 mV), the cell membrane proprieties change and a new AP is generated [27]. The five phases are illustrated as follows (Figure 8):

Phase 0:It is considered as the rapid depolarization, with a depolarization rate of about 250 mV, and a change in the membrane potential from –90 mV to +50 mV. This is due to the opening of the voltage-gated sodium channels, the membrane became more positive and triggers the opening of more sodium channels.

Phase 1:It is referred ad the “notch”, i.e. a transient repolarization period. Inward sodium current no longer depolarizes because the sodium channels start to become inactivated and the membrane fall to negative value (potassium ions continue the outward current). Two events occur simultaneously: the closure of potassium channel and the opening of the L-type calcium channels.

Phase 2: Also called “plateau phase”. The membrane potential is characterized by a dynamic balance and only small changes occurs, the calcium channels still continue to be open and most of the potassium channels closed in the phase 1 stay closed.

Phase 3:It is observed a repolarization following a reduction of calcium and sodium currents and an increasing of potassium current. The membrane potential value decreases to a more negative value.

Phase 4:The membrane potential returns to its resting values as well as the concentration of sodium, calcium and potassium.

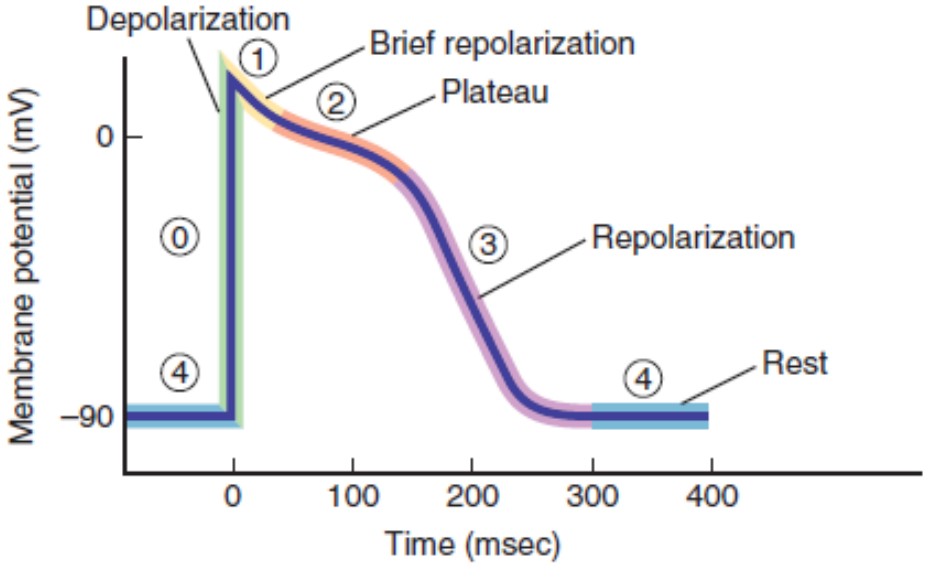

Figure 1.8: The cardiac action potential recorded from a ventricular myocyte [5]

Slow-response action potential

The slow-response AP is generated by pacemaker cells that can trigger AP without any external stimulus in a regular and periodic fashion. Pacemaker cells are characterized by an unstable resting potential, they slowly depolarize from –60 mv to a threshold of –40 mV generating an AP [28]. Afterword, the slow diastolic phase occurs, a specific feature of the SAN myocytes. The origin of this phase has been largely investigated and it is attributed to the presence of funny channel underling the cardiac pacemaker current or funny current [29]. This latter has unusual feature, which justified the name: it is an inward current activated on hyperpolarization to the diastolic range of voltages, with the ability to generate repetitive activity and modulate spontaneous rate allowing potassium and sodium to cross the plasma membrane [29, 5]. The funny channels remain open until the membrane potential reaches –55 mV, near the threshold but not sufficiently to generate the AP. But the initial depolarization triggers the opening of the transient (T-type) calcium channel through which the potential arrives at the threshold. At this stage, the T-type channel closes and there is the opening of the long-lasting calcium channel resulting in a large increase in the calcium concentration inside the cell which produce the rapid depolarization. This depolarization activates the opening of the potassium channel, and consequently an outward current, resulting in a fall of the potential membrane value and a stimulus for the closure of the calcium channels. The repolarization occurs and the AP terminates. Figure 1.9 shows the AP in the pacemakers cella and its three phases.

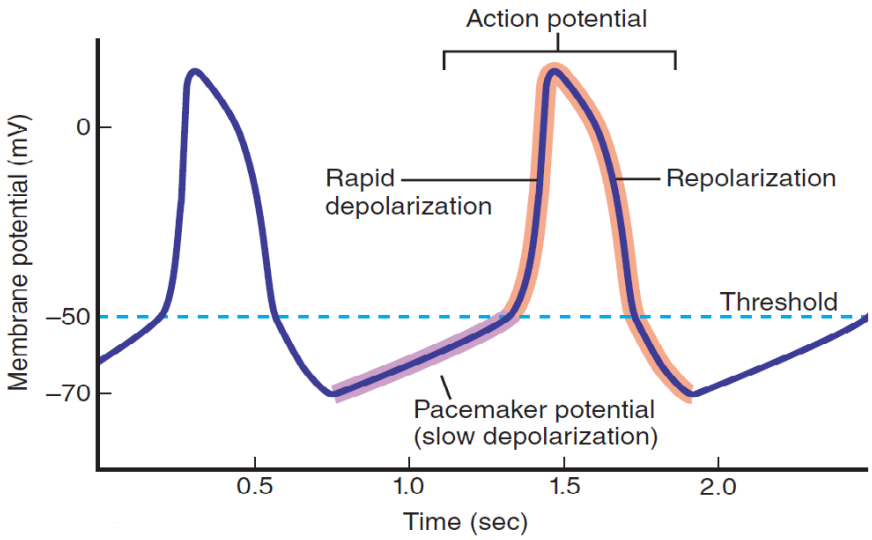

Figure 1.9: Action potential in the pacemaker cells and its three phases: **(1)** slow depolarization, **(2)** rapid depolarization, **(3)** repolarization [5]

1.2.2 The cardiac cycle

The cardiac cycle is a sequent of events associated with the flow and pressure of the blood through the heart during a single heartbeat. In a subject with normal heartbeat rate of 78 bpm (*beat*×) the duration is about 0.8-0.9 seconds. A single heartbeat is characterized by two distinct phases: ventricular contraction, systole, and ventricular relaxation, diastole. Their duration is not the same, the majority of the cardiac cycle is spent in diastole, about 0.6 seconds, whereas the systole lasts about 0.3 seconds. The Wiggers diagram is one of the most powerful tool for the understanding of the cardiac function and the mechanism by which the heart works. It is a graphic representation of the cardiac cycle plotted in a time scale [30]. In Figure 10 is displayed the Wiggers diagram: in the x-axis it is plotted the time course while in the y-axis are represented the ventricular pressure, aortic blood flow, ventricular volume, heart sound, venous pulse and electrocardiogram. The analysis of the different phases will start when the atria and ventricles are completely relaxed, so during the diastole.

1. *Ventricular filling*: The ventricles are filled with blood in two phases: diastole, relaxation of both atria and ventricles, and contraction of the atria. During the diastole, the blood flow via vena cava and pulmonary veins into the right and left relaxed atria, respectively, passes through the AV valves and into the ventricles. The process by which the blood flows back into the heart is called **venous return** and occurs when the pressure in the veins is higher respect that in the atria. Both semilunar valves are closed. At the end of the diastole, the atria contract pushing the remain amount of blood, the pressure in the ventricles increase above that of the

atria causing the closure of the atrioventricular valves.

2. *Isovolumetric contraction*: This phase is characterized by the beginning of systole that triggers the excitation-contraction of ventricles and a rapid increase in the intraventricular pressure. At this time, the AV valves are closed as well as the aortic and pulmonary veins. Consequently, blood cannot flow into or out the ventricles, the ventricular volume does not change thus the pressure inside increases, approaching the pressure in the aorta and pulmonary arteries.

3. *Ventricular ejection*: At this stage, the pressure within the ventricles overcomes that in the aorta and the pulmonary artery causing the opening of the semilunar valves. The blood effluxes from the ventricles and into the vasculature. The period of rapid ventricular ejection represents the 70% of the blood ejects in the first third of ventricular ejection, the slow ventricular ejection is the final 30% of the blood in the remainder of the time. The pressure reaches the peak and then starts to decrease until falls below the aortic pressure resulting in closure of the semilunar valve, the ending of systole and the beginning of diastole.

4. *Isovolumetric relaxation*: At the beginning of the diastole, the ventricles start to relax. During the period between the closure of the semilunar valves and the opening of the AV valves, the ventricular pressure decreases while the volume of blood is constant within the relaxing of the ventricles. Once the ventricular pressure is lower than atrial pressure, the AV valves open and the blood enters the ventricles again. This marks the beginning of a new cardiac cycle.

1.2.3 Cardiac output and its control

The heart is the centre of the cardiovascular system providing the force to deliver blood at high pressure into the arteries and ultimately to organs. This ability depends on the rate at which the ventricles are able to pump blood. In a healthy subject at rest, both ventricles pump more than 5 liters through the pulmonary and systematic circulation every minute. Therefore, the **cardiac output** (CO) is defined as the rate at which the left ventricle pumps blood into the aortic arch, and it is usually expressed in liters per minute [5]. At rest, the CO is 5-6 Lmin whereas in elite athletes during exercise is more than 35 Lmin and it depends on the heart as well as the circulatory system, veins and arteries [31]. It is also referred to:

$$CO = HR \cdot SV \tag{1.1}$$

HR is the number of times the heart beats in one minute and the normal range is between 60 to 100 beats per minute. The stroke volume (SV) is the amount of blood pumped out of the left ventricle during each systolic cardiac contraction and the average value of 70 kg male is 70 mL [32]. By considering the blood filling the heart by the end-diastolic volume (EDV) is not completely ejected from the heart during the systole, it must be regarded the volume left in the heart at the end of systole,

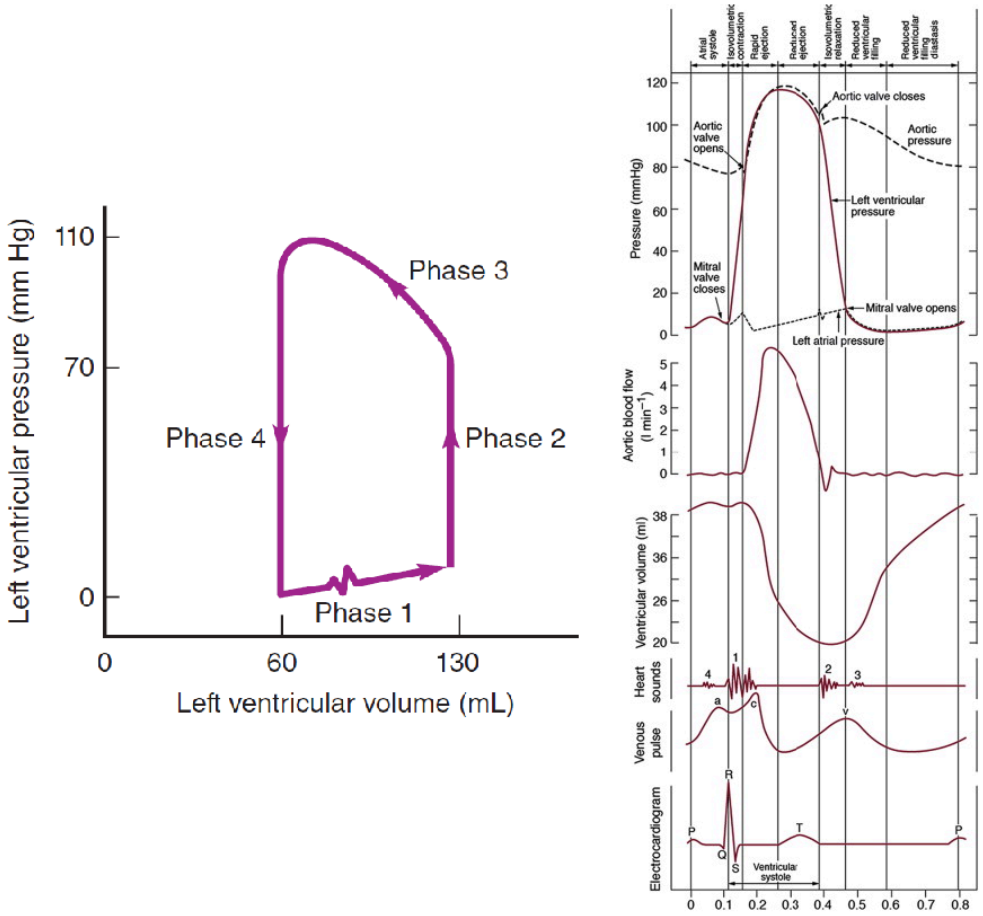

Figure 1.10: In the left, the left ventricular pressure-volume curve. In the right, the cardiac cycle

called end-systolic volume (ESV). Thus, the SV is equal to:

$$SV = EDV - ESV \tag{1.2}$$

The CO is involved in the essential mechanism that provides blood flows to the body, especially it ensures a continuous oxygen supply to the brain and other vital organs. But the body's demand for oxygen changes depending on the situation, for instance during exercise, and the control of the CO is performed by modulating both HR and SV [31]. The mechanism of neural control is complex, and it primarly involves the autonomic nervous system (ANS). The fibers involved belong to both the sympathetic and parasympathetic division exerting opposite effect: the sympathetic nervous system reacts in a "**fight-or-flight**" situation whereas the parasympathetic nervous system is referred to by the epithet of "**rest and digest**". The parasympathetic innervation is provided by Vagus nerve (cranial nerve X), which innervate only pacemaker structure (SAN and AVN) and exerts an inhibitory effect slowing the HR and reducing the number of depolarization generable in a fixed time interval. The

sympathetic system, through cardiac nerve, innervate SAN, AVN and muscle fibers of ventricular wall. It has an excitatory effect by increasing the HR and the frequency of depolarization of the action potential produced by pacemaker cells [5]. As regard the modulation of the SV, it depends on three factors: preload, afterload and contractility. An increase preload, which affects the passive muscle tension, enhances the passive stretching of the heart muscle by means a phenomenon called Frank-Starling law of the heart [33, 34]. Afterload is proportionate to systemic blood pressures and it is inversely related to stroke volume [33]. Lastly, contractility refers to the force of myocyte contraction, and when the force increases, the heart pumps out more blood increasing the SV [31]. An increase in preload leads to an increase in stroke volume (width of loop) because of the Frank-Starling mechanism. If afterload and inotropy do not change, then the end-systolic volume will not change and the heart simply ejects all the extra blood that filled it. However, increased stroke volume leads to an increase in cardiac output and arterial pressure; therefore, the afterload on the ventricle increases. This partially offsets the increased stroke volume by increasing the end-systolic volume. The reason for this is that the increased afterload reduces the velocity of fiber shortening and therefore the ejection velocity. Conversely, a decrease in preload reduces stroke volume, but this reduction is partially offset by the decreased afterload (reduced aortic pressure) so that the end-systolic volume decreases slightly.

1.3 Coronary circulation

The coronary circulation is a part of the systemic circulation: the coronary arteries provide blood and nutrients from the LV to the tissues of the heart, whereas the coronary veins are responsible for carrying deoxygenated blood away from the myocardium to the heart chambers. The primary coronary arteries originate from the sinuses of Valsalva behind the aortic valve leaflets. The right coronary artery (RCA), which arise from the anterior aortic sinus, supplies blood to the right heart, including SAN and AVN, and specific portions of the LV. From the left posterior aortic sinus, the left main coronary artery (LMCA) takes origin bifurcating into the left circumflex artery (LCX) and left anterior descending artery (LAD), which provide blood to the left side of the heart (Figure 1.11). A functional division classify the coronary arteries in epicardial vessels and intramuscular vessels. The role of the epicardial vessels is the conduction of the blood flow, they are superficially located and greater respect to intramuscular vessels. The latter are within the myocardium, they branch into arterioles to ensure a fine-tuned control of blood flow [35]. Lying immediately beneath the endocardium is a plexus of subendocardial arteries (Figure 1.12). In a normal condition, the heart receives about 75% of the available oxygen from the blood, a large amount with respect to other organs in the circulation, for instance, skeletal muscle extracts about 40% and the liver extracts 20%. Ongoing blood support to the heart is vital since obstruction of a

coronary artery leads to myocardial infarction, a partial death of heart muscle, to total heart failure, and in severe cases to death [36]. This degree of oxygen extraction stresses the continuous high metabolic activity of the myocardium. The myocardial oxygen demand can increase according to ventricular rate and contractility, thus, the increase of the coronary flow under this condition is fundamental. The mechanism of coronary regulation is not fully understood, therefore different studies have proposed a multifactorial model to explain it. The primary determinant of coronary flow is believed to be carbon dioxide and other metabolites of oxygen consumption. In addition, the localized hypoxia and hypercarbia can influence coronary vasodilation, in the physiological and pathophysiological condition. At any rate, multiple studies have demonstrated that the amount of oxygen and carbon dioxide is not sufficient to explain the degree of vasodilation in response to increased oxygen demand and an intermediate molecule could be involved [36]. Concerning the coronary veins, the oxygen-poor blood return to the systemic circulation after occurring gas exchange. The venous vascular network runs parallel to the epicardial coronary arteries. The two primary veins are the intraventricular vein (IVV) and the cardiac vein (Figure 1.11). The former vein is located near the LAD and it is involved in the anterior surface drainage derived from the LAD perfusion territory. The latter vein adjacently courses to the LCA by continuing the drainage system. Both coronary veins flow into the coronary sinus supplying 55% of the coronary backflow and returning into the RA. While the return in the RV is mediated by the anterior cardiac veins constituting about 35% of the venous drainage. The 10% left is accomplished by the thebesian vein [6].

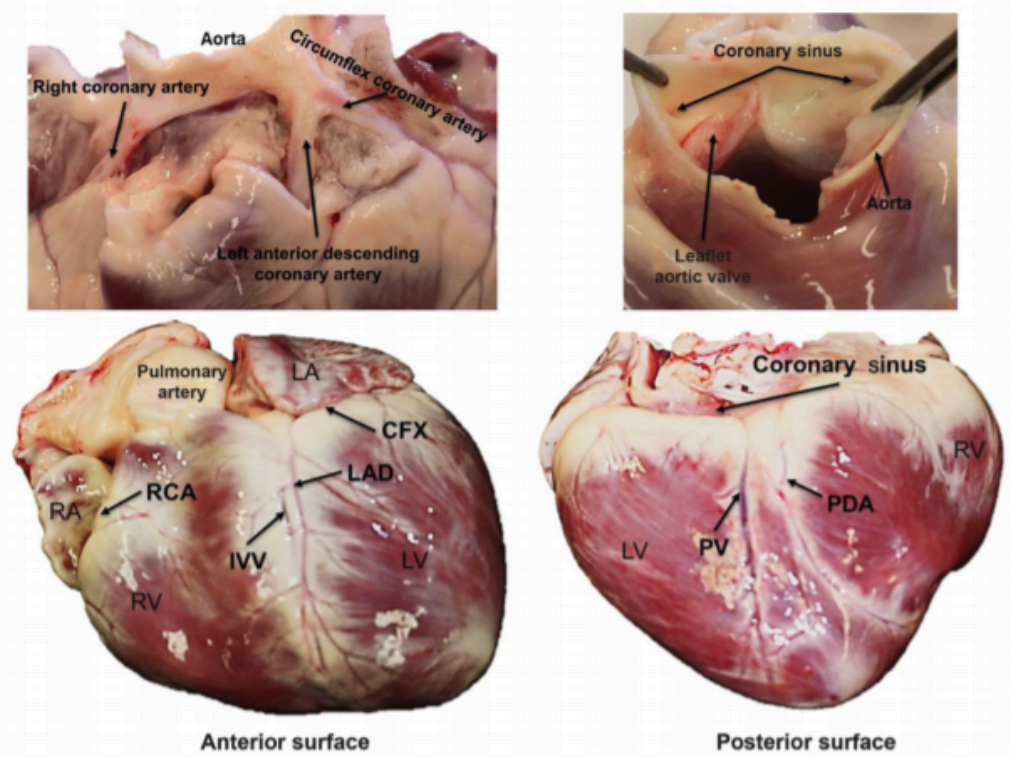

Figure 1.11: Anatomy of coronary circulation [6]. LA=left atria; LV=left ventricle; RA=right atria; RV=right ventricles; RCA=right coronary artery; LAD=left anterior descending artery; CFX=circumflex artery; PDA=patent ductus arteriosus; PV=pulmonary veins.

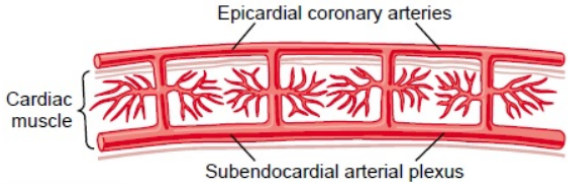

Figure 1.12: Epicardial, intramuscular and subendocardial coronary vasculature [7].

Chapter 2

Electrocardiogram and Electrocardiographic Alternans

Since the early 20th century, **electrocardiogram** (ECG) is the standard diagnostic tool for heart diseases able to detect critical information about human heart, contained in the cardiac electrical activity. The relevance of ECG has been largely demonstrated, firstly for its universality and permanence, which refers to the ability of performing biometric matches against templates that have been designed earlier in time. This essentially requires that the signal is stable over time. A second important concept is the uniqueness of the extracted features, because different subjects under examination have different physiological elements, depending on the activity they are performed, age, mental status and so on. Critical is the relevance of the connection between the identification of correct measures and unicity of subject-to-subject heart parameters. A further important issue is the lifetime availability to record ECG tracing for each living person in the world, allowing analysis all long-life course. The difficulties for the exact identification of the ECG features are generated by external noise, especially in ECG acquired during sport, since the internal environmental factors cannot distort the waveforms. [37]. The main sources of noise are: muscular activation during physical activity, power line noise, interference from heavy breathing movement and poor electrode-skin contact during motion. The added disturbances increase the difficulty in interpreting signal for the evaluation of athlete's heart status: the unseen parameters can be essential for the detection of heart failure or high-risk athletes. Hence, an automatic analysis, for the extraction of detailed and relevant feature of ECG, is needed, by using computer-based algorithm.

2.1 Genesis of electrocardiogram

The contraction of myocardial cells is characterized by a wave of electrical current which spreads through the whole heart triggering the systole or heartbeat. The pattern of electrical propagation coordinately travels over the heart resulting in coordinated systole and a measurable potential difference on the body surface of the subject. This amplified and filtered signal is defined as the ECG [9]. ECG is a non-invasive and painless measurement which allow the investigation of heart

problems and monitor the heart's health. Clearly, the understanding of ECG's genesis is critical for clinician in evaluating and diagnosing heart diseases. The first theory was introduced by William Einthoven at the beginning of the twentieth century and it considers the heart as a current dipole located in an infinite and homogenous volume conductor [38]. This mathematical model explains the relationship between the cardiac generator and the body surface potential. We will start the discussion from a cellular point of view. As explain in the previous chapter 1.2.1, the electrical activity of the heart is influenced by fluxes across the cell membrane of sodium, potassium, calcium and chloride ions. The cell membrane selectively allows the passages of ions through the presence of embedded channel proteins resulting in a different composition of fluid inside and outside the cell. Specifically, the inside is more negative respect the outside resulting in a negative potential [39]. Figure 2.1 shows the conduction of AP. In cell A the sodium channels are already open and cell A is starting to produce its own AP causing intracellular current flow from a fully depolarized cells on the left to cell B in the right. Cell B starts to be less negative and extracellular potential difference between cell A and cell B is generated. At this stage, the potential above cell B is higher than the potential above cell A triggering a net driving force from right to left. This flow is called extracellular current and it is responsible for the generation of the ECG.

In the mathematical model, the elementary electrical source of the surface ECG is the intracellular current, and it is referred to the current dipole. Against the direction of propagation, the flow of the extracellular current enables the conservation of charge, resulting in a current close-loop: the dipole field is formed (Figure 2.2). The generation of the ECG signal is triggered by the movement of the dipole relative to the ECG electrode. The depolarization is characterized by a positive leading edge of the activation wavefront and a negative charge in the rearmost edge. In the ECG, an upward and downward deflection depends on the movement toward and away from the recording electrode, respectively. During the repolarization, the ECG signal has inverse deflection [9]. The vectorcardiogram is the spatial representation of the

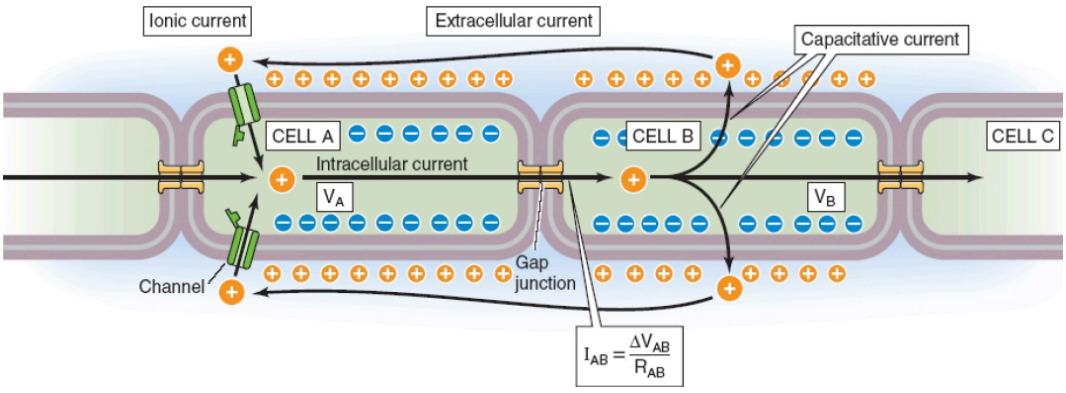

Figure 2.1: Conduction of action potential from two adjacent cell and the generation of the extracellular current [8].

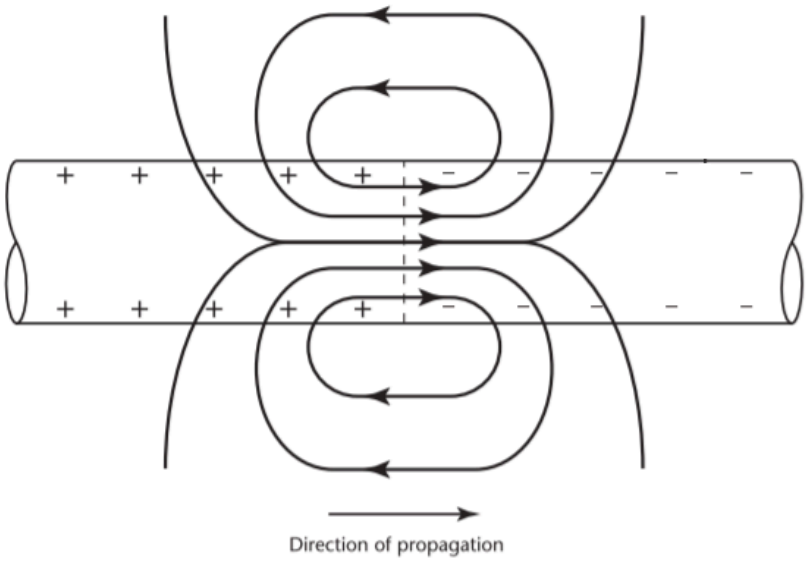

Figure 2.2: The dipole field generated by a current flow in the heart myocardial cell. [9]

forces generated during the cardiac cycle. The vector is characterized by an onset (origin) and end, the size of vector varies according to the magnitude, orientation and direction and the point of the vector is its positive side. The equivalent dipole moment is defined as time-dependent heart vector, which changes in magnitude and direction as each wave of depolarization spreads through the heart [40]. Figure 2.3 displays the heart's geometry and the resultant vector of the electrical activity of the heart throughout the cardiac cycle. By focusing on a normal heartbeat, the spontaneous depolarization is provoked by the cells in the SAN. The wave of depolarization travels from the right atrium to the left atrium in about 80 ms. On the body surface, the electrical activity of the SAN is not sufficiently high to be recorded, while the depolarization of atria produces the P wave on the ECG, reflecting the leading edge of the depolarization wavefront. In the AVN, the depolarization starts when the activation wavefront spreads to the lower right atrium, but the electrical activity is not registered on the ECG. The ventricular activation triggers a sequence of events that generates a signal recorded as the QRS complex. From the AVN, the depolarization wavefront reaches the heart septum, followed by the activation of the left and right apex, from the endocardium to epicardium free wall, and the base of the LV and RV. The QRS lasts about 90 ms, the time in which all the ventricular cells are depolarized. At the same time, the repolarization of atria occurs but the wave is relatively small in amplitude and it is masked by the QRS complex. The sequence of ventricular repolarization is opposite to that of the depolarization, the direction goes from epicardium toward endocardium, and the T wave is recorded in the surface ECG [41].

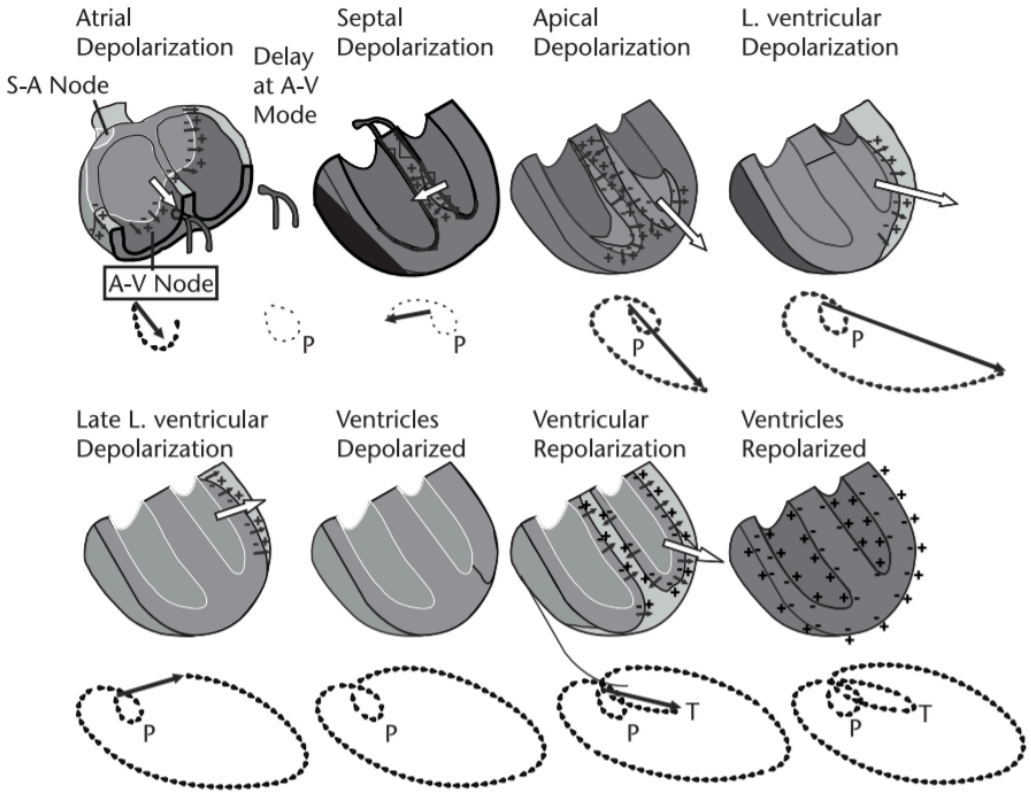

Figure 2.3: Trajectory of a normal cardiac vector [9]

2.2 Electrocardiographic leads

2.2.1 Lead Vector

The ECG lead is a graphical description of the electrical activity of the heart, detected by adhesive electrodes attached to the skin.The resulting measurements are referred to as leads. An electrode is a conductive pad attached to the skin for the recording of electrical activity. The ECG understanding is based on two essential concepts: the heart vector (discussed in Section 2.1) and the lead vector. Lead vectors are defined such that, when electrodes are placed along two different vectors that lie in the same plane as the cardiac vector, it can be fully defined. Firstly, William Einthoven contributes to the creation of the ECG, he is called "the father of electrocardiography" and he received a Nobel prize for his work in 1924. Einthoven defined the circuit **Einthoven triangle**, in which the electrical activity of the heart is lumped in heart vector H. This vector H is projected on an equilateral triangle, on the three leads I, II, III. All leads are equally sensitive. The amplitude in lead I, II, and III is associated with heart vector H, and if H changes direction or size, it will change ECG amplitude in each lead. The extremity leads I, II, and III have been called "Einthoven leads". Each lead detects the electrical potential difference between the positive and negative electrodes. Lead I computes the potential difference between left arm and right arm;

Lead II computes the potential difference between left leg and right arm; lead III computes the potential difference between left leg and left arm (Figure 2.4). In this model, the cardiac source is a two-dimensional dipole in a fixed location and the conductor can be infinite and homogenous or a homogenous sphere with the dipole source in the center. A few decades later, Ernest Frank developed an electrolytic

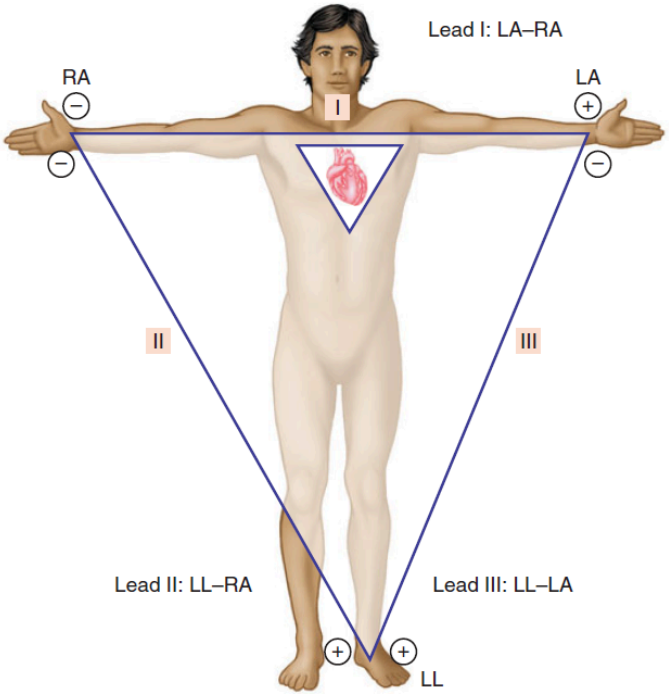

Figure 2.4: The Einthoven triangle [5]

tank model of the human torso. The source is a three-dimensional dipole in a fixed position in the thorax, representing the lumped electrical activity of the heart at a given moment. The conductor filled within the torso is a finite and homogenous medium. The triangle is called the **Frank triangle**, and it is illustrated in Figure 2.5b. It is obtained by measuring the lead vectors of the scalar leads by constructing an electrolytic tank model of the human torso. In this model, the lead vectors of standard lead were measured by using an inhomogeneous electrolyte tank model of the human torso, in order to introduce the effect of the lungs. The underlying idea is that each ECG lead is associated with a lead vector that represents the directionality (i.e. spatial orientation of the lead vector) and the sensitivity (i.e. lead vector magnitude) of the ECG lead. The ECG amplitude is expressed as the product between the fixed lead vector c and the heart dipole vector p(t). The **Burger triangle** replaces the Einthoven triangle. It's a graphical representation of the lead vector concepts. There are two triangles and a Heart Vector H, which is projected on these lead vectors and gives us the ECG amplitude. The inner triangle is formed by the lead vectors I', II' and III', and the direction of lead I is not horizontal but a bit upward whereas the leads II' and III' measure more vertically than in the Einthoven

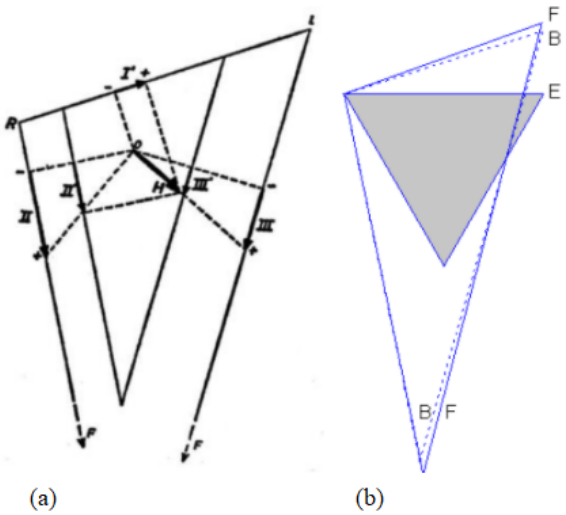

Figure 2.5: **(a)** The Burger triangle including the inner and outer triangles **(b)** Einthoven (E), Frank (F), and Burger (B) triangles

representation. The amplification in amplitude in leads II and III is represented by the outer triangle. Lead III is the most sensitive because it has the longest lead vector and for that, the relative distance between the inner and outer triangle is larger in lead III than lead II. Finally, the ECG amplitude is measured in leads I, II, and III of the outer triangle (Figure 2.5a). Figure 2.5b compares the Einthoven, Frank, and Burger triangles. It is possible to note that the Frank and Burger triangles vary according to the location of the assumed heart dipole whereas the Einthoven triangle lies in the frontal plane.

2.2.2 Lead system

Standard 12-lead ECG

The 12-lead ECG is a standard lead system used in clinical practice, able to generate a graphic representation of the electrical activity of the heart. The standard 12-lead ECG system is developed for displaying the frontal components of three-dimensional electric vector in six limb leads and the horizontal components in six precordial leads. The frontal components involve three bipolar standard lead (I, II, III) which measure the electrical differences between the combination of three limbs (see Section 2.2.1) and three augmented leads (aVR, aVL, aVF) are unipolar limbs where the positive pole is a single limb electrode, and the negative pole is the average of two electrode potentials. The precordial leads, or V leads, provide a three-dimensional view representing the orientation of the heart on a transverse plane and are attached over the areas of the left ventricle covering only half of the chest for the convenience of the patient (Figure 2.6).

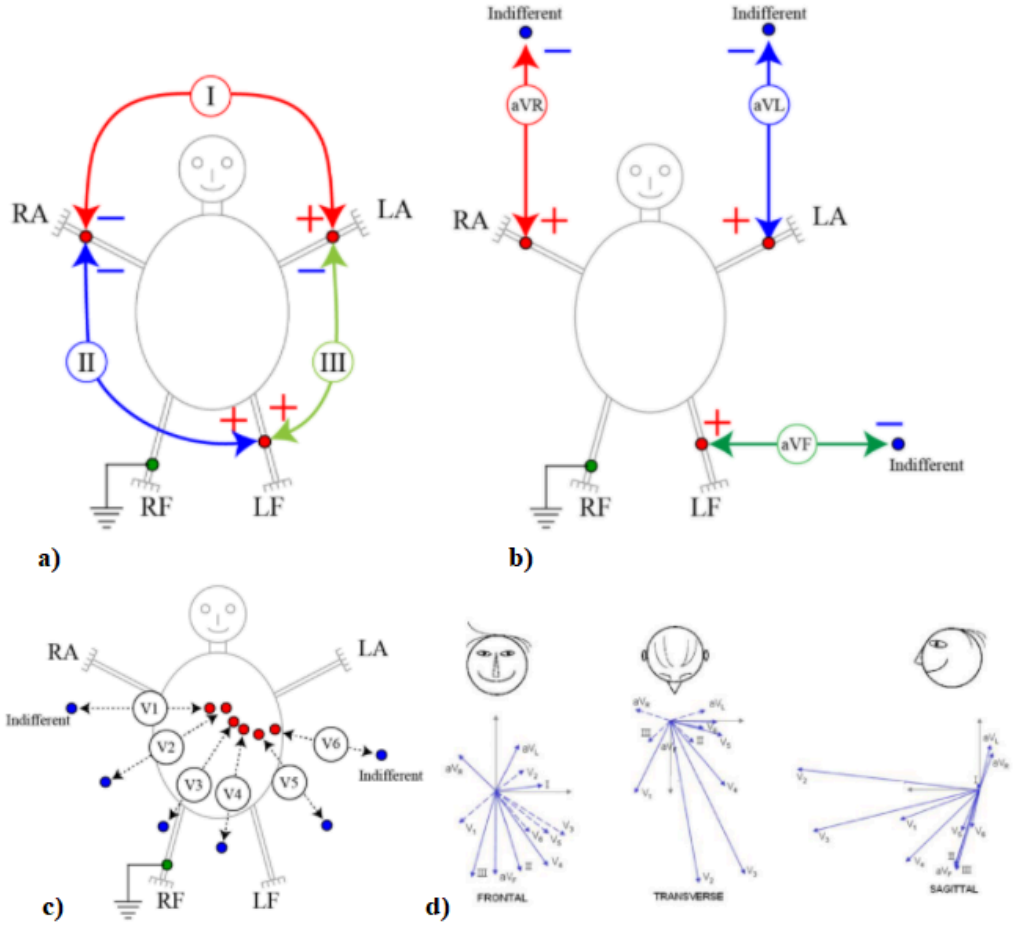

Figure 2.6: **(a)** The three standard Einthoven leads **(b)** The Augmented leads **(c)** The Precordial leads **(d)** The real lead vectors in all planes

In detail, chest leads:

V1-V2: septal view of the heart.

V3-V4: anterior view of the heart.

V5-V6:lateral view of the heart.

The other leads:

Lead I: lateral view (calculated by analysing activity between the RA and LA electrodes).

Lead II: inferior view (calculated by analysing activity between the RA and LL electrodes).

Lead III: inferior view (calculated by analysing activity between the LA and LL electrodes).

aVR:lateral view (calculated by analysing activity between LA+LL -> RA).

aVL: lateral view (calculated by analysing activity between RA+LL -> LA).

aVF: inferior view (calculated by analysing activity between RA+LA -> LL).

For the standard 12-lead ECG to be obtained, 10 electrodes are usually attached [**?**].

2.3 Acquisition of electrocardiogram

The electrocardiographic trace represents the most practical method to observe the electrical activity of the heart, in normal or pathological conditions. The general operation of the ECG is described through its block diagram (Figure 2.7), which depicts a diagram of a system where the principal parts or functions are represented by blocks connected by lines showing the relationships of the blocks.The electrical impulse in the heart acts as a voltage source, generating an electric current in the trunk and a corresponding electric potential on the skin and its distribution can be modeled as if the heart is an electric dipole that changes over time [**?**]. If two leads are connected between two points on the body (i.e. a vector is formed between them), the voltage observed between the two electrodes is given by the dot product of the two vectors [**?**]. Therefore, in order to obtain a complete vector image of the heart, multiple reference guide points and simultaneous measurements are required. The signal is collected by 10 electrodes connected to the left and right wrists and to the ankles of the patient, connected in this way to comply with the Einthoven triangle on which the ECG signal measurement is based, and are generally of the direct-contact type. The three bipolar leads (the three electrode application points) then record cardiac electrical activity from how it results from its projection onto the side of the triangle. Thus lead I (right wrist) is equal to the sum of lead II and lead III, lead II (left wrist) is equal to III+I, and lead III (ankles) is equal to I+II. Once the signal has been acquired, it enters an electric circuit that allows the extraction of the ECG trace. The blocks that constitutes the general scheme of an ECG are as follows:

Defibrillator Protection Circuit: the patient safety has the highest priority, therefore for the effect reduction of possible voltage surges and for the protection of the electronic circuitry from serious damage, ECG amplifiers must be protected with appropriate protection circuit. The end of the electrodes are connected to it. The protection circuit is equipped with buffer amplifier, to provide electrical impedance transformation from one circuit to another, in order to prevent the signal source from being affected by whatever currents (or voltages) that the load may be produced with, and voltage overload protection circuit.

Lead Selection Logic: this block helps to select the type of electrode lead system for the appropriate waveform or view. The conductor pair is selected via this selector switch, which can be switched to different conductor pairs depending on the type of waveshape needed.

Pre Amplifier: the amplitude level of the ECG signal is very weak. Therefore, it is necessary to enlarge the waveform for proper analysis and drawing purposes.

Instrumentation amplifiers and differential amplifiers with high gain and high CMRR (Common Mode Rejection Ratio) are used as preamplifiers. The CMRR is than set through the common-mode (CM) reduction amplifier.

Power Amplifier: the output unit is driven with it. After the signal amplification by pre-amplifier, it goes to the power amplifier. The output unit is attached with a pen motor. A high electrical power is required to initiate recording with pen recorder. Hence, a high power gain amplifiers are used as power amplifier.

The modulation blocks: it is located between the two amplifiers. Modulation is a transmission system in which the wave of the transmitted signal is associated with a carrier wave that has suitable characteristics for the transmission. There are two different systems to modulate in amplitude (AM), one non-coherent the other coherent; vice versa demodulation consists in reconverting in their original form the modulated signals, so it can be defined as the reverse process of modulation.

Two power supplies: the float power supply and the ground. The first one, connected to the modulator, is a power supply that has no reference or common point, where one of its outputs + or - can be connected to any part of another circuit or another power supply and not cause a short circuit. In the case of grounding, to which the demodulator is connected, the electrical circuit is connected directly to the ground, in the same way used to avoid damage due to short circuit, by discharging the excess voltage to the ground. The Defibrillator protection circuit, the CM reduction amplifier and the Power amplifier are also connected to the power supplies, as shown in the Figure 2.7

Output Display Unit: it can be either a Cathode Ray Oscilloscope (CRO), an instrument generally used in a laboratory to display, measure and analyze various waveforms, or a pen chart recorder acting as the output device.

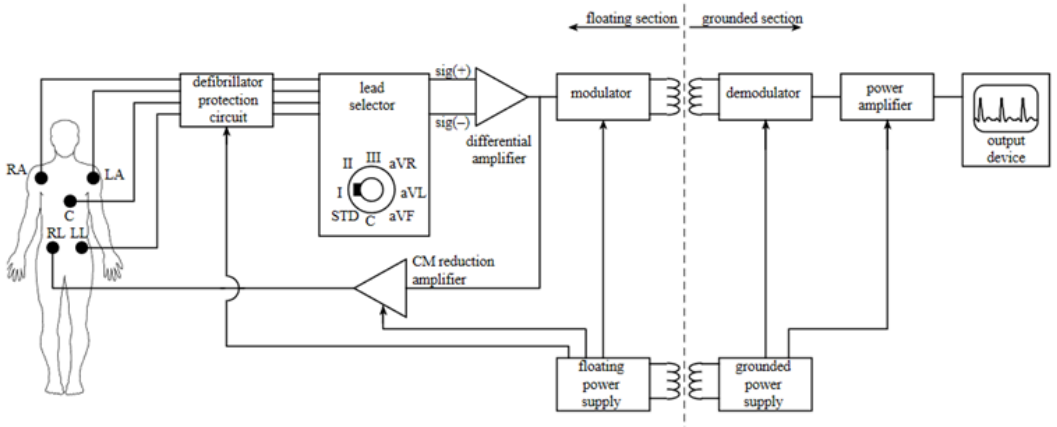

Figure 2.7: Block diagram of ECG system

2.4 Morphology of electrocardiogram

Every beat of the heart is a series of deviations from the baseline on the ECG. These deflections reflect changes in the electrical activity of the heart over time, which triggers muscle contraction. Traditionally, a sinus (normal) cycle of an electrocardiogram corresponds to a heartbeat, and each turning point is marked with the letters P, Q, R, S, and T (Figure 2.8) [?].

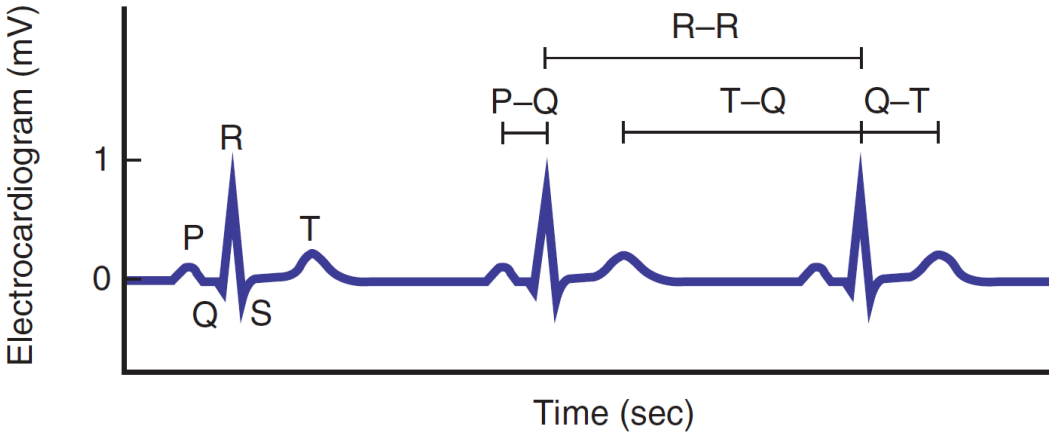

Figure 2.8: ECG morphology

The ECG may be divided into the following sections:

P-wave: is a slight low voltage deviation from the baseline caused by atrial depolarization prior to atrial contraction, as the activation wave front propagates from the SA node through the atria [?]. Although anatomically speaking, the atria are two different chambers, they almost act as one chamber electrically. Their muscles are relatively small and due to this reason produce a small P wave, that has an amplitude rarely exceeding 0.25 mV and a duration that should not exceed 0.12 s. Normal P waves may have slight notches, especially in the precordial (chest) leads. The bifid P wave is caused by a slight asynchrony between the depolarization of the left and right atria.

PQ interval: the time between the onset of atrial depolarization and the onset of ventricular depolarization. The PQ interval (sometimes called the PR interval because the Q wave is not always present) indicates the speed at which the action potential is transmitted from the atrium to the ventricle through the AVN. The measurement should start at the beginning of the P wave and end at the beginning of the QRS segment. The normal interval is between 0.12 and 0.20 s and a prolonged PQ indicates degeneration of the conduction system or increased vagus nerve tone (Bezold-Jarisch reflex), or it can be induced by pharmacology [?].

QRS complex: the largest-amplitude portion of the ECG, that represents the electrical forces generated by ventricular depolarization. Due to this reason, the QRS duration indicates how fast the ventricles depolarize and the normal length is less than 0.10 seconds.The atrial repolarization occurs before ventricular depolarization, but the QRS waveform has a large amplitude that makes the atrial repolarization not visible on the ECG [**?**].

QT interval: the time from the beginning of the QRS complex to the end of the T wave, which represents the total time spent on ventricular depolarization and repolarization [**?**]. At the end of the interval the ventricles are repolarized, becoming ready for a new cycle: the normal value for QT is below 450 ms for men and below 460 ms for women. Prolonged QT-interval may be related to delayed ventricular repolarization, which may lead to ventricular tachyarrhythmia leading to sudden cardiac death [**?**].

ST interval: the time between the end of S-wave and the beginning of T-wave [**?**]. It represents the period between the end of ventricular depolarization and the beginning of repolarization [**?**] by connecting the T-wave with the QRS complex. Since it is often difficult to accurately determine where the ST segment ends and the T wave begins, the relationship between the ST segment and the T wave should be checked together. The typical duration of the ST segment is usually about 0.08 seconds, with variations in the range of 0.005 to 0.150 sec.

T-wave:ventricular repolarization, whereby the cardiac muscle is prepared for the next cycle of the ECG [**?**]. The normal wave is asymmetrical, the first half having a more gradual slope than the second half: the interval from the beginning of the QRS complex to the apex of the T wave is referred to as the absolute refractory period; the last half of the wave is referred to as the relative refractory period or vulnerable period. T wave amplitude corresponds with the amplitude of the preceding R wave, and should generally be at least 1/8 but less than 2/3 of the amplitude of the corresponding R wave; T wave amplitude is at least 0.2 mV in leads V3 and V4 and at least 0.1 mV in leads V5 and V6 [**?**]. The duration, instead, is between 0.10 or 0.25 seconds or greater.

U-wave: a small deflection that follows the T-wave. It results from repolarization of the mid-myocardial cells, between the endocardium and the epicardium, and the His-Purkinje system [**?**]. It always follows the peak of the T wave and occurs before the next P Wave. It is not always seen on the ECG of normal patients, for this reason it is not represented in the typical ECG morphology 2.8. When present, a normal U wave is of low amplitude (less than one fourth the height of the T wave) and has the same polarity as its T wave. The duration of the U wave is normally not determined and is normally not significant, except in rare cases. The amplitude is usually less than 2mm and always smaller than that of the preceding T Wave.

2.5 Electrocardiographic alternans

Historically, the electrical alternans is defined as an electrophysiological phenomenon characterized by a beat to beat oscillation concerning the morphology of a one or more waves in the ECG. It is not considered a disease but an ECG sign of an underlying cardiac pathology providing crucial clues in this regard. The first report was a study presented by Theodor Herring in 1909 [42], who first recognized the phenomenon, further characterized by Thomas Lewins in 1910 [43] and firstly detected on the surface ECG in 1948 by Kalter and Schwartz [44]. In this study, they re-examined the world literature finding 41 reported cases, then they review ECGs from 6059 different patients finding 5 new cases. The most relevant discovery was the mortality associated with electrical alternans: 62% [44, 45]. Historically, this condition was considered a rare electrocardiographic abnormality associated with different diseases: acute ischemia [46], Prinzmetal's angina [47], electrolyte abnormalities [48, 49], and the long QT syndrome [50]. For most of the XIX century, the electrical alternans has been occasionally involved in conditions with an increased risk of ventricular arrhythmias but rarely encountered in clinical practice, difficult to identify, and with no specific clinical significance. The turning point cames in 1984 with the development of finite element computer simulation methods for the study of re-entrant arrhythmias [51]. The study demonstrates that the computer model electrical alternans precedes the occurring of re-entrant arrhythmias. But since the electrical alternans was considered a rare phenomenon, the underlying hypothesis was a microvolt level alternans as a marker of enhanced susceptibility to re-entrant ventricular arrhythmias [51, 45]. This hypothesis was reinforced by the fact that microvolt level alternans is too small to be detected by clinical in the ECGs but can be measured by using the computer analysis method. From a physiological point of view, the electrical excitation is a nonlinear physical process normally originated in the SAN, the driving force is the HR. Electrical alternans is defined as "*subharmonic bifurcation of this process, constituting an excitation at one-half of the driving frequency*" [52]. It may result from a mechanical "flip-flopping" of the heart on a beat-to-beat basis as a consequence of the mechanical movement of the heart within the pericardial sac, caused by electrophysiologic alteration, which can be related to cardiac electrical instability. Historically, the attention has focused on a specific wave of ECG, T-wave alternans (TWA), which is recognized worldwide as a powerful index to detect malignant ventricular arrhythmias and sudden cardiac death (SCD) [53, 54, 55, 56]. This might be a partial view of the AP if it is not integrated with the study of P-wave alternans (PWA) and QRS alternans (QRSA). In 2020, Marcantoni et al. propose a new approach based on the study of all the ECG waves: electrocardiographic alternans (ECGA) [**?**]. The study underlines the importance of finding a method to identify not only TWA but PWA and QRSA as well. P wave is associated with atrial depolarization, and PWA could be considered as an index of atrial electrical instabilities, including associated pathology. QRS

complex reflects both ventricles depolarization and atria repolarization, and QRSA is a clue in the case of supraventricular and ventricular tachycardias. Clearly, AP travels along all the heart sites, and alternans can affect all the ECG wave, but in this way, it is possible to obtain an electrically complete vision of heart health.

2.5.1 T-wave alternans

TWA is a beat-to-beat change in amplitude and morphology of the T-wave or ST-segment, appearing with regular rhythmicity and without relevant changes in the cycle length. TWA is considered a noninvasive index of malignant ventricular arrhythmias [57]. Ventricular repolarization induces the genesis of T wave, consequently, a spatiotemporal heterogeneity of repolarization generates the TWA, which is sensitive to perturbations in intracellular calcium handling and is responsible for the arrhythmogenesis by amplifying repolarization heterogeneity. The beat-to-beat alternation occurs at the level of cardiac myocytes by an alteration of AP [58]. It is possible to differentiate spatially concordant TWA when AP in a neighboring cell alternates in phase, or discordant TWA when AP alternates out of phase. In particular, discordant TWA is associated with a sharp increase in repolarization dispersion and a high percentage of developing ventricular tachyarrhythmias [59]. Even the transition from concordant to discordant alternans causes either marked changes in T-wave complexity and heterogeneity and TWA magnitude spikes. Additional studies attribute the growth of TWA to the derangements in calcium cycling and conduction during myocardial ischemia and heart failure [60, 61]. During this latter, the derangement is provoked by a reduction in calcium ions, resulting from impaired reuptake and release of calcium in the sarcoplasmic reticulum [61]. Studies conducted in cardiomyopathy patients demonstrate that oscillations in the AP plateau may cause TWA which is best explained by reduced calcium uptake into the sarcoplasmic reticulum, in a computational model [58, 62, 63]. An important factor that influences the TWA is the HR, presumably for intracellular calcium cycling and engaging the steepest portions of the electrical restitution curve. Initially, human studies of microvolt TWA (mTWA) were performed by using atrial pacing to measure TWA at increased HR with relatively low noise levels. In 1994, Rosenbaoum et al. have firstly found the strong relationship between microvolt TWA and ventricular arrhythmias during electrophysiology testing [64]. Over the following year, several studies and a great number of advances in signal processing and noise reduction allow the measure of microvolt TWA during exercise. In particular, it has been shown that TWA amplitude increases with increasing HR, and most of TWA analysis is performed at accelerated HRs, reached during exercise, with respect to resting conditions [53, 65, 66, 67, 68]. In 2002, Bloomfield et al. demonstrated that exists a specific HR threshold from which TWA starts to significantly increase its amplitude, named TWA-onset HR, about 90 beats per minute (bpm) [66]. From this value, TWA keeps being raise till HR reaches 120-125 bpm, and then declines to its initial value, even with higher HRs.

The presence of this phenomenon is confirmed in different studies [68, 69, 70, 71], suggesting that the peak of alternans that can be gained during exercise or at the end depends on the patient HR reaction to exercise. In 2016, Burattini et al have performed an observational study by investigating the dependency of TWA from HR during either HR-increasing exercise and HR-decreasing recovery phase to evaluate the potential predictive value of TWA during recovery in patients with an implanted cardiac defibrillator (ICD) [68]. During the recovery phase, it has been observed an increase TWA around 120-135 bpm, even it is much less marked with respect to TWA during exercise, meaning that recovery TWA may assist the identification of subjects with increased risk of arrhythmic events. In conclusion, microvolt TWA is recognized worldwide as a powerful test for the evaluation of patients at increased risk of SCD or potentially lethal cardiac arrhythmia.

2.5.2 QRS alternans

QRSA is an electrocardiographic phenomenon defined as alternating amplitude or axis of the QRS complexes in any or all leads [**?**]. Microvolt QRSA is a novel phenomenon in cardiomyopathy patients, considered a strong ECG-based risk-stratified for ventricular tachyarrhythmia. It can manifest itself with and without TWA and it is associated with QRS prolongation [**?**]. It is important to highlight that few clinical studies have evaluated macrovolt and microvolt QRSA, therefore the pathogenesis and its precise relation to ventricular arrhythmias is still not clear. Brembilla-Perrot et al. have demonstrated the presence of visible QRSA and TWA during rapid ventricular pacing and a retrograde His-Purkinje/AVN conduction alternans [**?**]. Low-magnitude, rate-dependent QRSA was observed by a limited number of studies in a patient with rapid supraventricular tachycardia and normal ventricular function [**?**, **?**]. The first microvolt evaluation of QRSA and TWA has been performed by Rosenbaum et al. By applying the spectral method in a mixed patient population with normal and depressed LV ejection fraction: QRSA results lower in prevalence and magnitude with respect to TWA [64]. The most recent study, proposed by Suszko et al. in 2020, has investigated the presence of microvolt QRSA and TWA in 100 cardiomyopathy patients with prophylactic defibrillators [**?**]. Their results show that since microvolt QRSA is both not rate dependent between 100 and 120 bpm and is associated with QRS prolongation, a potential mechanism of QRSA generation is His-Purkinje and/or myocardial conduction alternans. In the same year, a case report of a 34-year-old man without structural heart disease displays the presence of QRSA accompanied by RR alternans which may be considered a clue to the diagnosis of atrioventricular reciprocating tachycardia [**?**]. In general, a complete and well-understood definition of the phenomenon is not present, it is clear the need for a detailed understanding of how it is generated and the cardiovascular disease associated with it. The studies presented in these years demonstrate the diagnostic potential of QRSA.

2.5.3 P-wave alternans

P-wave electrical alternans is a beat to beat alternation in the morphology of the P-wave. No literature studies are present but case report [**?**, **?**, **?**]. PWA is considered a rare phenomenon and a predictor of atrial fibrillation. In particular, the case reported by Siniorakis et al is the first work that correlates PWA with imminent atrial flutter [**?**]. The PWA pathogenesis is unknown and several studies are needed for a better understanding of the mechanism underlying within.

Chapter 3

Athlete and athlete's heart

3.1 Definition of the athlete

The complete and well-describe definition of the athletes is a fundamental building block in aiding clinicians and biomedical engineers to understand the degree of cardiac changes in response to a variety of exercise training. On the other hand, the standardization is considered a crucial challenge of the modern-day caused by the population heterogeneity, loosely or overly restrictive definition and difficult understanding of the association between exercise and health medical parameters [72]. In the literature the description varies from amateur exercise to professional sports men and women, but in most cases the definitions are unable to detect the type, duration and intensity of activity. These aspects are not negligible since the ability of the athletes evolves with the time and depends on the amount of training, type of competition and type of exercise underlying the relation of the load variance on the cardiovascular system. The critical analysis begins with the study of etymology: the word 'athlete" derives from the Greek word "athletes" related with '*prize-fighter, contestant in the games*' and from Latin "athlete" which means a '*wrestler, combatant in public games*', often viewed with superior physical ability [73]. In order to facilitate the standardization, several organizations have suggested a definition of athletes discussing medical issue combine to athletes/. The American Heart Association (AHA) define a competitive athlete as "*One who participates in an organized team or individual sport that requires regular competition against others as a central component, places a high premium on excellence and achievement, and requires some form of systematic (and usually intense) training*" [**?**]. The European Society of Cardiology (ESC) has drawn attention on sports participation, in particular a competitive athletes is: "*individuals of young and adult age, either amateur or professional, who are engaged in exercise training on a regular basis and participate in official sports competition. Official sports competition (local, regional, national, or international) is defined as an organized team or individual sports event that, placing a high premium on athletic excellence and achievement, is organized and scheduled in the agenda of a recognized Athletic Association*" [**?**].

3.2 Athlete's heart

The athlete's heart is a nonpathological enlargement of the heart combined with electrical changes, resulting in individual who participate in intense exercise with high aerobic component, consequently it is not a medical condition. The heart is a biological system able to adapt to physical and metabolic load allowing heart to increase its ability to supply blood and oxygen to exercising tissues. The principle mechanism for the heart to increase its output is to increase the amount of blood ejected per beat (also known as the stroke volume). This is achieved by increasing chamber size and compliance. A prolonged training causes hemodynamic effects on the cardiac chambers: the increase of pressure and volume results in an increase of the ventricle's wall stress, similarly, occurs in the atria. In particular, the myocardium is primarily involved in the adaptations to exercise affected by both isotonic and isometric stress. Isotonic stress occurs when a large amount of blood moved into the cardiovascular system and refers to endurance sporting disciplines (long-distance running). In contrast, the generation of high intravascular pressure causes isometric stress, characteristic of short but intense sporting disciplines. As regard the left heart, published data suggest that 30% of healthy athletes are likely to develop a LV chamber dimension that exceed the limits of normal [72]. Eccentric LV remodelling, characterized by balanced chamber dilatation and wall thickening, occurs in athletes participating in sport with significant isotonic physiology; while concentric LV remodelling, where wall thickening manifests itself in the absence of chamber dilatation, develops in individuals performing a predominant isometric physiological sport. The diastolic function is enhanced in isotonic sport and it is normal or slightly reduced in isometric training, while the systolic function is not affected by both form of exercise training. The right heart, instead, can run into a right ventricular dilation following an isotonic physiology, whereas it is irresponsive to isometric stress. In general, RV hypertrophy is an uncommon adaptation in athlete's population and may be considered a pathology condition rather than remodelling physiology [74]. Studies have demonstrated that ventricular volume increases with exercise till arriving an approximating anaerobic threshold from which ventricular volume begins slowly to reduce and most likely during a moderate-to-high intensity, the structural and functional adaptation takes place [72]. Difficulties to estimate the degree of expected remodelling arise when the concept of volume and pressure load needs to be incorporated with the effect of strength and power training, demonstrated to be more significant on cardiovascular adaptation. In the recent work "A Modern Definition of the Athlete's Heart—for Research and the Clinic", the authors suggest the simplest definition of the athlete's heart based on two variables, exercise intensity and duration, which result to be closely associated with cardiovascular adaptation with respect to previous studies. In the athlete population, the overlap between physiology and pathology is a crucial issue owing to the difficulty of discriminate healthy physiological adaptation of the myocardium from the pathological remodelling caused

by congenital disease, cardiomyopathies and hypertensive heart disease. The most common adaptation is the left ventricular hypertrophy (LVH) of training which is in contrast with the pathologic hypertrophy of a hypertrophic cardiomyopathy (HCM) with an occurrence of approximately 2% in athletes, reversible with detraining. In the sports literature, different studies have proposed important tool to differentiate the two clinical entities by focusing on the grey zone of hypertrophy, defined by means of septal wall thickness (between 12 mm to 16 mm). In 1991, Pelliccia et al. have observed that in elite athletes with a wall thickness of more than 16 mm in combination with nondilated LVH are associated with pathologic hypertrophy [75]. Although, this finding may be incomplete or not reliable for all the different categories of athletes. Several researches have proposed left ventricle (LV) cavity dimension, LV diastolic function and left atrial dimension as a good discriminator between athlete's heart and pathological HCM [76]. A most recent study presented by Lynne Martina Millar et al. identifies as a modest discriminating value the combination of different techniques including ECG, Holter monitoring, baseline echocardiographic. But even in this case, the limitations arise from the categories application since the study is conducted on male and may be not reliable for female athletes or black athletic population [77]. Anyway, distinguishing physiological from pathological condition for athletes continues to be challenging despite the access to multi parametric approach and the combination of different innovative technologies. A misdiagnosis can have devastating consequences on the athlete's career with the interruption of training and elimination from competition. Conversely, an incorrect diagnosis of an athlete's heart without the support of genetic test can considerably increase the risk of cardiac attack and sport related sudden cardiac death (SrSCD) which may affect the sports word [78].

3.3 Electrocardiographic changes in athlete

Electrocardiographic changes in competitive athletes have an occurrence of about 80% further to physiological adaptation to exercise training, but the pathological cardiomyopathy hidden in these changes are present in 10-14% [11]. The gold standard for the evaluation at all levels of competition is the standard 12 lead electrocardiogram which gain information that can be integrated with continuous ECG monitoring, measurement of heart rate variability and signal averaged ECGs. The ECG interpretation has been widely studied by publishing guidelines and consensus documents for the differentiation of normal adaptation from cardiac disease. Figure 3.1 shows the significant evolution of athlete's ECG interpretation over the last years ending up with the most recent publication of the international recommendations for ECG interpretation (Figure 3.2). Endurance physical exercises strongly affect the cardiac autonomic nervous system (ANS) by a continuous modulation sympathetic nervous system (SNS) and parasympathetic nervous system (PNS). The ANS is primary involved in the regulation of HR becoming an important determinant in

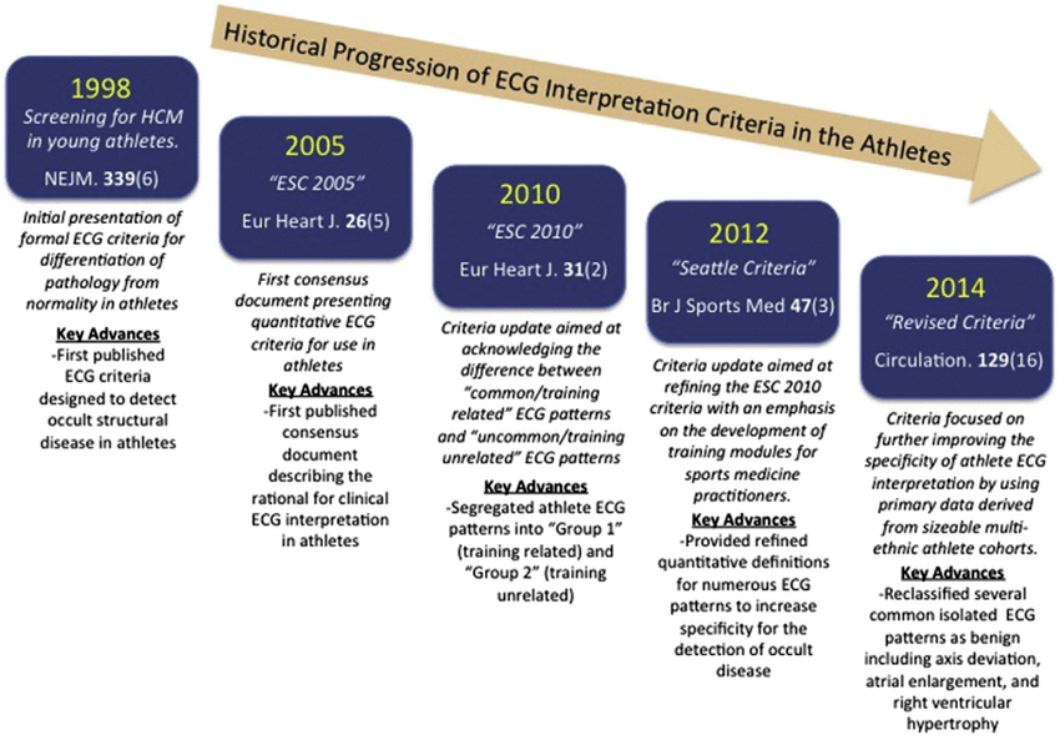

Figure 3.1: Evolution of the interpretation of the athlete's ECG [10]

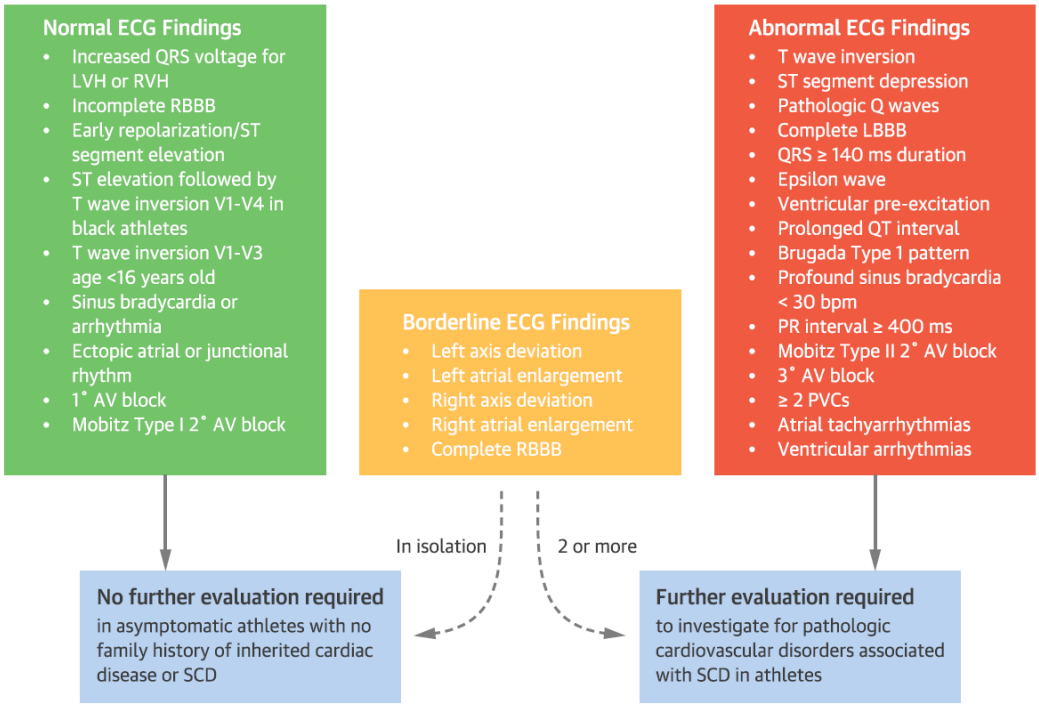

Figure 3.2: International recommendations for ECG interpretation in athletes [11]

training adaptation. Athletes are characterized by an overall increase in HR variability and parasympathetic cardiac modulation. During exercise, HR variability is reduced,

and R-R intervals are shorter as a result of increased HR: augmented sympathetic and attenuated parasympathetic activity is observed and their relationship strongly depends on training intensity. The parasympathetic component of HR variability decreases during long-term high-intensity training sessions, while increases during the recovery phase. The sympathetic component demonstrates the opposite tendency. The inability to return HRV parameters in optimal levels can lead to a reasonable condition and a chronic disturbance in ANS activity, which may cause an overtraining and heart adaptation. In detail:

Sinus bradycardia:The physiological adaptation is intrinsic structural and ion's channel remodelling of sinus node. In some cases, the form of bradycardia is extreme with a resting sinus rhythm of less than 30 beats per minute [**?**]

Sinus arrhythmia:It has an occurrence of 15-20% in athletes and is defined as sinus pauses that last longer than 2 seconds, whether at night or during the day [**?**]

First degree AV block:it is observed in 10-33% of athletes and usually for a few seconds. Figure 3.3 displays the ECG of a male marathon runner recorded during patient sleeping where the AV block is present in the three last beats.

Incomplete right bundle branch block:occurs mainly in endurance training, resulting from an increase right ventricular dimension and prolonged conduction. The occurrence is 30-40% of athletes.

Ectopic atrial rhythm:P waves are negative in the inferior leads with different morphologies compared with the sinus P wave.

Junctional escape rhythm:It is present in athletes with marked bradycardia, reflecting a faster QRS rate than the resting P wave rate. P waves can be inverted or be present after QRS complex, as well as no visible. Figure 3.4 illustrates the ECGs of two different type of junctional escape rhythm.

Early repolarization:The origin of the mechanism is still uncertain, presumably it arises from a parasympathetic modulation of ventricular repolarization and it may be a direct effect of the vagus nerve in the ventricle or the enhanced vagal effects on sympathetic nervous activity. This latter alteration may account for the increased T wave amplitude in athletes. Literature research have demonstrated a highly association between early repolarization pattern and increased risk of sudden cardiac death, but a distinction of exercise-induced early repolarization from the variation linked to the sudden death is crucial for the clinical evaluation. The most significant differentiation proves that the increased risk of death is confined in subjects between 40 to 50 years old, the early repolarization in the athletes occurs instead in the peak of fitness [74]. Anyway, the current pattern is present in over half of competitive athletes, arriving at 80-90% in black individuals.

Repolarization pattern in black athletes: Includes J-point elevation, convex ST-segment elevation, and T-wave inversions in leads V1 to V4 occurring in 5-15% of black athletes [**?**].

Juvenile pattern: T wave inversion extending to V3 or an isolated biphasic T-wave in V3 and are a normal finding in the adolescent athlete (age <16) with a prevalence of 4 to 9.5% [**?**]

Isolated QRS voltage criteria for left ventricular hypertrophy: It includes atrial enlargement, left axis deviation, a 'strain' pattern of repolarisation, ST-segment depression, T-wave inversion or pathological Q waves [**?**].

Figure 3.3: ECG of male athletes with AV block [**?**]

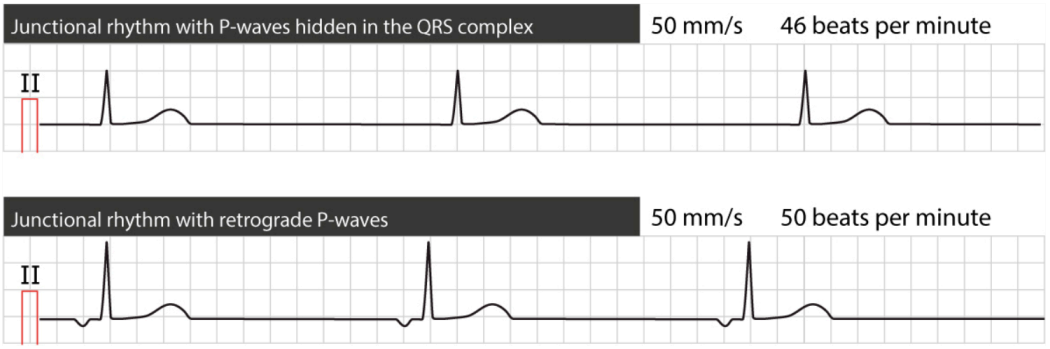

Figure 3.4: ECGs of subject affected by junctional rhythm [**?**]

The ECG criteria for the interpretation of physiological adaptation is an important reference for clinicians and the significant evolution has improved the detection of cardiovascular disease and reduced false positive with a particular regard for family history, personal experience and the context of symptoms. Despite the improvements, the growing of mixed population remains a great limitation since same class of society are not adequately represented as well as black ethnicity.

3.4 Electrocardiographic alternans in athlete

The dependence of TWA on HR increase and variability makes it a remarkable instrument for the athlete's population, able to achieve significantly high HR during exercise training or stress test. In the literature research, few studies have been performed for the evaluation of TWA diagnostic potential in athletes. The interest in this fields emergens from studies proving that young competitive athletes with silent arrhythmogenic heart disease have a high risk of srSCD respect to sedentary

subjects with the same age [79, 80, 81]. In 2004, the first study is proposed by Furlanello et al in order to assess the predictive value of the microvolt TWA in 100 competitive and noncompetitive athletes [82]. Their findings suggest that mTWA may be considered a useful and noninvasive tool for assessing arrhythmic risk in the athlete's population considering its high negative predictive value using both electrophysiology test (EPT) and the follow-up observation for severe arrhythmic cardiac events as endpoint. The limited number of positive TWA does not allow to obtain a significant positive predictive value but, in any case, the subjects under examination are considered at high risk of srSCD [82]. In 2007, Inama et al. have performed a cardiological evaluation on 43 athletes with no history of cardiovascular disease, by comparing TWA and EPT [83]. Their study has reported a significant correlation between negative TWA and non-inducibility of ventricular arrhythmias, but no significant association between positive or indeterminate TWA (test that does not meet the criteria for being classified as positive or negative) and the result from EPT. The high value of negative predict value in forecasting the result of EPT is consistent with the Furlanello et al. findings [82]. The predictive accuracy of TWA is at least comparable to the invasive programmed ventricular stimulation and TWA seems to be useful to improve risk stratification for ventricular arrhythmia and srSCD [83]. Similar results have been obtained the following year by the same team Inama et al. [84]. In 2017, Simova et al have presented an evaluation of TWA prevalence in athletes compared with a group of non-athlete subjects with high expected TWA prevalence during the cardiopulmonary stress test (CPT) [85]. The first analysis has shown an unexpected result: the presence of TWA in athletes is far higher with respect to non-athletes with diagnosed heart disease and high cardiovascular risk. This finding can be explained by the different conditions during CPT: athletes test lasts almost twice that of non-athletes, which is interrupted by fatigue before reaching the maximum HR. Actually, the athlete's HR is significantly higher compared to non-athletes when performing sport, and TWA is an HR-dependent phenomenon, therefore the results found may have underlying clinical significance. A second analysis was performed by considering a lower HR range level attainable by either athlete and non-athlete group: the results have drastically changed demonstrating that higher TWA prevalence is found in the non-athletes group. The main finding of this study shows that the prognostic relevance of TWA in the analyzed classes is different depending on the HR range, but its diagnostic value is still confirmed [85]. Nevertheless, a complete vision of electrical activity (or inactivity) during the entire cardiac cycle may be helpful for a distinct overview of clinical cardiac situation, by the inclusion of the two parameters: QRSA and PWA. In sport literature, there is a lack of studies for the identification of cardiac risk through ECGA analysis. The present thesis aims to propose ECGA as new approach for the evaluation of athlete's risk.

Chapter 4

Background on methods

4.1 R-peak extraction

R peak detection in ECG is a widely used method to detect heart rhythm irregularities and estimate HRV [86]. The reference waveform is the QRS complex for its largest amplitude and its steep slope (high-frequency spectrum in the range 10-50 Hz) and its examination is the starting problem. The performance of an algorithm based on heart rate variability, by means of variation in RR intervals, depends on the accuracy of QRS detection. In addition, the P and T wave's locations can be identified by their relative position to the QRS complex. The study is indeed performed based on the extracted features from the morphology of the fiducial points. The correct detection of these features is crucial for doctors to make a correct clinical diagnosis [87]. Difficulties arise from highly noisy ECG which hides fundamental parameters for the assessment of cardiac risk and uncorrected automatic R-peak detection can lead to false identification and evaluation of fiducial point [88]. In 1987, J. Pan and J. W. Tompkins have presented a real-time QRS detection algorithm, the so-called 'Pan-Tompkins algorithm', capable to adapt each threshold and RR interval autonomically [89]. It has been the first adaptive approach able to provide accurate signal characteristics, QRS morphologies and heart rate changes. It is considered the gold standard for R-peak extraction, with later studies demonstrating same limitation in terms of accuracy and performance in noise and long ECG signals [90]. Several examination methods have been proposed to detect R-peak. In particular, the application of the Empirical Model Decomposition (EMD) and the Ensemble Empirical Model Decomposition (EEMD) on the extraction algorithm has been widely used in the past decades. The EMD is a data-driven process developed in 1998 by Huang et. al. The underlying mechanism is the decomposition of data into intrinsic mode functions (IMFs) which provide the basis of expansion. Recent research studies have figured out a serious mode mixing phenomenon, overcame through the adoption of noise-assisted data analysis method, the EEMD: the effect of mode mixing is weakened by adding white noise to signal analysis [91].In this chapter,the discussion will be focused on R-peak detection algorithm based on EMD and EEMD. These algorithms can be functionally divided in three different classes. The class 1 is dispalyed in Table 4.1. The underlying mechanism of the algorithm

is divided in three mean steps: pre-processing, feature extraction and classification. The EEMD is used for the finding of fiducial points, and it is the starting point, then the identification of R-peak is performed based on morphology or classifier tool [92].

Table 4.1: Class 1 of R-peak detection algorithm: pre-processing, feature extraction and classification

Reference	**Method**	**ECG database**	**Results**
Zhao *et al.*	The preprocessing is followed by ECG decomposition into IMFs by EEMD and the power spectrum of each IMF component is estimated by Welch method. The features set size is reduced by using PCA. The K-nearest neighbors method is applied as the classifier.	1) the MIT/BIH ST change database 2) Long-term ST database 3) The PTB database by the National Metrology Institute of Germany	Performance: 1) IMF = 95.3% 2) Power spectrum of IMF = 80.9% 3) MIMFs + Power spectrum= 98.1%

Table 4.2 shows class 2. The EMD or EEMD is employed to the filtering of ECG and reduction of noise to enhance the R-peak detection [93, **?**, **?**]. The third class is expalined in Table 4.3. The algorithm is composed by two steps: decomposition of signal and reconstruction from particular IMFs to improve the visualization of QRS complex [**?**, **?**, 94]. In the end, these literature studies have demonstrated the pressing need to find a precise and efficient method for the correct detection of R-peak location, usually compared to the gold standard Pan-Tomkins algorithm. The newest approach based on EEMD seems to be the more efficient in terms of accuracy and robustness.

Table 4.2: Class 2 of R-peak detection algorithm: EEMD is employed to the filtering of ECG and reduction of noise to enhance the R-peak detection

Reference	**Method**	**ECG database**	**Results**
K.M. Chang	The filtering performance of Butterworth filter, Wiener filter, EMD and EEMD was compared based on filtered ECG peak detection and phase delay between filtered ECG and clean ECG	1) Clean synthetic ECG signal 2) Real arrhythmia ECG database 3) Synthetic noises 4) Real noise stress database	Analysis based on mean square error: EEMD has the best performing in ECG noise reduction procedure
Lin *et al.*	Decomposition (EMD)-based ECG signal denoising algorithm is proposed in a smart clothing for ECG acquisition and HR monitoring	1) MIT-BIH Arrhythmia Database 2) ECG from university students during the walking exercise.	1) Accuracy=99.8% Sensitivity= 94.87% 2) Accuracy=96.46% Sensitivity=98.75%
Chang *et al.*	Assessment of noise-filtering performance between EEMD and FIR Wiener filters based on the IMF containing more QRS components and less Gaussian noise	1) standard ECG template derived from ECG simulator 2) MIT/BIH arrhythmia database	Analysis based on mean square error: EEMD has the best noise-filtering performance

Table 4.3: Class 3 of R-peak detection algorithm: decomposition of signal and reconstruction of particular IMFs to improve the visualization of QRS complex Abbrevation: MSE = mean square error; MAE= mean absolute value; var.= variance; s.=sample

Reference	**Method**	**ECG database**	**Results**
Pal *et al.*	EMD based ECG signal enhancement, partial reconstruction by a set of IMF for a visualization improvement of QRS	1) Physionet PTB diagnostic database 2) MIT/BIH arrhythmia database	1) Sensitivity=98.8% Specifity=99.2% 2) Sensitivity=99.8% Specificity=99.9%
Zhu *et al.*	EMD decomposition method, reconstruction of 3 IMFs and application of adaptive threshold to the detect QRS complex	MIT/BIH Arrhythmia Database	Detection rate=99.6%
Safari *et al.*	EEMD decomposition, application of ICA algorithm on IMFs and R-peak detection by the implementation of Pan-Tompkins	QT database	1) MSE= 3.025 s. 2) MAE=1.22 s. 3) MSE var.=0.61s.

4.2 Electrocardiographic alternans detection

In literature, several studies have investigated alternans focusing on a specific ECG wave, TWA, considered a powerful index to predict ventricular arrythmias and SCD. In particular, the development of method for automatic detection of non-visible TWA is still challenging [95]. The current prevalent algorithms are mainly designed in two domains: time and frequency. The advantage of the spectral analytical technique is the evaluation of the power spectrum for each sample point allowing the recognition of the alternans along the T wave. On the other hand, the main disadvantage comes out from the initial hypothesis: the alternans signal is considered a stationary wave with constant amplitude and phase. In general, it is not true, and it may lead to a lack in the detection of nonstationary features [96]. The first quantitative study is the Energy Spectral Method published by Adam et al. in 1981, identifying the correlation between TWA and myocardial instability [**?**]. The underlying idea was that alternans is usually observed as a 0.5 cycles-per-beat (cpb) fluctuation in the beat-to-beat measured T wave energy. TWA magnitude was measured as the periodogram evaluated at 0.5 cpb of the normalized T wave energy series minus an estimate of the spectral background noise. After that, Table 4.4 displays the

most common methods developed in frequency domain: fast fourier transform (FFT) method [97], complex demodulation (CD) method [97], and Karhunen-Loève (KL) transformation method [98].

Table 4.4: TWA detection method: Frequency Domain

Reference	**Method**	**ECG database**	**Results**
Rosenbaum *et al.*	FFT spectral method: the registration of the Alternans along the T-wave is enabled by analysis of the power spectrum for each sample point	1) High Risk Group 2) Low Risk Group	Sensitivity=70% Specificity=80%
Rosenbaum *et al.*	CD method: Describe the slowly variation of T-wave amplitude as a sinusoid with slowly varying amplitude and phase	1) High Risk Group 2) Low Risk Group	Sensitivity=90% Specificity=5%
Laguna *et al.*	KL transformation: Fourier transform of KL series with beat order as a temporal reference. The ratio of the power in the band around 0.5 cycle/beat for the total power is used as an indicator for alternans presence.	Simulated alternating ECG with added moving artifacts, EMD and baseline wander noise	Sensitivity > 95% Specificity > 95%

In the time-domain, the proposed methods involve approach as Modified Moving Average Method (MMAM) [99], the Correlation Method (CM) [100] and the most recent Heart Rate Adaptive Match Filter (HRAMF) (Table 4.5). The detection of TWA occurs in short-time and in non-stationary signal by the using of Holter data. Besides above reported methods, several nonlinear and statistical methods of TWA detection are proposed: Laplacian Likelihood Ratio (LLR) method [101], Statistical Tests (ST) Method [102], Poincaré Mapping (PM) method [103] and Continuus Wavelet Transform (CWT) method [**?**] which is a time–frequency analysis (Table 4.6).

Table 4.5: TWA detection method: Time Domain
Abbreviation: CAD=coronary artery disease; TWAD=TWA duration; TWAA= TWA amplitude; TWAM=TWA magnitude; pv=p value

Reference	**Method**	**ECG database**	**Results**
Nearing *et al.*	MMA method: The alternans estimate for any ECG segment is determined as the maximum difference between A and B modified moving average computed beats within the ST segment and T-wave region.	Experimental laboratory ECGs with dynamically changing alternans	Sensitivity=100% Specificity=100%
Burattini *et al.*	CM: TWA detection by computing, for each consecutive T wave, an alternans correlation index based on a cross- correlation technique.	39 ECGs from digital Holter of long QT syndrome	Identification of 44% patients with nonstationary TWA
Burattini *et al.*	Method based on HRAMF: filtering in a narrow frequency band (to consider the physiological variability of the heart rhythm) around the alternans frequency, defined by half of the heart rate.	Holter ECG recordings: 1) 176 healthy subject 2) 200 CAD patients	TWAD: pv<0.001 TWAA: pv<0.05 TWAM: pv<0.001

Historically, the study of electric alternans was primarily focused on the analysis of macroscopic and microscopic TWA which is associated with severe life-threatening arrhythmias. Therefore, the methods proposed in the past year are developed for TWA only. In literature, there is a lack of detection mechanism for PWA and QRSA. Only two study have been performed for the detection of QRSA and TWA by using spectral method. In 1994, Rosenbaum et al firstly evaluate microvolt QRSA and TWA by using spectral method in a mixed patient population with normal and depressed LV function with syncope or ventricular tachyarrhythmia [64]. In 2020, Suszuko et

Table 4.6: Nonlinear and statistical TWA detection methods

Reference	**Method**	**ECG database**	**Results**
Martinez *et al.*	LLR method: It is derived from a GLRT TWA detector and amplitude estimator for Laplacian noise. The resulting estimator is a "median filtered complex demodulation"	MIT/BIH Noise Stress Test database	Sensitivity=95% Specificity=95%
Srikanth *et al.*	ST method: three statistical tests including Student's tests for independent and paired samples to test the differences between T wave features in odd and even beats, and Rayleigh's test for periodicity	European ST database	Detection accurancy=100%
Strumillo *et al.*	PM method: is obtained by representing pairs of consecutive beat-to-beat differences in the phase space. Alternans is identified when two clusters of points are present in the Poincaré maps	Digital ECG recordings with increased HB by medication	Correlation coefficient of $= 0.91$ between TWA levels calculated by comparing the method with FS method
Addison *et al.*	CWT method: time–frequency signal analysis methods for simultaneous interpretation of the signal in both time and frequency	Porcine experimental model of ventricular fibrillation	It allows a signal to be decomposed such that frequency characteristics and the location of features in a time series may be highlighted simultaneously

al. have quantified microvolt QRSA and TWA by using the spectral method [**?**]. In this study, 100 cardiomyopathy patients with prophylactic defibrillators are tested. The first approach including the identification of ECGA is proposed by Marcantoni et al. [**?**]. In particular, they have adapted the use of HRAMF in detecting and analyzing the ECGA and they have validated its effectiveness and its relevance in the diagnostic field. The detection of different types of alternans and the identification of the prevalent alternating wave pave the way for a complete overview of cardiac electrical activity and for possible correlates pathologies.

Chapter 5

Methods analysis of the real population

5.1 Database description

This work aims to evaluate ECGA in subjects performing sport. Therefore, the dataset "Wrist PPG during exercise", from the Physionet website, https://physionet.org/works/WristPPGduringexercise/, has been selected [**?**]. The database is designed for the creation of signals heavily corrupted by motion artifacts as a result of exercise conditions. The presence of artifacts underlines the need to assess a signal processing algorithm for removing the motion interference and extracting heart rate and heart rate variability, allowing the extraction of true heart related information from ECG signals. The recording of chest ECGs are performed to providing a reference/comparison heart rate to be found, during four different activities:

1) Walk on a treadmill.

2) Run on a treadmill.

3) Easy bike ride set to a low resistance (giving high cycling speeds).

4) Hard bike ride set to a high resistance (giving low cycling speeds).

The data is stored in Physionet WaveForm DataBase (WFDB) format [**?**] and each record is composed of two files: .hea extension and a .dat extension. The .hea file holds header information, including the signal name, units, sampling frequency (256 Hz), number of samples, and parameters required to load the data values stored in the .dat file, automatically handled by the Physionet toolkit software. The ECG measurement has been conducted by using an ECG unit placed on the chest. Specifically, the Activewave (CamNtech, Cambridge, UK) recorder [**?**] and pre-gelled self-adhesive Silver-Silver Chloride (Ag/AgCl) electrodes are used, and

a single-channel ECG recording is obtained. The two electrodes are placed on the upper chest with one electrode on either side of the heart, as shown in Figure 5.1. The 4mm snap connector electrodes were connected to the 1mm non-touch-proof connector on the Activewave using 15 mm converter cables provided by CamNtech, whose motions introduce artifacts in the ECG recording [**?**]. In this ECG trace, R peaks are identified by hand and are included in the database as a gold standard reference. After the electrodes' application, participants could choose to perform one or more different types of exercises, which included walking on a treadmill at a

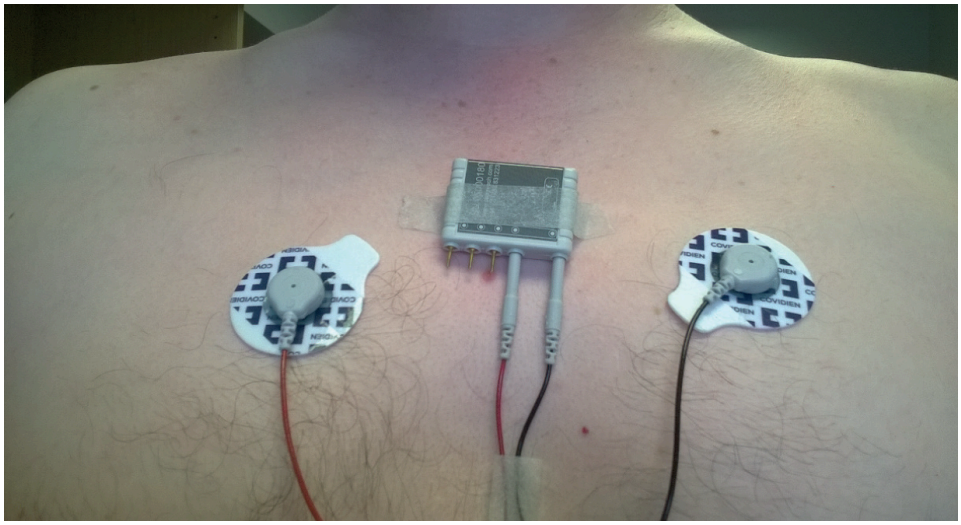

Figure 5.1: Actiwave unit used for recording the single-channel, two-electrode, ECG [**?**]

normal pace with a maximum length of 10 min; light jog/run on a treadmill, with a maximum length of 10 min; pedal on an exercise bike set at a low resistance with a maximum length of 10 min; pedal on an exercise bike set at a higher resistance with a maximum length of 10 min. It is important to stress the goal of the exercise's application: introduction of a wide variety of motion artifacts into the collected heart signals. To this end, the pace of the treadmill and pedal rate on the bike setting is not fixed but it is set by the participants themself, to make them feel comfortable. The number of participants is eight, three male and five female, aged 22-32 (mean age 26.5 years old). The duration of each record is different for each activity and subject, from 4 to 10 min, as shown in Table 5.1.

Table 5.1: Duration of each data record. The symbol "–" indicates the absence of this activity for this participant. LR=low-resistance; HR=high-resistance.

Subject ID	**Walk** (min:sec)	**Run** (min:sec)	**LR Bike** (min:sec)	**HR Bike** (min:sec)
1	9:48	-	9:39	9:48
2	6:39	-	5:41	6:54
3	4:47	5:07	4:54	4:41
4	-	4:52	-	-
5	-	5:08	4:40	-
6	5:36	5:02	4:40	-
8	6:42	4:47	-	-
9	3:40	-	-	-

Each participant started from a rest condition; thus, the heart rate began at a low resting value rising during the activity. For subjects performing more than one type of exercise, the record is still single with a break of at least 10 min present between each activity, and then the recording is segmented offline into the portions corresponding to different activities [**?**]. The number of available records is nineteen, allowing a standard leave-one-out cross validation approach. All possible combinations can be used proving to get very good generalisability [**?**].

5.1.1 ECG signals classification

The ECG signals under examination are highly corrupted by noise and for some of them the visual recognition of the main waves is extremely difficult. For this purpose, the 19 signals are firstly classified into three groups by visual inspection and afterward confirmed by the signal to noise ratio (SNR) calculation. They are defined as: recognizable signals, moderate signals and hard signals.

The **recognizable signals** allow a easier interpretation of the main ECG landmarks, they represent the 42% of the total signals, and the signal morphology is shown in Fig 5.2.

The **moderate signals** can be considered as a trade-off between the best and worst cases. The noise increases, but the visual recognition is still possible. They include the 42% of the total signals, Fig 5.3.

The last classification identifies signals difficult to analyze and process caused by the massive presence of noise, the **hard signals**. They are the 16% of total signals, Fig 5.4.

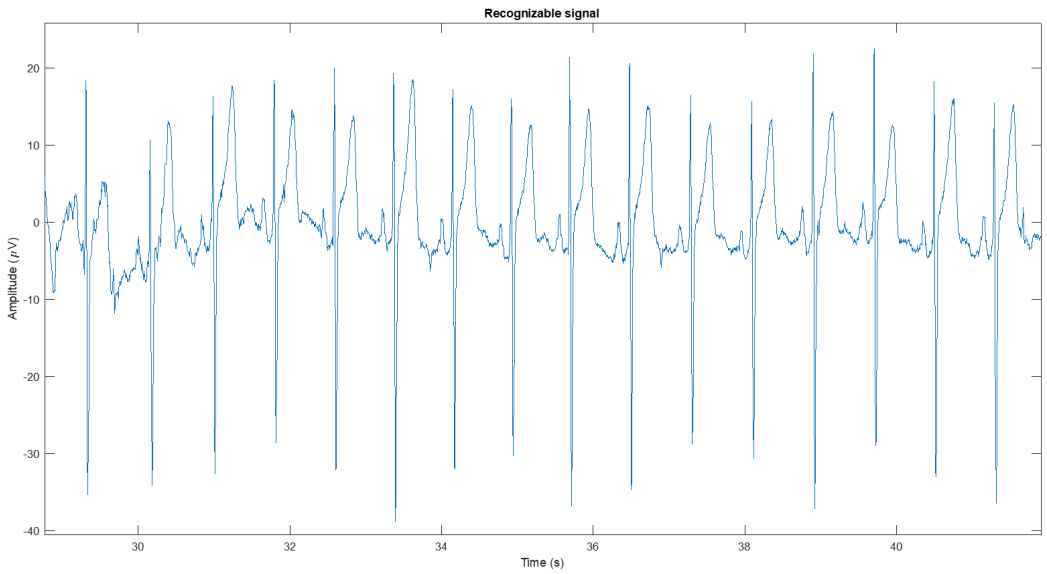

Figure 5.2: Recognizable morphology signals

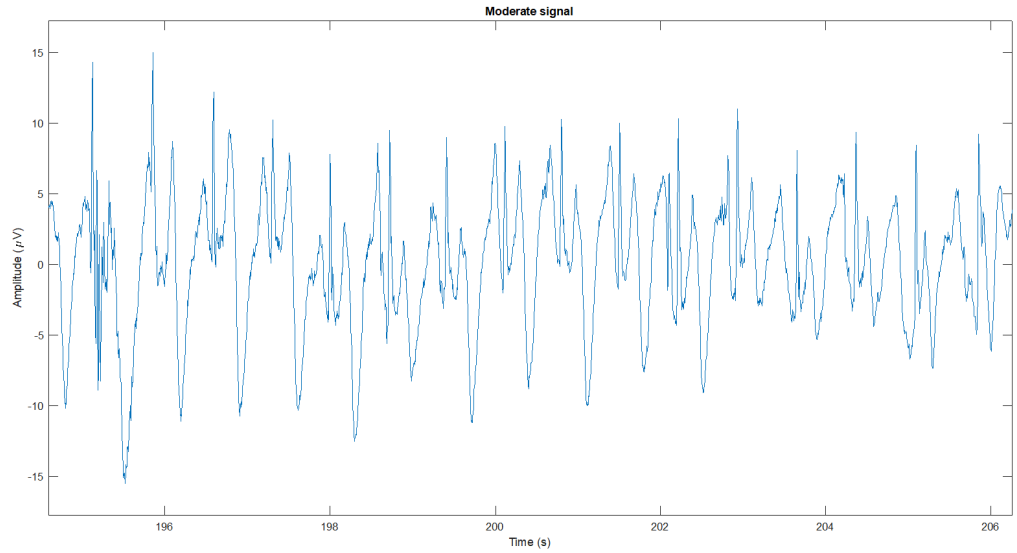

Figure 5.3: Moderate morphology signals

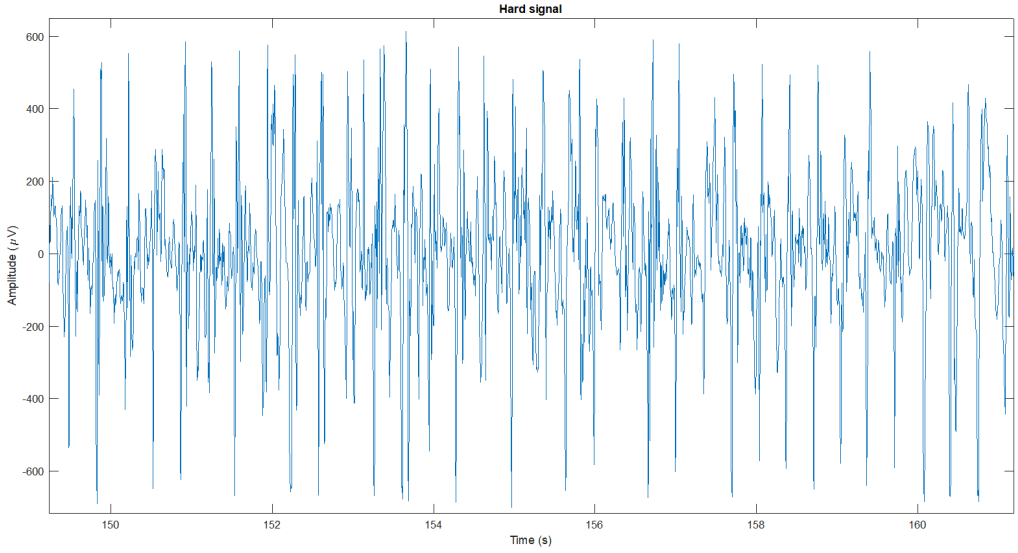

Figure 5.4: Hard morphology signals

5.2 R-peak identification method

The proposed method for R-peak identification is made up of nine steps (Figure 5.5).

Hereinafter referred to the description of each step. The input is a single channel ECG.

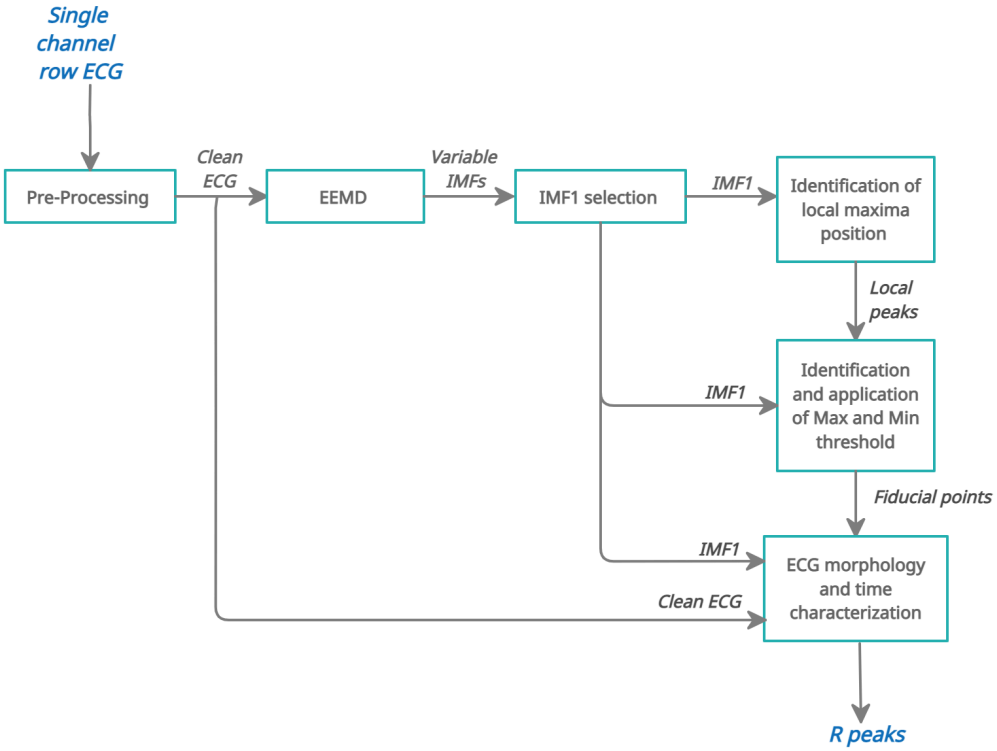

Figure 5.5: Block scheme of the proposal method for R-peak identification

1) Pre-Processing: This step includes the removal of the mean, the resampling of the signal at 200 Hz, and the application of a Notch filter at 50 Hz for the elimination of power line.

2) EEMD: The EEMD algorithm, described in Section 4.1, is applied to the pre-processed ECG signal. The EEMD function inputs are:

-The ensemble number (NE), set to 500 and representing the number of rounds performed by the algorithm;

-The standard deviation of the added noise (0.2; Nstd);

-ECG signals expressed in microvolts (μV) to be comparable with the white noise added by the algorithm.

The output is a varying number of IMFs, depending on the ECG length.

3) IMF1 selection: After the extraction of IMFs, the IMF with the highest frequencies (IMF1) is selected and considered.

4) Identification of local maxima position: The local maxima in the IMF1 are detected and considered as local peaks.

5) Identification and application of Max and Min threshold: The first screening includes peaks between a minimum threshold (min-thr) and a maximum threshold (max-thr). The min-thr is fixed and defined as double the absolute value of the first percentile of IMF1 amplitude distribution. The max-thr depends on the standard deviation of IMF1: if the standard deviation is lower than 100 µV, max-thr is the maximum amplitude of IMF1, if its standard deviation is higher than 100 µV, max-thr is $n \cdot 5 \cdot$ first percentile in absolute value (n is a higher integer over which there are less than 3% of IMF1 local peaks). After this application, the local peaks able to pass the control are termed fiducial points.

6) ECG morphology and time characterization: This step includes different ECG controls: noisy ECG-segment control, first time control, maximum adjustment and a second time control. The noisy ECG-segment control is the algorithm's section that examines ECG-segment with a standard deviation of more than 80 µV . The control is composed of two parts, that should be both verified: the duration in time of QRS complexes must be greater than 0.1 s, and the slope of the rising edge of the QRS complex higher than 70°. The following steps include all the identified fiducial points. The first control on time is applied to comply with the refractory period of 0.25 s and prevents that two or more peaks occur extremely closer in time by selecting the highest one. The Maximum Adjustment is performed on the selected R-peak to guarantee and select the right position of the maximum. Further control on time is implemented: the distance between two consecutive peaks must be greater than the 40% of the RR interval mode. The final output is a vector with the position of the identified R peaks.

5.3 Enhanced adaptive matched filter algorithm for identification of ECGA

The algorithm used for the identification of ECGA is the enhanced adaptive matched filter (EAMF), and it represents an enhancement of the HRAMF algorithm, originally designed for the detection of one kind of alternans, the TWA [95]. The analysis is performed in an ECG tracing containing a number of heartbeats (NHB) set to 64. If the ECG signal is higher than NHB, an overlapping and sliding window of NHB is extracted and processed until the whole length of the signal is reached. The time between the extraction of two subsequent windows, named the number of seconds (NS), is set to 1s [68, **?**], while the sampling frequency (SF) of the ECG tracing is 200 Hz. The EAMF-based procedure identifies and measures ECGA automatically and it consists of two successive steps:

1) **Pre-Processing:** filtering, ECG suitability assessment and signal enhancement.

2)**EAMF:** identification and measurement of alternans, including signal filtering and extraction of alternans features.

The raw ECG is preprocessed by a 6-order bidirectional Butterworth filter with cut-off frequency at 35Hz (standard high-frequency noise removal), heartbeat segmentation, R-peak determination, and the removal of baseline through a cubic spline interpolation. A specific control for the presence of noisy or non-sinus heartbeats is added in order to replace artifacts and ectopic heartbeats. The check is carried out through a correlative approach. The first move is the sectioning of three adjoint sections: the P-wave section (P section), including between the P-wave onset (Pon) and the Qwave onset (Qon); the QRS-complex section (QRS section), including between Qon and the J point (J); and the T-wave section (T section), including between J and the T-wave end (Tend). The heartbeat landmarks can be annotated and used in the ECG sections or otherwise, they need to be estimated through experimental formula or visual form. In this study, the heartbeat landmarks are experimentally calculated. Thereafter, the correlation between the ECG waveforms included in the QRS and T sections of each heartbeat and the corresponding ECG waveforms of the median heartbeat (computed over the available heartbeats) is executed. The heartbeat under examination is entirely replaced by the median heartbeat if the correlation of either QRS and T waves is lower than 0.85; in the opposite case, the heartbeat is considered to be sinus and not affected by artifacts. Additionally, the R peaks are used for the determination of the mean RR interval (mRR; s) and RR standard deviation (stdRR; s). For each considered ECG tracing, the ECG suitability assessment inspects the number of replaced heartbeats (lower than 10% NHB) and stdRR(lower than 10%mRR). If both the conditions are satisfied the ECG tracing is considered suitable for analysis and undergoes the signal enhancement by setting to baseline all ECG sections but the one for which occurrence of alternans has to be evaluated. If classified as not suitable, the ECG tracing is no further analyzed. For each of it is obtained three signals: the P signal (baseline set to all section but the P signal); the QRS signal (baseline set to all section but QRS signal); and the T signal (baseline set to all section but the T signal). In terms of frequency, the alternans has a specific frequency, equal to half heart rate, only in a unlikely state of fixed heart rate (I.e. null heart rate variability). The realistic condition includes a finite but limited physiological variability, consequently, the ECGA is characterized by a narrow frequency band around half the mean heart rate. The selected EAMF is a band-pass filter for the extraction of the alternans signal. After the computation of the alternans frequency (fA = 1/2mRR; Hz), the band-pass filter is implemented as a 6th-order bidirectional (to avoid phase delay) Butterworth filter with high-pass cut-off frequency of fL=$fA - 0.06$ Hz and low-pass cut-off frequency of fH=fA+0.06 Hz [95] . When this filter is applied to a preprocessed signal (P signal, QRS signal, or T signal), the frequency component outside the alternans band are delated and the output obtained is a pseudo-signal named PWA signal, if the input signal is the P signal, QRSA signal, if the input signal is the QRS signal and TWA signal, if the input signal is the T signal. The outgoing vector contains a value of alternans (in terms of amplitude μV) for each beat if the ECGA is detected, differently the value

of alternans is set to 0. To conduct the analysis, from each alternans signals five parameters are extracted, the first three are computed for each sliding window, while the last two are subsequentially calculated:

1) The mean amplitude of alternans considering the 0 (AAm; μV), defined as the difference between the maximum and the minimum of the alternans signal [95];

2) The mean amplitude of alternans without considering the beats that the method does not consider alternating (AA0m; μV)

3) Alternans duration (AD; beat), defined as the total number of beats with alternating T-waves, P-waves or QRS complexes.

4) The alternans area (AAr; μV$\times$ ms), defined as the product of AAm and the length of the analyzed wave (i.e. P-wave length, QRS-complex length and T-wave length, respectively).

5) The alternans magnitude (AM; beatμV), defined as the product between the AAm and AD.

5.4 Statistical analysis

5.4.1 R-peaks identification

The validation of the proposed method for the identification of R-peak is done through the comparison with the annotation of the database. Firstly, the number of true positive (TP), corresponding to the correct identifications, the number of false-negative (FN), that wrongly indicates the peak's absence, and false positive (FP), which incorrectly indicates the presence of R-peak, were identified and counted. Then, positive-predictive value (PPV) (Eq. 5.1) , sensitivity (SE) (Eq. 5.2), false-negative rate (FNR) (Eq. 5.3), and false discovery rate (FDR) (Eq. 5.4) were computed as follows [**?**]:

$$\mathrm{PPV} = \frac{\mathrm{TP}}{\mathrm{TP+FP}} * 100 \tag{5.1}$$

$$\mathrm{SE} = \frac{\mathrm{TP}}{\mathrm{TP+FN}} * 100 \tag{5.2}$$

$$\mathrm{FNR} = \frac{\mathrm{FN}}{\mathrm{FN+TP}} * 100$$

(5.3)

$$\mathrm{FDR} = \frac{\mathrm{FP}}{\mathrm{N}^{\circ}\ \mathrm{Annotation}} * 100$$

(5.4)

The highest performance is obtained when PPV and SE are as close as possible to 100.00%, and consequently when FNR and FDR are as close as possible to 0.00%. The single cumulative statistical index (CSI), defined as a linear combination of the above-defined indexes, is evaluated to describe the performance of the proposed method Eq. 5.5.

$$\mathrm{CSI} = \frac{\mathrm{PPV} + \mathrm{SE} - \mathrm{FPR} - \mathrm{FNR}}{2}$$

(5.5)

The more CSI gets close to 100.00%, the better the performance of R-peaks detector method compared to reference annotation.

5.4.2 ECGA detection

The statistical analysis is led in terms of correlation between the HR and the features extracted by the ECGA analysis. For every parameter vector is calculated the mean except for the '-1' values because they identified the rejected windows. The intra-subject correlation analysis evaluates the correlation between: the mean AAm-HRmean , the mean AA0m-HRmean, the mean AD-HRmean, the mean AAr-HRmean, and the mean AM-HRmean, for each activity (run, walk, high-resistance bike, and low-resistance bike) and for each subject. Hence, for each signal five correlation coefficients and p-value are evaluated for PWA, five for QRSA and five for TWA. The second inter-subject correlation analysis shall be carried out for a complete overview of the alternans: the mean, among each activity and each subject, of AAm, AA0m, AD, AAr and AM are obtained and correlated with the total mean, among each activity and each subject, of HR, for all kind of alternans (PWA, QRSA and TWA). Therefore five correlation coefficients and p-value are displayed for each type of alternans, PWA, QRSA and TWA.

Chapter 6

Results

6.1 R-peaks identification

The proposed EEMD-based method for the identification of the R-peaks results to have a SE of 95%, PPV of 94%, FNR of 5%, FDR of 4% and CSI of 89%. Table 6.1 shows SE, PPV, FNR, FDR, CSI, TP, FN and FP for each subject (the last row is the total). In order to obtain a satisfactory description of the results, the number of R peaks detected by the EEMD-based method, the number of R peaks in the annotation and the SNR of ECG signals are reported in Table 6.1. The SNR values are extracted by a reference paper [**?**]. Table 6.2 displays SE, PPV, FDR, FNR, CSI and SNR differentiated by the three signal classes: recognizable, moderate and hard. The final output of the algorithm is a R-peak position vector. Examples of ECG segment (10s) with the identified peaks are displayed in Fig 6.1 for recognizable signals, in Fig 6.2 for moderate signals and in Fig 6.3 for hard signals.

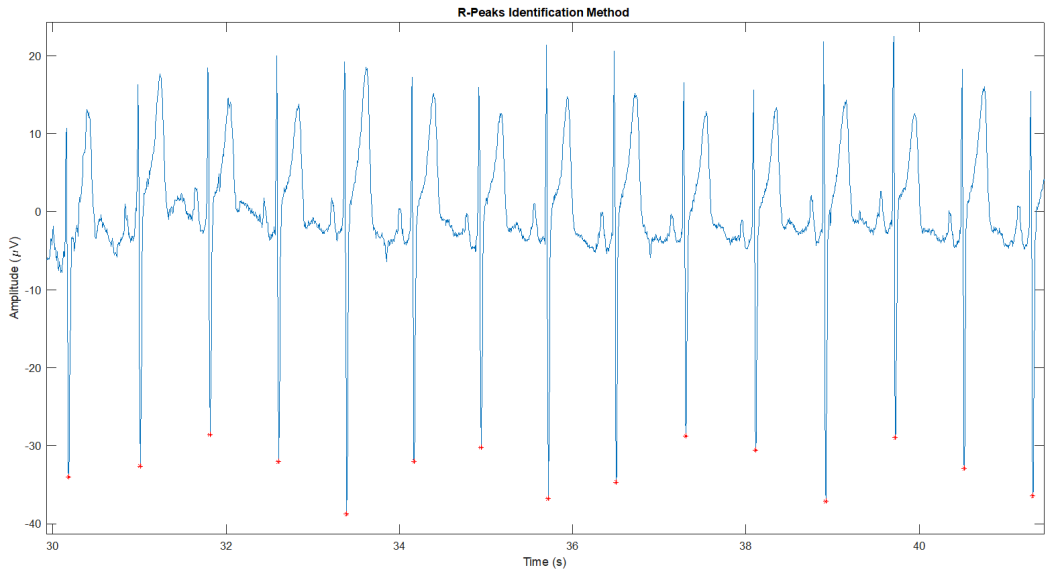

Figure 6.1: Example of the proposed method application: recognizable signals

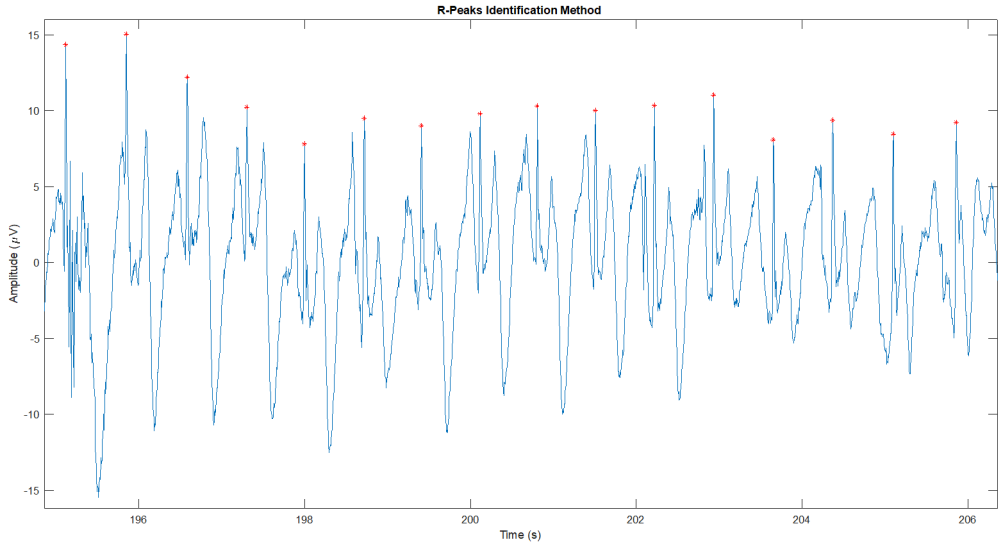

Figure 6.2: Example of the proposed method application: moderate signals

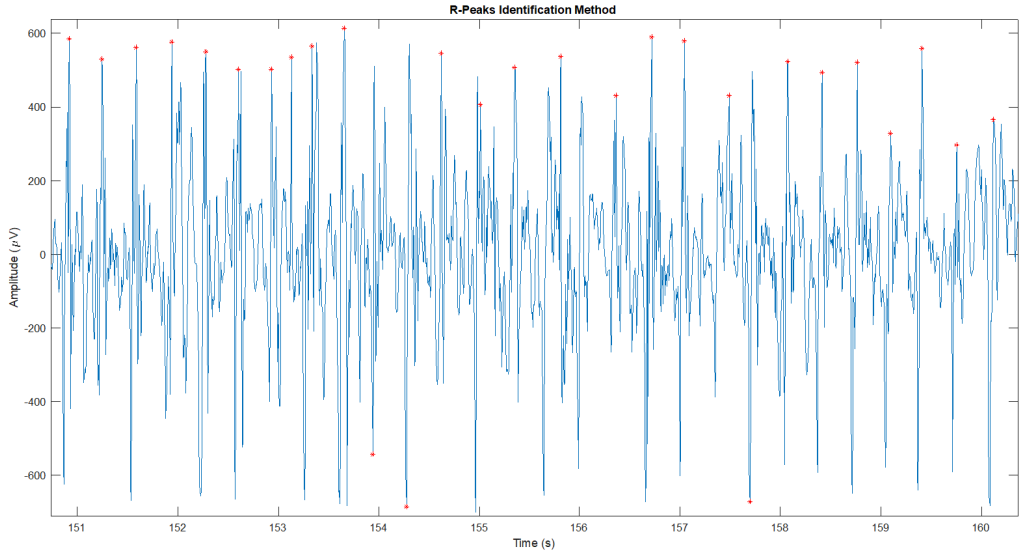

Figure 6.3: Example of the proposed method application: hard signals

Additionally, a correlation analysis is performed between the CSI and SNR, in order to assess the dependence of the proposed method with the presence of noise. The correlation coefficient is 0.5 with a p-value of 0.02. Figure 5.5 shows the distribution of data with linear regression line and R squared.

Table 6.1: Statistical indexes for assessment of the EEMD-based method in comparison to database annotation. Subj=subject ID; Ann=annotation;PM=proposed EEMD-based method; LRB=low-resistance bike; HRB=high-resistance bike

Subjects	**Ann. (n°)**	**PM (n°)**	**TP (n°)**	**FN (n°)**	**FP (n°)**	**SE (%)**	**PPV (%)**	**FNR (%)**	**FDR (%)**	**CSI (%)**	**SNR (dB)**
S1-Walk	512	563	493	70	19	88	96	3	12	85	-6
S1-LRB	796	798	794	2	4	100	99	0	1	99	9
S1-HRB	1040	1038	1026	14	12	99	99	1	1	98	9
S2-Walk	566	593	509	84	57	90	86	10	14	76	-5
S2-LRB	611	643	555	56	88	91	86	9	14	77	5
S2-HRB	805	882	751	54	131	93	85	7	15	78	3
S3-Walk	458	462	451	7	11	99	98	1	2	97	-1
S3-Run	565	568	564	1	4	100	99	0	1	99	5
S3-LRB	523	532	485	38	47	93	91	7	9	84	-5
S3-HRB	593	592	536	7	56	90	91	10	9	81	-4
S4-Run	839	839	753	86	86	90	90	10	1	80	0
S5-Run	640	640	673	3	3	100	100	0	0	100	9
S5-LRB	576	577	571	5	6	99	99	1	1	98	0
S6-Walk	513	514	507	6	7	99	99	1	1	98	-3
S6-Run	478	478	431	47	47	90	90	10	10	80	-3
S6-LRB	536	542	497	39	4	93	92	7	8	85	4
S8-Walk	498	504	490	8	14	98	97	2	3	95	-1
S8-Run	417	439	375	42	55	90	87	10	13	77	-8
S9-Walk	372	369	363	9	6	98	98	2	2	96	2
Tot.	**597**	**608**	**567**	**30**	**35**	**95**	**94**	**5**	**6**	**89**	**1**

Table 6.2: Statistical indexes for assessment of the EEMD-based method differentiated by the three signal classes

Classes	**SE (%)**	**PPV (%)**	**FDR (%)**	**FNR (%)**	**CSI (%)**	**SNR (dB)**
Recognizable	97	96	3	4	96	4
Moderate	92	94	8	6	86	-1
Hard	92	89	8	11	82	-3

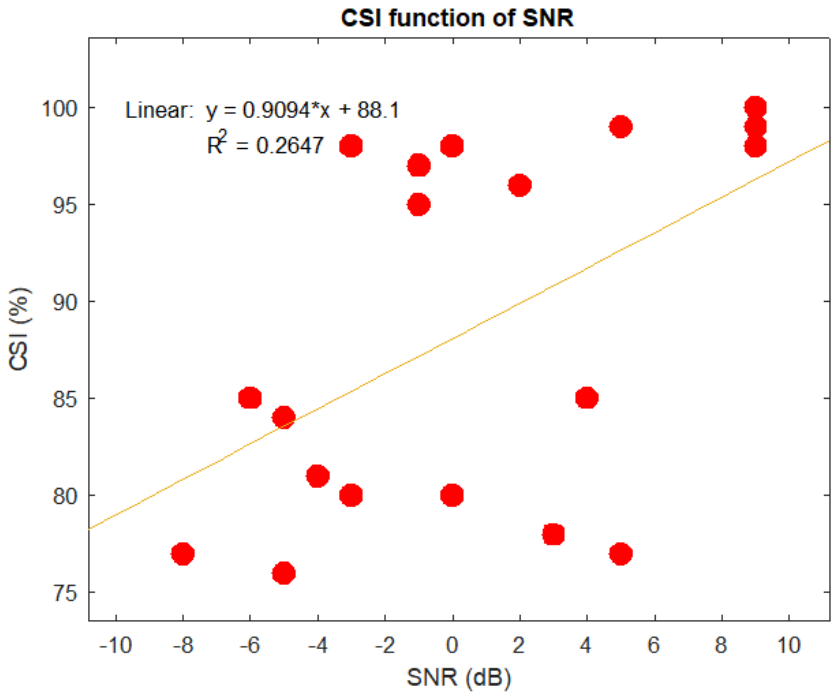

Figure 6.4: CSI function of SNR

6.2 ECGA detection

The results obtained after applying the EAMF to the ECG signals are expressed in terms of: mean value of alternans features (AAm, AA0m, AAr, AD and AM) for each types of alternans (PWA, QRSA and TWA), intra-subject correlation analysis and inter-subject correlation analysis. Table 6.3, 6.4 and 6.5 show the feature extracted by the EAMF for the analysis of ECGA: the amplitude of alternans considering the beats that the method does not consider alternating (AAm; μV), the amplitude of alternans not considering the beats that the method does not consider alternating (AA0m;μV), the alternans duration (AD; beat), the alternans area (AAr;$\mu\times$ms), and the alternans magnitude (AM; beatμV) for each subject and each activity (PWA Table 6.3, QRSA Table 6.4 and TWA Table 6.5 respectively). Additionally, the percentage of rejected windows and the mean HR of each ECG signals are included in the analysis in Table 6.6. The 75% of the recognizable signals and the 50% of the moderate signals are analyzed, none of hard signals has the quality to pass the suitability control.

Table 6.3: Alternans feature extracted by the EAMF for PWA

Feature	*S1* **LRB**	*S1* **HRB**	*S2* **LRB**	*S2* **HRB**	*S3* **Run**	*S3* **LRB**	*S5* **LRB**	*S6* **LRB**	*S8* **Walk**	*S9* **Walk**
AAm (μV)	10	10	9	9	6	7	2	5	6	10
AA0m (μV)	14	12	12	11	8	9	4	7	8	12
AD (Beat)	45	51	50	53	43	47	30	49	45	52
AAr ($\mu\times$ms)	1927	1982	1809	1839	1127	1351	413	992	1125	1929
AM (BeatμV)	453	520	463	494	266	328	63	248	255	502

Table 6.4: Alternans feature extracted by the EAMF for QRSA

Feature	*S1* **LRB**	*S1* **HRB**	*S2* **LRB**	*S2* **HRB**	*S3* **Run**	*S3* **LRB**	*S5* **LRB**	*S6* **LRB**	*S8* **Walk**	*S9* **Walk**
AAm (μV)	19	17	16	15	13	17	19	10	10	18
AA0m (μV)	24	21	18	18	17	20	21	13	15	22
AD (Beat)	51	52	54	54	50	51	58	52	44	53
AAr ($\mu\times$ms)	1555	1373	1274	1212	1046	1330	1488	836	820	1474
AM (BeatμV)	1005	905	888	668	668	879	1076	545	453	973

Table 6.5: Alternans feature extracted by the EAMF for TWA

Feature	*S1* **LRB**	*S1* **HRB**	*S2* **LRB**	*S2* **HRB**	*S3* **Run**	*S3* **LRB**	*S5* **LRB**	*S6* **LRB**	*S8* **Walk**	*S9* **Walk**
AAm (μV)	44	28	28	22	14	30	9	10	12	35
AA0m (μV)	49	32	30	23	16	33	10	11	17	40
AD (Beat)	56	56	58	59	57	57	58	56	47	57
AAr ($\mu\times$ms)	4362	2849	2771	2154	1447	3017	907	969	1225	3532
AM (BeatμV)	2473	2849	1625	1282	845	1763	523	545	574	2026

Table 6.6: Percentage of rejected windows (RW) and mean HR

Feature	*S1* **LRB**	*S1* **HRB**	*S2* **LRB**	*S2* **HRB**	*S3* **Run**	*S3* **LRB**	*S5* **LRB**	*S6* **LRB**	*S8* **Walk**	*S9* **Walk**
RW (%)	26%	0%	50%	29%	0%	60%	73%	78%	64%	83%
mHR (bpm)	83	106	111	117	111	108	127	113	74	102

The intra-subject correlation analysis involves the computation of the correlation coefficient and its p-value between the HR and AAm, AA0m, AD, AAr, and AM,

for each subject and each activity. Table 6.7 refers to the correlation coefficient of PWA, Table 6.8 refers to the correlation coefficient of QRSA and Table 6.9 refers to the correlation coefficient refers to p-value of TWA. The symbol (*) means that the correlation is signficant with a p-value < 0.005.

Table 6.7: PWA: Intra-subject correlation analysis: Correlation Coefficient,* identifies a p-value lower than 0.005

Subjects	*HR-AAm*	*HR-AA0m*	*HR-AD*	*HR-AAr*	*HR-AM*
S1-LRB	0.4*	0.3*	0.4*	0.4*	0.4*
S1-HRB	0.3*	0.1	0.4*	0.2*	0.3*
S2-LRB	0.2	0.3*	-0.2	0.2	0.07
S2-HRB	0.3*	0.3*	0.1	0.3*	0.2*
S3-Run	-0.5*	-0.5*	-0.4*	-0.5*	-0.5*
S3-LRB	0.6*	0.6*	0.6*	0.6*	0.6*
S5-LRB	-0.1	-0.3*	0.1	-0.1	0.01
S6-LRB	0.3	0.5*	0.01	0.2	0.1
S8-Walk	-0.8*	-0.5	-0.9*	-0.8	-0.9*
S9-Walk	-0.1	0.4	-0.6*	-0.1	-0.3

Table 6.8: QRSA: Intra-subject correlation analysis: Correlation Coefficient, * identifies a p-value lower than 0.005

	HR-AAm	*HR-AA0m*	*HR-AD*	*HR-AAr*	*HR-AM*
S1-LRB	0.4*	0.4*	0.1	0.4*	0.4*
S1-HRB	0.2*	0.02	0.3*	0.2*	0.3*
S2-LRB	0.2	0.09	0.5*	0.2	0.3*
S2-HRB	0.1	0.02	0.2*	0.1	0.2
S3-Run	0.3*	0.2	0.3*	0.3*	0.3*
S3-LRB	**0.7***	**0.7***	0.4*	**0.7***	0.6*
S5-LRB	-0.2*	-0.1*	-0.3*	-0.2*	-0.2*
S6-LRB	**0.7*** *	**0.9***	-0.8*	**0.7***	0.3
S8-Walk	-0.1	-0.4	0.3	-0.1	0.1
S9-Walk	-0.5	-0.6*	**0.8***	-0.	-0.3

Table 6.9: TWA: Intra-subject correlation analysis: Correlation Coefficient,* identifies a p-value lower than 0.005

	HR-AAm	*HR-AA0m*	*HR-AD*	*HR-AAr*	*HR-AM*
S1-LRB	**0.8***	**0.8***	0.5*	**0.8***	**0.8***
S1-HRB	0.01	-0.01	0.3*	0.01	0.04
S2-LRB	0.3	-0.3*	-0.3*	0.2*	-0.2
S2-HRB	**0.7***	**0.7***	0.5*	**0.7***	**0.7***
S3-Run	**0.7***	**0.7***	0.1	**0.7***	**0.7***
S3-LRB	0.6*	0.6*	0.5*	0.6*	0.6*
S5-LRB	0.1	0.1	0.2	0.1	0.11
S6-LRB	0.02	0.1	-0.3	0.03	-0.1
S8-Walk	**0.7**	-0.2	0.2	**0.7**	0.
S9-Walk	-0.6*	-0.2	-0.9*	-0.6*	-0.7*

The inter-subject correlation analysis is conducted by the correlation of the mean, among each activity and each subject, of AAm,AA0m, AD, AAr and AM with the total mean, among each activity and each subject, of HR, for all kind of alternans (PWA, QRSA and TWA). The correlation coefficient and the p-value are reported. The mean amplitude value (AAm0) of PWA is 10 μV, QRSA is 19 μV and TWA is 26 μV. Considering AAm, the PWA ampitude is 7 μV, the QRSA amplitude is 15 μV and the TWA amplitude is 23 μV. The results are showed in Table 6.10 .

The following figures represent the feature extracted by the ECGA analysis (AA0m, AAm, AD, AAr, and AM) in relation to HR (Fig 6.6, Fig 6.5, Fig 6.7, Fig 6.8, Fig 6.9 respectively). In particular, different markers are displayed: the shape of the markers (star, triangle, circle, square, hexagon, and rhomb) identify the six subjects under examination, while the marker color refers to the four different activities (red for low resistance bike, magenta for high resistance bike, green for run and blue for the walk). In order to obtain a better description of the set and trend of given data,

Table 6.10: Inter-subject correlation analysis. CC= correlation coefficient.

CC(p-value)	**PWA**	**QRSA**	**TWA**
HR-AAm	-0.4(0.3)	0.2(0.5)	-0.3(0.3)
HR-AA0m	-0.4(0.2)	-0.1(0.9)	-0.4(0.2)
HR-AD	-0.2(0.6)	**0.8**(0.003)	**0.8**(0.01)
HR-AAr	-0.3(0.4)	0.2(0.6)	-0.4(0.3)
HR-AM	-0.2(0.5)	0.3(0.4)	-0.2(0.5)

the regression line and R-squared are added. The latter is a statistical measure of how close the data are to the fitted regression line, it is always between 0 and 100% and in general, the higher the R-squared, the better the model fits data.

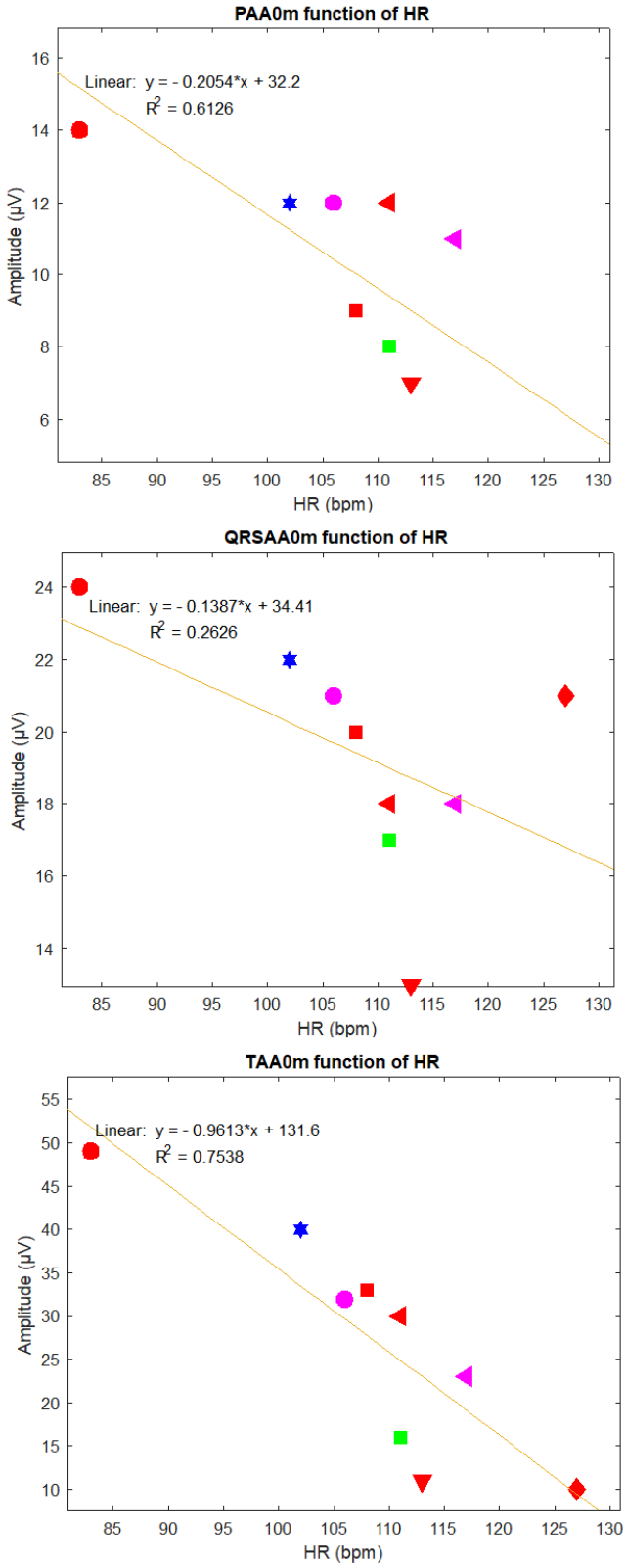

Figure 6.5: AA0m in relation to HR: markers shape identifies different six analyzed subjects, markers color refers to the activities (red for low resistance bike, magenta for high resistance bike, green for run and blue for the walk). AA0m=Amplitude not considering the not alternating beats. HR= heart rate.

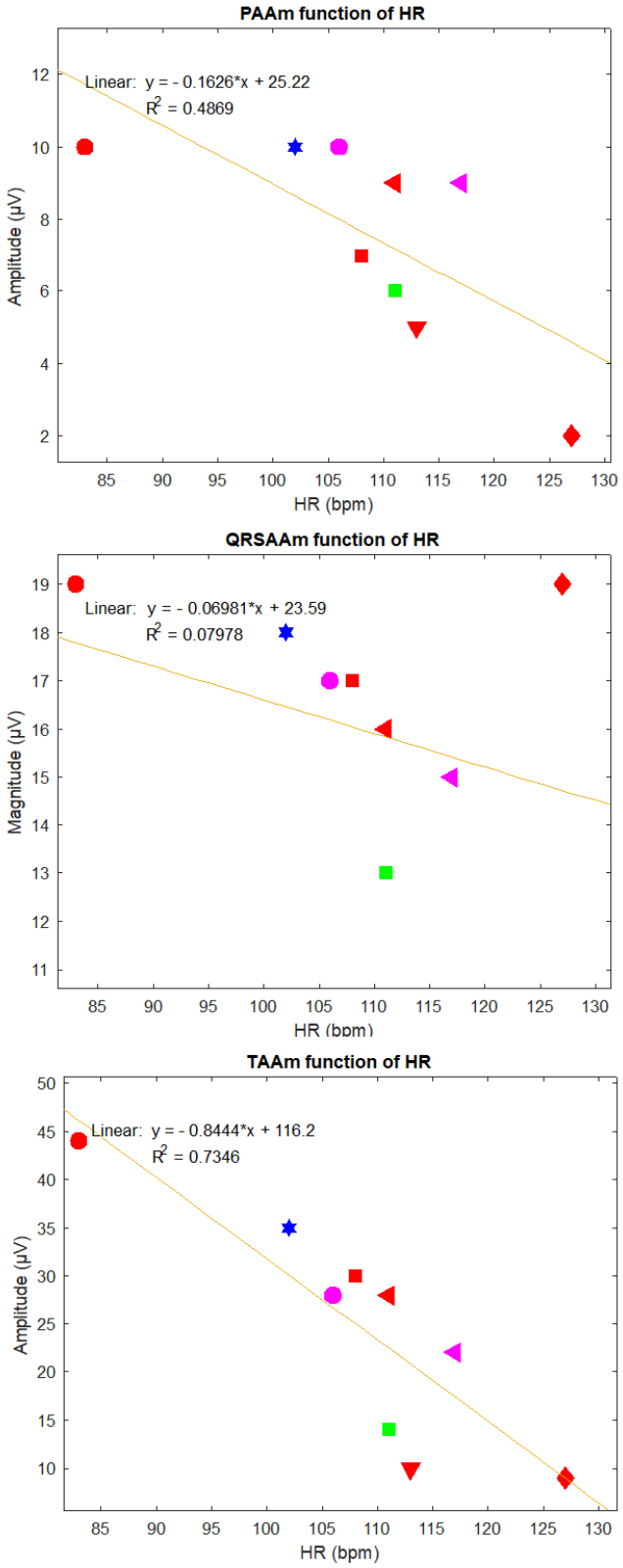

Figure 6.6: AAm in relation to HR: markers shape identifies different six subjects, markers color refers to the activities (red for low resistance bike, magenta for high resistance bike, green for run and blue for the walk). AAm= alternans amplitude considering the not alternating beats. HR=heart rate.

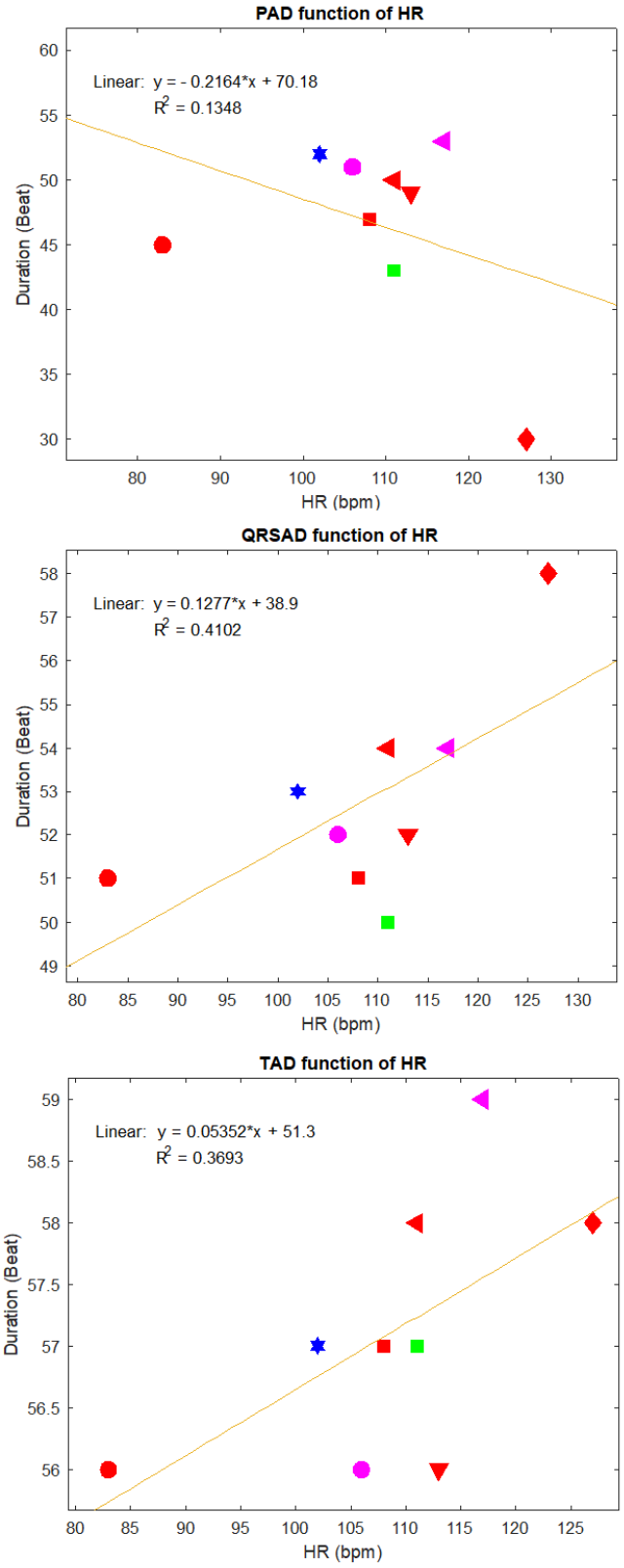

Figure 6.7: AD in relation to HR: markers shape identifies different six subjects, markers color refers to the activities (red for low resistance bike, magenta for high resistance bike, green for run and blue for the walk).AD= alternans amplitude. HR=heart rate

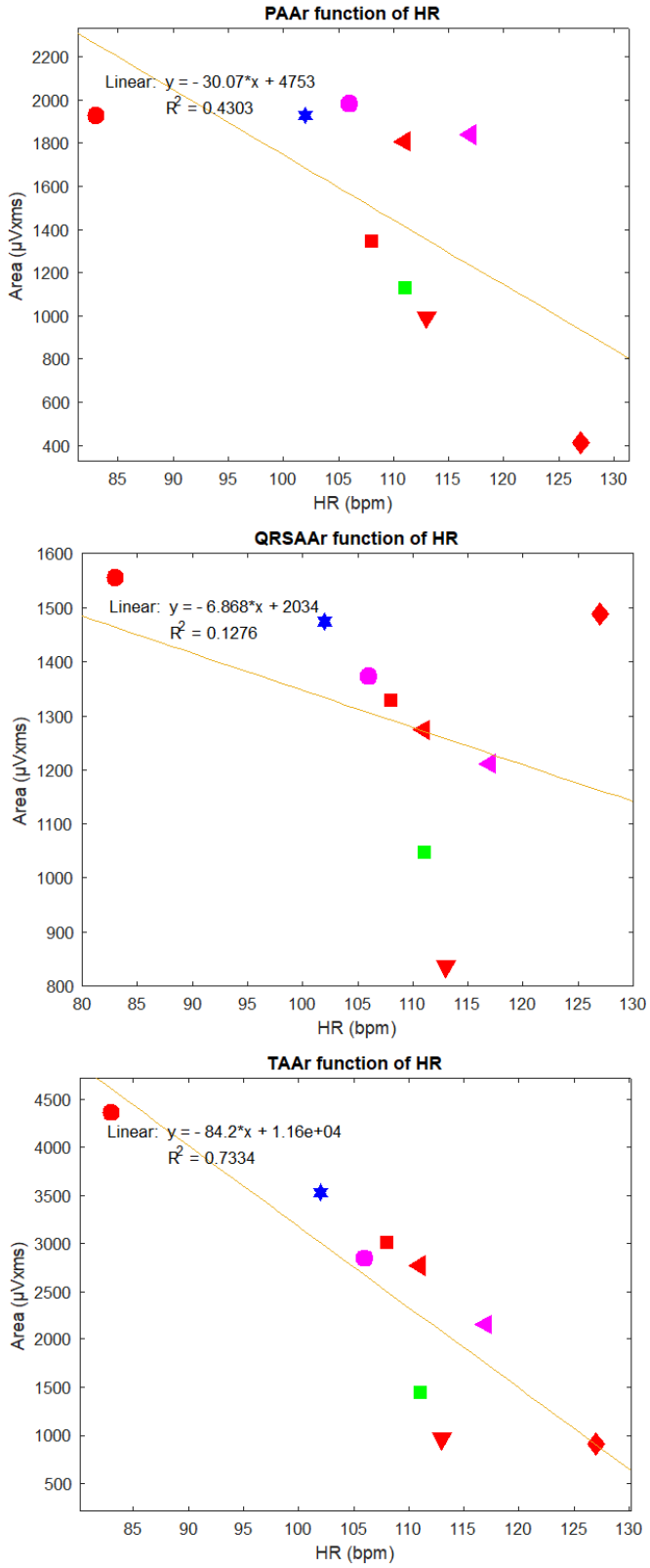

Figure 6.8: AAr in relation to HR: markers shape identifies different six subjects, markers color refers to the activities (red for low resistance bike, magenta for high resistance bike, green for run and blue for the walk).AAr=alternans area. HR=heart rate.

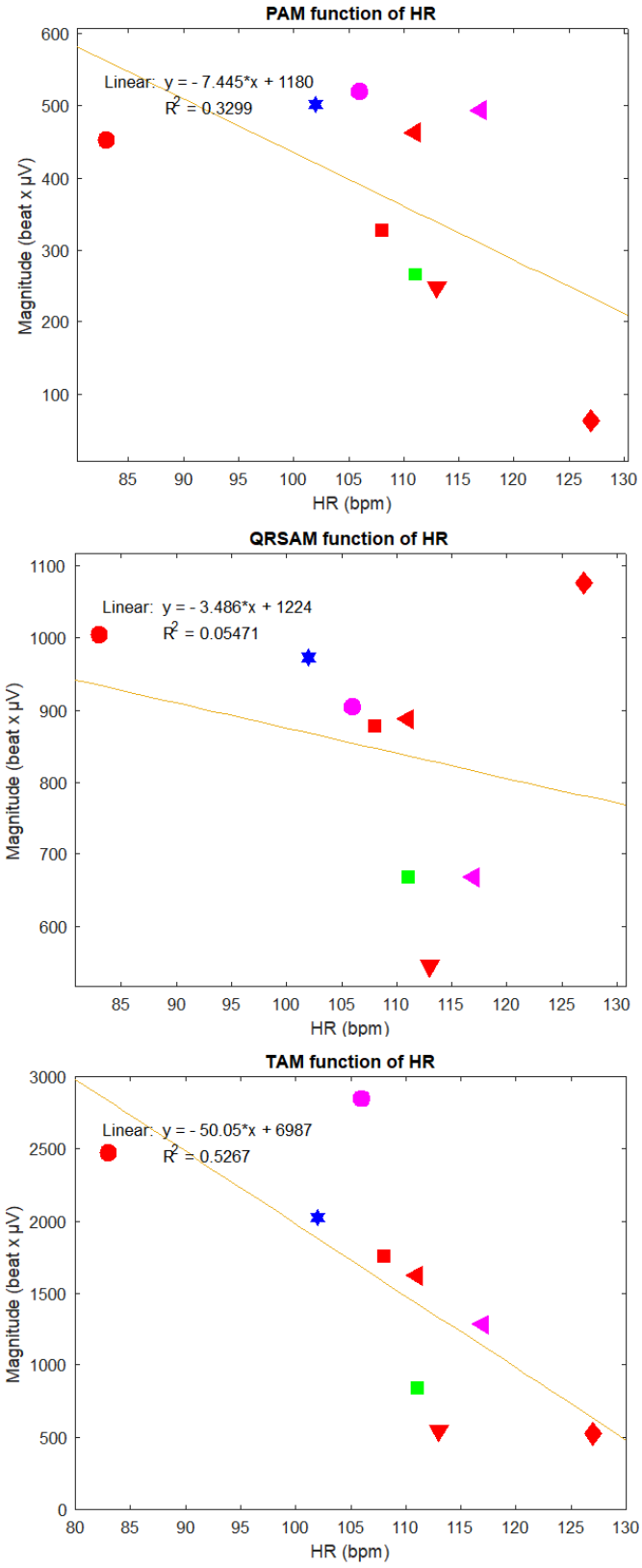

Figure 6.9: AM in relation to HR: markers shape identifies different six subjects, markers color refers to the activities (red for low resistance bike, magenta for high resistance bike, green for run and blue for the walk).AM=alternans magnitude. HR= heart rate

Chapter 7

Discussion

The present thesis aims to achieve a dual purpose: the development of an algorithm for the identification of R peaks and the detection of ECGA in ECG signals acquired on subjects while performing sport. The achievement of the first aim is fundamental to pursue the second aim. Consequently, the correct identification is necessary to obtain a reliable ECGA analysis. The selected ECG signals are classified into three classes (recognizable, moderate and hard signals) in order to assess the performance of the algorithm depending on the noise presence, considering that the acquisition during physical activity introduces noise and artifacts. The first part is focused on the development of a technique able to correctly identify R peaks in very noisy ECG signals acquired during sports activity. This algorithm is based on EEMD method. Differently from other works proposed in the literature, this method does not imply the filtration or the reconstruction of the signal from IMFs [92, 93, ?, ?, ?, ?, 94]. The method considers only the first among the IMFs computed by EEMD. On this IMF1, fiducial points were firstly identified, and considered as the position of potential R peaks. The consideration of the IMF1 provides two major advantages. Firstly, it contains the highest frequencies of the signal, including also the frequency band 10-50 Hz characterizing the QRS complex [92, ?]. Secondly, IMF1 characterizes the narrow band amplitude-frequency modulation linked with the ventricular depolarization because it better reproduces the ondulatory mode and pseudo-periodic presence of the QRS complex. The setting of EEMD, i.e. NE and power of added noise, is chosen based on literature results. Specifically, the NE should be of the order of hundred to produce good quality IMFs [?], and in this work, it is set to 500 and the standard deviation of the added noise is fixed and set to 0.2. The ECG morphology control is performed only in the ECG segment where the R peaks are hidden in the noise because standard values (the length and the slope of the rising edge of the QRS complex) better identify the peaks. The application of the same control in the entire ECG length would have been too restricted considering the variable nature of the signals. The validation of the proposed method is done through the comparison with the annotations of the database.The PPV, SE, FNR, FDR and CSI were computed and analyzed. The results show a good level of performance working on noisy and raw ECG signals, with a SE value of 95%, PPV of 94%, FNR of 5%, FDR of 6% and CSI of 89%. The best performance is obtained in

the recognizable signals with a higher CSI (96%) with respect to moderate signals (86%) and hard signals (82%). The same value of SE for both moderate and hard signals demonstrates a good algorithm quality. Actually, a low correlation coefficient between CSI and SNR confirms the ability to work independently from noise or artifacts. After a correct identification of R peaks, the ECGA analysis can be reliably performed. ECGA is an index of susceptibility to malignant ventricular arrhythmias and sudden cardiac death. The algorithm used for the identification of ECGA is the enhanced adaptive matched filter (EAMF), and it represents an enhancement of the HRAMF algorithm, originally designed for the detection of one kind of alternans, the TWA [95]. The advantage of the selected algorithm is the introduction of an enhancement procedure since the possible presence of different kinds of alternans simultaneously affecting the ECG alternans identification and it can bias the correct interpretation of the phenomenon. This issue is resolved by deleting all waves but the one of interest allowing an independent but contemporary analysis. Moreover, for the first time, the insertion of the alternans area provides information about the cumulative amount of alternans related to a specific wave and permit a reliable comparison of different forms of ECGA, and so, the identification of the prevalent one. And lastly, because of its theoretical approach, it is able to be robust against noises and interferences in most frequency bands. The analysis is performed in an ECG tracing containing a number of NHB set to 64. Infact, in case of particularly noisy signals it is preferable to set a small dimension of the moving window. Short ECG windows more likely respect the required HR stability criterion and their frequent extraction allows a continuous adapting alternans analysis along the ECG. The time between the extraction of two subsequent windows is set to 1s to increase the number of analysed windows and to reduce the percentage of rejected windows. The EAMF-based procedure identifies and measures ECGA automatically and it consists of two successive steps: the pre-processing, including filtering, ECG suitability assessment and signal enhancement and EAMF, with the identification and measurement of alternans, including signal filtering and extraction of alternans features. For each alternans signals five parameters are extracted, the first three are computed for each sliding window, while the last two are subsequentially calculated: 1) the mean amplitude of alternans considering the beats that the method does not consider alternating (AAm;µV); 2) the mean amplitude of alternans without considering the beats that the method does not consider alternating (AA0m;µV); 3) the alternans duration (AD; beat); 4) the alternans area (AAr;µV×ms); 5) the alternans magnitude (AM; beatµV). The considered parameters allow a complete characterization of the ECGA phenomenon. The EAMF correctly identifies the presence of the three kinds of alternans in ten subjects, while in nine signals the percentage of rejected windows is 100%. Although the filter is quite sturdy to work with the presence of noise, none of the hard signals has the quality to pass the suitability control, whereas 75% of the recognizable signals and 50% of the moderate signals are analyzed. Anyway, the positive aspect of rejecting windows is the greater

reliability of the results. The analysis indicates that highest values of amplitude alternans (AAm and AA0m) are found in TWA, as well as magnitude and area. The mean amplitude value AAm0 of TWA is 26 µV, respect to PWA of 10 µV and QRSA of 19 µV. Considering AAm, the TWA amplitude is 23 µV while PWA amplitude is 7 µV and QRSA amplitude is 15 µV. Even if the duration is similar in all three waves, the prevalent alternans wave is the T wave. Since there are no reference value for ECGA in athletes it is not possible a comparison, but the low amplitude range suggests a not-risk alternans presence in healthy subjects. The evaluation on a large number of healthy athletes could provide reference values to compare with, especially useful in the case of automatic ECGA identification, potentially integrated into wearable devices that acquire and analyze the ECG. A statistical analysis has been carried out to evaluate the dependence of the alternans with HR. Overall, a non-significant correlation between HR and the parameters extracted is found, except for the duration. The alternans duration, which is the total number of alternating beats, is related to HR even if it is not reached its maximum, and it can be used as a useful index for the evaluation of alternans in resting condition or low HR range. Regarding the intra-subject analysis, a correlation coefficient between HR and alternans amplitude higher than 0.7 is found only for TWA (four subjects) and QRSA (two subjects). In general, a significant correlation is seen in subjects with the highest amplitude value and with a HR trend almost always above 100 bpm, according to literature findings. The activities proposed by the database are not really functional for the purpose since higher HR and recovery phases should be needed. Anyway, it has been selected for the presence of R peaks annotation. These results are justified by a limited HR variability, a low range of HR (83-127 bpm), and the absence of the recovery phase, considering that previous study has been conducted under stress conditions to increase HR to a critical level for TWA detection. The fewer number of participants and the even lower number of signals analyzed for the ECGA detection can affect the results, and a precise and accurate understanding of the phenomenon is not obtained. Additionally, in sports literature, there is a lack of studies for the identification of cardiac risk through PWA and QRSA analysis.The inclusion of PWA and QRSA in the analysis is important because the AP travels along all the heart sites, and in this way is possible to obtain an electrically complete vision of heart health. P wave is associated with atrial depolarization, and PWA could be considered as an index of atrial electrical instabilities. QRS complex reflects both ventricles depolarization and atria repolarization, and QRSA is a clue in the case of supraventricular and ventricular tachycardias. Few studies have been performed for the evaluation of TWA, but it does not give useful information (i.e. reference alternans value for athletes) but only the confirmation of high HR range to highlight its dependence with alternans [82, 83, 84, 85]. At any rate, the prognostic significance of exercise-induced ECGA in athletes appears to change depending on the HR range. The present thesis has demonstrated the presence, even if low, of alternans despite the low HR range and the limited HR variability. These findings,

in healthy subjects, allow us to define the alternans as a continuous phenomenon, whose associated electrical risk increases while alternans amplitude and HR increase. Furthermore, they allow to define the physiological values of alternans in case of healthy athletes. A complete characterization of the phenomenon is useful to know the reference values to compare with. To obtain a complete understanding of the prognostic relevance of alternans in athletes, it is necessary to find the HR value for which the alternans reach its maximum.

Conclusion

In conclusion, the primary aim of the study is the evaluation of ECGA, for subjects performing different type of sports. For the first time, the evaluation of alternans is done through a complete characterization of the phenomenon in terms of amplitude, duration, area, and magnitude. Considering the total absence of literature reference value for both healthy and high-risk athletes, this work proposes a first approach for the identification of cardiac risk in subjects performing sport. A basilar step for the evaluation of ECGA is the correct identification of R peaks on the ECG. The proposed algorithm for R peaks detection based on EEMD method shows a good level of performance, despite a very low SNR mostly related to movement artefacts. The low correlation of the CSI with SNR confirms its robustness that does not depend on the presence of noise, extending the algorithm application field. Thus, it can be used for a successive evaluation of ECGA, where the correct extraction of R peaks position is crucial for a valid investigation. The ECGA is an HR-dependent phenomenon and the achievement of the maximum HR is relevant for a correct characterization of ECGA. The results of the study demonstrates the presence of alternans in healthy subjects even if a wider range of HR values may be useful. At any rate, the low range value suggests the presence of not-risk alternans in healthy individuals. The present study presents a limitation in achieving the specific activity of reaching the maximum HR with incremental exercise. Further follow-up study firstly may involve a consistent population of athletes to significantly evaluate the reference alternans value for healthy subjects. Secondly, a specific protocol of the activity must be designed to achieve the maximum HR through incremental fatigue steps. It should include an incremental exercise and a resting phase before the exercise as well as the final recovery. Despite the limited knowledge, the ECGA seems to be a valid instrument for the evaluation of athlete's risk during physical activity, paving the way for continuous monitoring of athletes through wearable sensors.

Bibliography

[1] I. Rehman; A. Nassereddin; A. Rehman. Anatomy, torax, pericardium. *StatPearls Publishing*, pages 1–2, 2020.

[2] J.M.H. Wanga; R. Raib; M. Carrascoc; T. Sam-Odusinac; S. Salandyc; J. Gieleckid; A. Zuradae; M. Loukasc. An anatomical review of the right ventricle. *Elsevier GmbH*, pages 1–9, 2019.

[3] K.P. McCarthy; L. Ring; S.B. Rana. Anatomy of the mitral valve: understanding the mitral valve complex in mitral regurgitation. *European Journal of Echocardiography*, 11:3–9, 2010.

[4] I.E. Charitos; H.H. Sievers. Anatomy of the aortic root: implications for valve-sparing surgery. *The Annals of Cardiothoracic Surgery*, 2(1):3–56, 2013.

[5] P.W. Bridgman. *Handbook of Cardiac Anatomy, Physiology and Devices*, volume 4. Springer, 2005.

[6] M. Dick; A. M. Kiel; J. D. Tune A. G. Goodwill; G. Regulation of coronary blood flow. *Comprehensive Physiology*, 7(2):321–382, 2018.

[7] BrainKart. Medical physiology.

[8] W. Boron; E. Boulpaep. *Medical physiology.* 2016.

[9] A. Reisner; G. Clifford; R. Mark. The physiological basis of the electrocardiogram. 2006.

[10] A.L.Baggish. A decade of athlete ecg criteria: Where we've come and where we're going. *Journal of Electrocardiology*, 48(3):324–328, 2015.

[11] J. Basu; A. Malhotra. Interpreting the athlete's ecg: Current state and future perspectives. *Current Treatment Options in Cardiovascular Medicine*, 20:104, 2017.

[12] C. L. Standfield. *Principle of human physiology*, volume 5. Pearson Education, 2012.

[13] B.J.B. Grant; D.R Dantzker. *Pathophysiology of the Pulmonary Circulation*, volume 1. Springer, 1984.

[14] T. Nikolaidou; O.V. Aslanidi; H. Zhang; I.R. Efimov. Structure/function relationship in the sinus and atrioventricular nodes. *Pediatric Cardiology*, 33(3):890–899, 2012.

[15] F. Saremi; S. Yen Ho; J.A. Cabrera; D. Sanchez-Quintana. Right ventricular outflow tract imaging with ct and mri: Part 1, morphology. *American Journal of Roentgenology*, 2013.

[16] A. Kosiński; M. Grzybiak; A. Dubaniewicz; K. Kędziora; W. Makarewicz; D. Kozłowski. False chordae tendineae in right ventricle of adult human hearts – morphological aspects. *Archives of Medical Science*, 8:834–840, 2012.

[17] D. Goor; C. Lillehei. *Congenital Malformations of the Heart*, volume 3. Grune Stratton, 1975.

[18] M. Ifrim; E. Bontaş; D. Cochior; I. Ţintoiu. *Right Heart Anatomy: A Short Uptodate*, volume 2. Springer, Cham, 2018.

[19] B.D. Hoit. Left atrial size and function: role in prognosis. *American College of Cardiology*, 63:1–2, 2014.

[20] S. Yen Ho. Anatomy and myoarchitecture of the left ventricular wall in normal and in disease. *European Journal of Echocardiography*, 10:iii3–iii7, 2009.

[21] N. Piazza;P. de Jaegere; C. Schultz; A.E. Becker; P.W. Serruys; H.R. Anderson. Anatomy of the aortic valvar complex and its implications for transcatheter implantation of the aortic valve. *Journal of the American Heart Association*, 1:78–81, 2008.

[22] B. Husse; W.M. Franz. Generation of cardiac pacemaker cells by programming and differentiation. *Biochimica et Biophysica Acta*, 1863:1948–1952, 2016.

[23] C.B. Estigoy; F. Pontén; J. Odeberg; B. Herbert; M. Guilhaus; M. Charleston; J.W.K. Ho; D. Cameron; C.G. dos Remedios. Intercalated discs: multiple proteins perform multiple functions in non-failing and failing human hearts. *Biophysical Reviews*, 1:43–49, 2009.

[24] D.A. Goodenough; D.L. Paul. Gap junctions. *Cold Spring Harbor Perspectives in Biology*, 1, 2009.

[25] D. Garrod; M. Chidgey. Desmosome structure, composition and function. *Biochimica et Biophysica Acta*, 1778:572–587, 2008.

[26] R.E. Klabunde. Cardiac electrophysiology: normal and ischemic ionic currents and the ecg. *Advances in Physiology Education*, 41:29–37, 2017.

[27] L.F Santana; L.F. Cheng; W.J. Lederer. How does the shape of the cardiac action potential control calcium signaling and contraction in the heart? *Journal of Molecular and Cellular Cardiology*, 49(6):901–903, 2010.

[28] A.M. Campbell; J.A. Hulf. Aspects of myocardial physiology. *Update in Anaesthesia*, 18:1–4, 2004.

[29] D. Di Francesco. Funny channels in the control of cardiac rhythm and mode of action of selective blockers. *Pharmacological Research*, 53:399–406, 2006.

[30] B.E. Wright; G. LeFever Watson; N.J. Selfridge. The wright table of the cardiac cycle: a stand-alone supplement to the wiggers diagram. *Advances in Physiology Education*, 44:554–563, 2020.

[31] J. King; D.R. Lowery. Physiology, cardiac output. *Treasure Island (FL): StatPearls Publishing*, 2020.

[32] Z.S. Bruss; A. Raja. Physiology, stroke volume. *Treasure Island (FL): StatPearls Publishing*, 2020.

[33] J.M. Norton. Toward consistent definitions for preload and afterload. *Advances in Physiology Education*, 25:53–61, 2001.

[34] P. LaCombe; A. Jose; S.L. Lappin. Physiology, starling relationships. *Treasure Island (FL): StatPearls Publishing*, 2020.

[35] S. Rehman; A. Khan; A. Rehman. Physiology, coronary circulation. *Treasure Island (FL): StatPearls Publishing*, 2020.

[36] The Editors of Encyclopaedia Britannica. Coronary circulation. 2014.

[37] Z. Zhao; L. Yang; D. Chen; Y. Luo. A human ecg identification system based on ensemble empirical mode decomposition. *Sensors (Basel, Switzerland)*, 13:6832–6864, 2013.

[38] M. Rivera-Ruiz; C. Cajavilca; J. Varon. Einthoven's string galvanometer: The first electrocardiograph. *Texas Heart Institute Journal*, 35:174–8, 2008.

[39] D. A. Jaye; Y.F. Xiao; D. C. Sigg. *Basic Cardiac Electrophysiology: Excitable Membranes*, pages 41–51. 08 2010.

[40] Meneghini; C. Ferreira; E. Schapacknik; S. Dubner; P. Moffa A. R. Perez Riera; A. H. Uchida; C. F. Filho; A. Significance of vectorcardiogram in the cardiological diagnosis of the 21st century. *Clinical Cardiology*, 30:319–323, 2007.

[41] E.P. Walsh; M. E. Alexander; F. Cecchin. *Electrocardiography and Introduction to Electrophysiologic Techniques*, pages 145–181. 2006.

[42] HE. Hering. Experimentelle studien an saugethieren uber das elektrocardiogram. *Zchr f exper path u therapie*, 7:363, 1909.

[43] T. Lewis. Notes upon alternation of the heart. *QJM: An International Journal of Medicine*, 4:141–144, 1910.

[44] HH. Kalter; M.L. Schwartz. Electrical alternans. *New York state journal of medicine*, 48(10):1164–6, 1948.

[45] A. A. Armoundas; R. J. Cohen. Clinical utility of t-wave alternans. *Cardiac Electrophysiology Review*, 3:390–394, 1997.

[46] JA. Salerno; M. Previtali; C. Panciroli; C. Klersy; M. Chimienti; M. Regazzi Bonora; E. Marangoni; C. Falcone; L. Guasti; C. Campana; R. Rondanelli. Ventricular arrhythmias during acute myocardial ischaemia in man: The role and significance of r-st-t alternans and the prevention of ischaemic sudden death by medical treatment. *European Heart Journal*, 7:63–75, 1986.

[47] MJ. Kleinfeld; JJ. Rozanski. Alternans of the st segment in prinzmetal's angina. *Circulation*, 55:574–577, 1977.

[48] C.V.R. Reddy; JP. Kiok; RG. Khan; N. El-Sherif. Repolarization alternans associated with alcoholism and hypomagnesemia. *American Journal of Cardiology*, 53:920–921, 1984.

[49] Z. Shimoni; E. Flatau; D. Schiller; E. Barzilay; D. Kohn. Electrical alternans of giant u waves with multiple electrolyte deficits. *American Journal of Cardiology*, 54:920–921, 1984.

[50] P. Schwartz; A. Malliani. Electrical alternation of the t wave: Clinical and experimental evidence of its relationship with the sympathetic nervous system and with the long q-t syndrome. *American Heart Journal*, 89:45–50, 1975.

[51] J.M. Smith; R.J. Cohen. Simple finite-element model accounts for wide range of cardiac dysrhythmias. *Proceedings of the National Academy of Sciences*, 81:233–237, 1984.

[52] M. Joseph; M.D. Smith; E.A. Clancy; C.R. Valeri; J.N. Ruskin; R.J. Cohen. Electrical alternans and cardiac electrical instability. *Circulation*, 77:110–121, 1988.

[53] L. Burattini; S. Man; S. Fioretti; F. Di Nardo; C.A. Swenne. Dependency of exercise-induced t-wave alternans predictive power for the occurrence of ventricular arrhythmias from heart rate. *Annals of Noninvasive Electrocardiology*, 20:345–354, 2015.

[54] T. Ikeda; H. Yoshino; K. Sugi; K. Tanno; H. Shimizu; J. Watanabe; Y. Kasamaki; A. Yoshida; T. Kato. Predictive value of microvolt t-wave alternans for sudden cardiac death in patients with preserved cardiac function after acute myocardial infarction: Results of a collaborative cohort study. *Journals of the American College of Cardiology*, 48:2268–2274, 2006.

[55] S.M. Narayan. T-wave alternans and the susceptibility to ventricular arrhythmias. *Journals of the American College of Cardiology*, 47:269–281, 2006.

[56] K. Sakaki; T. Ikeda; Y. Miwa; M. Miyakoshi; A. Abe; T. Tsukada; H. Ishiguro; H. Mera; S. Yusu; H. Yoshino. Time-domain twave alternans measured from holter electrocardiograms predicts cardiac mortality in patients with left ventricular dysfunction: A prospective study. *Heart Rhythm*, 6:332–337, 2009.

[57] A.A. Armoundas; G.F. Tomaselli; H.D. Esperer. Pathophysiological basis and clinical application of t-wave alternans. *Journal of the American College of Cardiology*, 40:207–17, 2002.

[58] R. L. Verrier; T. Klingenheben; M. Malik; N. El-Sherif; D. V. Exner; S.H. Hohnloser; T. Ikeda; J.P. Martínez; S.M. Narayan; T. Nieminen; D. S. Rosenbaum. Microvolt t-wave alternans: Physiological basis, methods of measurement, and clinical utility. *Journal of the American College of Cardiology*, 58(13):1309–1324, 2011.

[59] M. Chinushi; D. Kozhevnikov; E.B. Caref; M. Restivo; N. El-Sherif. Mechanism of discordant t wave alternans in the in vivo heart. *Journal of Cardiovascular Electrophysiology*, 14:632–638, 2003.

[60] W.T. Clusin. Mechanisms of calcium transient and action potential alternans in cardiac cells and tissues. *American Journal of Physiology: Heart and Circulatory Physiology*, 294:1–10, 2008.

[61] L.D. Wilson; D. Jeyaraj; X. Wan; G.S. Hoeker; T.H. S; M. Gittinger; K.R. Laurita; D.S. Rosenbaum. Heart failure enhances susceptibility to arrhythmogenic cardiac alternans. *Heart Rhythm*, 6:251–9, 2009.

[62] S.M. Narayan; J.D. Bayer; G. Lalani; N.A. Trayanova. Action potential dynamics explain arrhythmic vulnerability in human heart failure: a clinical and modeling study implicating abnormal calcium handling. *Journals of the American College of Cardiology.*, 52:1782–92, 2008.

[63] J.D. Bayer; S.M. Narayan; G.G. Lalani; N.A. Trayanova. Rate-dependent action potential alternans in human heart failure implicates abnormal intracellular calcium handling. *Heart Rhythm*, 7:1093–101, 2010.

[64] D.S. Rosenbaum; L.E. Jackson; J.M. Smith; H. Garan; J.N. Ruskin; R.J. Cohen. Electrical alternans and vulnerability to ventricular arrhythmias. *The New England Journal of Medicine*, 330:235–241, 1994.

[65] L. Burattini; M. Sumche; G. Ottaviano; S. Fioretti; F. Di Nardo ; C.A. Swenne. T-wave alternans rate of change with exercise for cardiac risk assessment. *Computing in Cardiology*, 41:177–180, 01 2014.

[66] D.M. Bloomfield; S.H. Hohnloser; R.J. Cohen. Interpretation and classification of microvolt t wave alternans tests. *Journal of Cardiovascular Electrophysiology*, 13:502 – 512, 05 2002.

[67] K. Tanno; S. Ryu; N. Watanabe; Y. Minoura; M. Kawamura; T. Asano ; Y. Kobayashi; T. Katagiri. Microvolt t-wave alternans as a predictor of ventricular tachyarrhythmias: A prospective study using atrial pacing. *Circulation*, 109:1854–8, 04 2004.

[68] L. Burattini; S. Man; S. Fioretti; F. Di Nardo; C.A. Swenne. Heart rate-dependent hysteresis of t-wave alternans in primary prevention icd patients. *Annals of Noninvasive Electrocardiology*, 21:460–469, 12 2015.

[69] H. Kitamura; Y. Ohnishi; K. Okajima ;A. Ishida; E. Galeano; K. Adachi; M. Yokoyama. Onset heart rate of microvolt-level t-wave alternans provides clinical and prognostic value in nonischemic dilated cardiomyopathy. *Journal of the American College of Cardiology*, 39:295–300, 01 2002.

[70] E.J. Rashba; A. Osman; K. MacMurdy; M. Kirk; S. Sarang; R.W. Peters; S.R. Shorofsky; M.R. Gold. Exercise is superior to pacing for t wave alternans measurement in subjects with chronic coronary artery disease and left ventricular dysfunction. *Journal of cardiovascular electrophysiology*, 13:845–50, 09 2002.

[71] M. Minkkinen; M. Kähönen; J. Viik; K. Nikus; T. Lehtimäki; R. Lehtinen; T. Kööbi; V. Turjanmaa; W. Kaiser; R. Verrier; T. Nieminen. Enhanced predictive power of quantitative twa during routine exercise testing in the finnish cardiovascular study. *Journal of cardiovascular electrophysiology*, 20:408–15, 11 2008.

[72] R. Beaudry; M.J. Haykowsky; A. Baggish; A. La Gerche. A modern definition of the athlete's heart-for research and the clinic. *Cardiology Clinics*, 34(4):507–514, 2016.

[73] https://www.etymonline.com/word/athlete?ref=etymonline_crossreference.

[74] R. Kovacs; A.L. Baggish. Cardiovascular adaptation in athletes. *Trends in Cardiovascular Medicine*, 26(1):46–52, 2016.

[75] A. Pelliccia; B.J. Maron; A. Spataro; M.A. Proschan; P. Spirito. The upper limit of physiologic cardiac hypertrophy in highly trained elite athletes. *The New England Journal of Medicine*, 324(5):295–301, 1991.

[76] N. Sheikh; M. Papadakis; F. Schnell; V. Panoulas; A. Malhotra; M. Wilson; F. Carré; S. Sharma. Clinical profile of athletes with hypertrophic cardiomyopathy. *Circulation: Cardiovascular Imaging*, 8(7), 2015.

[77] L. M. Millar; Z. Fanton; G. Finocchiaro; G. Sanchez-Fernandez; H. Dhutia; A. Malhotra; A. Merghani; M. Papadakis; E.R. Behr; N. Bunce; D. Oxborough; M. Reed; J. O'Driscoll; M.T. Tome Esteban; A. D'Silva; G. Carr-White; J. Webb; R. Sharma; S. Sharma. Differentiation between athlete's heart and dilated cardiomyopathy in athletic individuals. *Heart (British Cardiac Society)*, 106(14):1059–1065, 2020.

[78] M.W. Martinez; S.U. Nair. The athlete grey zone: Distinguishing pathologic from physiologic left ventricular hypertrophy. *American College of Cardiology*, 2014.

[79] L. Jordaens; R. Tavernier; J. Kazmierczak; C. Dimmer. Ventricular arrhythmias in apparently healthy subjects. *Pacing and Clinical Electrophysiology*, 20:2692 – 2698, 10 1997.

[80] B. Maron. *Cardiovascular Causes and Pathology of Sudden Death in Athletes: The American Experience*, pages 31–48. 01 2000.

[81] G. Thiene; C. Basso; D. Corrado. *Pathology of Sudden Death in Young Athletes: The European Experience*, pages 49–69. 01 2000.

[82] F. Furlanello; G. Galanti; P. Manetti; A. Capalbo; N. Pucci; A. Michelucci; D. Marangoni; F. Terrasi; G. Pettinati; R. Cappato. Microvolt t-wave alternans as predictor of electrophysiological testing results in professional competitive athletes. *Annals of noninvasive electrocardiology : the official journal of the International Society for Holter and Noninvasive Electrocardiology, Inc*, 9:201–6, 08 2004.

[83] G. Inama; R. Pizzi; G. Donato; O. Durin; M. Nanetti; C. Pedrinazzi. Ventricular arrhythmias in competitive athletes: risk stratification with t-wave alternans. *Heart International*, 3:58–67, 2009.

[84] G. Inama; R. Pizzi; G. Donato; O. Durin; M. Nanetti; C. Pedrinazzi; D. Assanelli. Microvolt t-wave alternans for risk stratification in athletes with ventricular arrhythmias: Correlation with programmed ventricular stimulation. *Annals of Noninvasive Electrocardiology*, 13:14 – 21, 2008.

[85] I. Simova; I. Gruev; G. Bortolan; I. Christov; S. Georgieva. T-wave alternans presence in young competitive athletes to be or not to be accepted as a prognostic factor? pages 1–4, 2017.

[86] J.S. Park; S.W. Lee; U. Park. R peak detection method using wavelet transform and modified shannon energy envelope. *Journal of Healthcare Engineering*, 2017:1–14, 2017.

[87] Y.C. Yeh; W.J. Wang. Qrs complexes detection for ecg signal: The difference operation method. *Computer methods and programs in biomedicine*, 91:245–54, 2008.

[88] A. Nimunkar; W. Tompkins. R-peak detection and signal averaging for simulated stress ecg using emd. *Conference proceedings : ... Annual International Conference of the IEEE Engineering in Medicine and Biology Society. IEEE Engineering in Medicine and Biology Society. Conference*, 2007:1261–4, 2007.

[89] Jiapu Pan and Willis Tompkins. A real-time qrs detection algorithm. *Biomedical Engineering, IEEE Transactions on*, 32:230–236, 1985.

[90] F. Liu; C. Liu; X. Jiang; Z. Zhang; Y. Zhang; J. Li; S. Wei. Performance analysis of ten common qrs detectors on different ecg application cases. *Journal of Healthcare Engineering*, 2018:1–8, 2018.

[91] L. Xie; Z. Li; Y. Zhou; Y. He; J. Zhu. Computational diagnostic techniques for electrocardiogram signal analysis. *Sensors (Basel, Switzerland)*, 20:6318, 2020.

[92] Z. Zhao; L. Yang; D. Chen; Y. Luo. A human ecg identification system based on ensemble empirical mode decomposition. *Sensors (Basel, Switzerland)*, 13:6832–6864, 2013.

[93] Kang-Ming Chang. Arrhythmia ecg noise reduction by ensemble empirical mode decomposition. *Sensors (Basel, Switzerland)*, 10:6063–80, 2010.

[94] A. Safari; H. Danandeh; M. Mohebbi; F. Faradji. A novel method for r-peak detection in noisy ecg signals using eemd and ica. pages 155–158, 2016.

[95] L. Burattini; W. Zareba; R. Burattini. Adaptive match filter based method for time vs. amplitude characterization of microvolt ecg t-wave alternans. *Annals of biomedical engineering*, 36:1558–64, 2008.

[96] X. Wan; K. Yan; D. Luo; Y. Zeng. A combined algorithm for t-wave alternans qualitative detection and quantitative measurement. *Journal of cardiothoracic surgery*, 8:7, 2013.

[97] D. Rosenbaum; X. Fang; J. Mackall. 1027-40 how to detect ecg t-wave alternans in patients at risk for sudden cardiac death. *Journal of the American College of Cardiology*, 25:409, 1995.

[98] P. Laguna; M. Ruiz; G.B. Moody; R.G. Mark. Repolarization alternans detection using the kl transform and the beatquency spectrum. volume 10, pages 673 – 676, 1996.

[99] Bnearing Nearing and Richard Verrier. Modified moving average analysis of t-wave alternans to predict venricular fibrillation with high accuracy. *Journal of applied physiology (Bethesda, Md. : 1985)*, 92:541–9, 02 2002.

[100] L. Burattini; W. Zareba; A. Moss. Correlation method for detection of transient t-wave alternans in digital holter ecg recordings. *Annals of Noninvasive Electrocardiology*, 4:416 – 424, 2006.

[101] J.P. Martínez; S. Olmos. A robust t wave alternans detector based on the glrt for laplacian noise distribution. volume 2002, pages 677 – 680, 2002.

[102] T. Srikanth; D. Lin; N. Kanaan; H. Gu. Presence of t wave alternans in the statistical context - a new approach to low amplitude alternans measurement. In *Computers in Cardiology*, pages 681–684, 2002.

[103] Pawel Strumillo and Jan Ruta. Poincare mapping for detecting abnormal dynamics of cardiac repolarization. *Engineering in Medicine and Biology Magazine, IEEE*, 21:62 – 65, 2002.